Published for SISSA by Springer

Received: December 10, 2019
Revised: January 31, 2020
Accepted: April 16, 2020
Published: May 8, 2020

JHEP05(2020)035

χSB of cascading gauge theory in de Sitter

Alex Buchel

Department of Applied Mathematics, Department of Physics and Astronomy,
University of Western Ontario,
London, ON N6A 5B7, Canada
Perimeter Institute for Theoretical Physics,
Waterloo, ON N2J 2W9, Canada

E-mail: abuchel@uwo.ca

Abstract: $\mathcal{N}=1$ supersymmetric $\mathrm{SU}(N)\times\mathrm{SU}(N+M)$ cascading gauge theory of Klebanov et al. [1, 2] spontaneously breaks chiral symmetry in Minkowski space-time. We demonstrate that in de Sitter space-time the chiral symmetry breaking occurs for the values of the Hubble constant $H\lesssim 0.7\Lambda$, as well as in the narrow window $0.92(1)\Lambda\leq H\leq 0.92(5)\Lambda$. We give a precise definition of the strong coupling scale Λ of the cascading gauge theory, which is related to the glueball mass scale in the theory $m_{\rm glueball}$ and the asymptotic string coupling g_s as $\Lambda\sim g_s^{1/2}m_{\rm glueball}$.

Keywords: AdS-CFT Correspondence, Black Holes in String Theory, Spontaneous Symmetry Breaking

ArXiv ePrint: 1912.03566

https://doi.org/10.1007/JHEP05(2020)035

Contents

JHEP05(2020)035

1 Introduction and summary

Consider $\mathcal{N} = 1$ supersymmetric $\mathrm{SU}(N+M) \times \mathrm{SU}(N)$ gauge theory with two chiral superfields A_1, A_2 in the $(N+M, \overline{N})$ representation, and two chiral superfields B_1, B_2 in the $(\overline{N+M}, N)$ representation, in four dimensional Minkowski space-time $\mathbb{R}^{3,1}$. This theory has two gauge couplings g_1, g_2 associated with the two gauge group factors, and a quartic superpotential

$$W \;\sim\; \mathrm{Tr}\,(A_i B_j A_k B_\ell)\,\epsilon^{ik}\epsilon^{j\ell}\,. \tag{1.1}$$

When $M = 0$, both gauge couplings are exactly marginal, and the theory flows to a strongly coupled superconformal fixed point — the Klebanov-Witten (KW) theory [3]. KW infrared (IR) fixed point global symmetry

$$G: \qquad \underbrace{\mathrm{SU}(2) \times \mathrm{SU}(2)}_{\text{flavour}} \times \underbrace{\mathrm{U}(1)}_{R-\text{symmetry}}\,, \tag{1.2}$$

together with the superconformal invariance implies non-perturbatively large anomalous dimensions for the chiral superfields:

$$\gamma(A_i) = \gamma(B_j) = -\frac{1}{4}\,. \tag{1.3}$$

When $M \neq 0$, conformal invariance of $\mathrm{SU}(N+M) \times \mathrm{SU}(N)$ gauge theory is broken: while the sum of the gauge coupling remains exactly marginal [2],

$$\frac{4\pi^2}{g_1^2} + \frac{4\pi^2}{g_2^2} = \frac{\pi}{g_s} = \text{const}\,, \tag{1.4}$$

where g_s is the asymptotic string coupling of the gravitational dual [4], the perturbative β-function of the difference of the couplings is nonzero [4]:

$$\frac{8\pi^2}{g_1^2} - \frac{8\pi^2}{g_2^2} = M \ln \frac{\Lambda}{\mu}\Big(3 + 2(1 - \gamma(\mathrm{Tr}(A_i B_j)))\Big) = 6M \ln \frac{\Lambda}{\mu}\left(1 + \mathcal{O}\left(\frac{M^2}{N^2}\right)\right)\,. \tag{1.5}$$

Λ is the strong coupling scale of the theory. Given (1.4) and (1.5), the effective weakly coupled description of $\mathrm{SU}(N+M) \times \mathrm{SU}(N)$ gauge theory exists only in a finite-width energy band centered about Λ — one encounters Landau poles both in the IR

$$g_2^2 \to \infty \qquad \text{as} \qquad \mu \to \mu_{IR} \equiv \Lambda e^{-\frac{\pi}{3 g_s M}}\,, \tag{1.6}$$

JHEP05(2020)035

and the ultraviolet (UV),

$$g_1^2 \to \infty \qquad \text{as} \qquad \mu \to \mu_{UV} \equiv \Lambda e^{+\frac{\pi}{3g_s M}} \,, \tag{1.7}$$

to leading order in M^2/N^2. As explained in [2], to extend the theory past the strong coupling regions one must perform the self-similar transformations (Seiberg dualities [5]): $N \to N - M$ for $\mu \lesssim \mu_{IR}$ and $N \to N + M$ for $\mu \gtrsim \mu_{UV}$. Thus, extension of the effective $\mathrm{SU}(N+M) \times \mathrm{SU}(N)$ description to all energy scales involves an infinite sequence — a *cascade* — of Seiberg dualities with the renormalization group flow of the effective rank [6–8]

$$N = N(\mu) \;\sim\; g_s M^2 \ln \frac{\mu}{\Lambda} \,. \tag{1.8}$$

Although there are infinitely many duality steps in the UV, there is only a finite number of the duality transformations as one flows to the IR — when N is an integer multiple of M (plus 1) one ends up in the IR with the $\mathrm{SU}(M+1)$ gauge theory. The latter theory confined in the IR with a spontaneous breaking of the $\mathrm{U}(1)_R$ (chiral symmetry),

$$\mathrm{U}(1)_R \to \mathbb{Z}_2 \,. \tag{1.9}$$

The IR properties of the cascading gauge theories were reviewed in [4] (see also [9]); an important feature of the theory is the characteristic scale in the glueball mass spectrum:

$$m_{\text{glueball}} \equiv \frac{\epsilon^{2/3}}{M g_s \alpha'} \,, \tag{1.10}$$

where ϵ is a conifold deformation parameter of the holographic dual [2], and $\alpha' = \ell_s^2$ is the string scale.

Previous studies focused on the fate of the chiral symmetry and the confinement in the cascading gauge theory at finite temperature. At finite temperature, there are three different spatially homogeneous and isotropic phases of the theory. We classify them as follows:

- PhaseA$_s$ — the deconfined phase with the unbroken chiral symmetry, i.e., U(1), see [6, 10–12];
- PhaseA$_b$ — the deconfined phase with the broken chiral symmetry, i.e., $\mathbb{Z}_2$, see [13, 14];
- PhaseB — the confined phase with the broken chiral symmetry, i.e., $\mathbb{Z}_2$, see [2].

Notice that confinement triggers the spontaneous breaking of the chiral symmetry [2]: there is no spatially homogeneous and isotropic phase which is confined with U(1) chiral symmetry. It will be instructive to have a geometrical classification of these phases, in the warped-deformed conifold holographic dual of the theory [2, 13, 15]. To this end, consider analytical continuation along the time direction $t \to t_E \equiv it$. Euclidean time t_E is then periodically identified as

$$t_E \qquad \sim \qquad t_E + \frac{1}{T} \,, \tag{1.11}$$

JHEP05(2020)035

where T is the equilibrium temperature of the phase. Topologically, the compact directions of the holographic dual are

$$\begin{aligned} &\text{unbroken chiral symmetry}: && \underbrace{S^1}_{\text{thermal circle}} && \times && \underbrace{S^1\times S^2\times S^2}_{\text{U(1)}-\text{symmetric } T^{1,1}}\ ; \\ &\text{broken chiral symmetry}: && \underbrace{S^1}_{\text{thermal circle}} && \times && \underbrace{S^2\times S^3}_{\mathbb{Z}_2-\text{symmetric } T^{1,1}}\ . \end{aligned} \tag{1.12}$$

We can thus geometrically characterize different phases depending on which cycle shrinks to zero size in the interior of the ten-dimensional Euclidean type IIB supergravity dual:

$$\begin{aligned} &\text{PhaseA}_s: && \underbrace{S^1}_{\text{thermal circle}} \to 0 && \& && S^1\times S^2\times S^2 \text{ is finite}\,; \\ &\text{PhaseA}_b: && \underbrace{S^1}_{\text{thermal circle}} \to 0 && \& && S^2\times S^3 \text{ is finite}\,; \\ &\text{PhaseB}: && \underbrace{S^1}_{\text{thermal circle}} \text{ is finite} && \& && S^2\to 0 \quad \& \quad S^3 \text{ is finite}\,. \end{aligned} \tag{1.13}$$

According to [12] there is the first-order confinement/deconfinement phase transition between PhaseA$_s$ and PhaseB at[1]

$$T_c = 0.614(1)\ \frac{\Lambda_{\text{thermal}}}{P g_s^{1/2}} = 0.614(1)\ \frac{3^{1/2}e^{1/3}}{2^{7/12}}\ \frac{\epsilon^{2/3}}{P g_s^{1/2}} = 0.220(2)\ g_s^{1/2} m_{\text{glueball}}\,, \tag{1.14}$$

where the relation between P and M is given by (2.7) and m_{glueball} is defined as in (1.10). At temperature $T < T_c$ the phase PhaseA$_s$ is metastable — it becomes perturbatively unstable below $T_{\chi\text{SB}} < T_c$ [13],

$$T_{\chi\text{SB}} = 0.542(0)\ \frac{\Lambda_{\text{thermal}}}{P g_s^{1/2}} = 0.194(3)\ g_s^{1/2} m_{\text{glueball}}\,. \tag{1.15}$$

The symmetry broken deconfined phase PhaseA$_b$ exists only for $T \geq T_{\chi\text{SB}}$ or for energy densities $\mathcal{E} \leq \mathcal{E}_{\chi\text{SB}}$ [14],

$$\begin{aligned} \mathcal{E}_{\chi\text{SB}} &= 1.270(1)\ \frac{\Lambda_{\text{thermal}}^4}{16\pi G_5} = 1.270(1)\ \frac{2^{2/3}e^{4/3}}{192\pi^4}\ (M g_s)^4\ m_{\text{glueball}}^4 \\ &= 4.089(6)\times 10^{-4}\ \times\ (M g_s)^4\ m_{\text{glueball}}^4\,, \end{aligned} \tag{1.16}$$

where G_5 is given by (2.8). PhaseA$_b$ has larger thermal free energy density than that of the chirally symmetric deconfined phase PhaseA$_s$ at the corresponding temperature, and thus it does not dominate the canonical ensemble. On the other hand, PhaseA$_b$ is entropically favored over PhaseA$_s$ at the corresponding energy density, and thus is the dominant phase in the microcanonical ensemble. According to [14] the phase PhaseA$_b$ is thermodynamically unstable, and thus it is dynamically (perturbatively) unstable towards developing spatial inhomogeneities [17].

[1]The precise expression for Λ_{thermal} was reported in [16].

JHEP05(2020)035

In this paper we would like to understand vacua of the cascading gauge theories in de Sitter space-time (flat or closed spatial slicing)[2]

$$ds_4^2 = -dt^2 + e^{2Ht} d\boldsymbol{x}^2 \,, \qquad \text{or} \qquad ds_4^2 = -dt^2 + \frac{1}{H^2}\cosh^2(Ht)\left(dS^3\right)^2 \,, \tag{1.17}$$

where H is a Hubble constant. Specifically, we would like to provide the classification of late-time states of the cascading gauge theory akin to spatially homogeneous and isotropic thermal phases {PhaseA$_s$, PhaseA$_b$, PhaseB} reviewed above. Of course there are crucial differences between the thermal equilibrium physics and the late time de Sitter dynamics:

- Thermodynamics can be studied in canonical or microcanonical ensembles.[3] The latter one is suitable to study the dynamics of the equilibration process. The de Sitter evolution of the gauge theory states is eternally sourced by the space-time accelerated expansion and thus is (loosely) equivalent to the microcanonical ensemble; there is no correspondence to the canonical ensemble.

- Insisting on spatial homogeneity and isotropy, an initial state typically[4] relaxes to a thermal equilibrium configuration, which can be assigned a thermal (time-independent) entropy density. The holographic dynamics of the conformal gauge theories with a simple scale transformation can be mapped to an evolution in Minkowski space-time [19] — here the late-time de Sitter vacua are conformally equivalent to the equilibrium states of the microcanonical ensemble. There is no equilibration of non-conformal gauge theories at late-times in de Sitter [19]:[5] the comoving entropy density production rate is nonzero. In [21] it was pointed out that the comoving entropy production rate $\mathcal{R}$ can be attribute entirely to the spatial expansion

$$\text{volume}\Big|_{\text{physical}} = e^{3Ht}\ \text{volume}\Big|_{\text{comoving}} \,,$$

while the physical entropy density s approaches a constant (time-independent) entanglement entropy s_{ent}:

$$\lim_{t\to\infty} s \equiv s_{\text{ent}} = H^3\ \mathcal{R}\,. \tag{1.18}$$

In holography, the non-equilibrium entropy density $s = s(t)$ is associated with the Bekenstein entropy of the dynamical apparent horizon (AH) [22, 23]. In [24] an example of a fully nonlinear holographic evolution from initially homogeneous and isotropic state in de Sitter was presented where the late-time dynamics approaches de Sitter vacuum with entanglement entropy (1.18).

Implementing de Sitter holographic dynamics as in [24] for the cascading gauge theories is outside the scope of this paper. Rather, as in [19] and [20], we assume that we

[2] There is no difference between them at late times as the curvature effects are diluted as $\propto \exp(-2Ht)$.

[3] As we emphasized above the thermal equilibrium phase structure is different in the two ensembles of the cascading gauge theory.

[4] Not all strongly interacting systems equilibrate. See [18] for a holographic example.

[5] See also [20] for a detailed recent analysis.

JHEP05(2020)035

specify a well-defined spatially homogeneous and isotropic initial state[6] (a well-defined initial condition for the gravitation evolution) in a holographic dual. This would correspond to some coarse grained state in the gauge theory specified with the density matrix ρ. We identify the von Neumann entropy $\mathcal{S}$

$$\mathcal{S} = -\operatorname{Tr}(\rho \ln \rho)\,,$$

with the Bekenstein entropy of the AH in the holographic dual.[7] Partial differential equation of the gravitational dual at late times reduce to system of ordinary differential equations [24] which we analyze in details here. Inequivalent de Sitter vacua of the cascading gauge theory are characterized with different values of the entanglement entropy density $s_{\rm ent}$. The true (dominant) vacuum is the one which results in the largest $s_{\rm ent}$ for a fixed Hubble constant H and a fixed strong coupling scale of the theory Λ, see (B.80),

$$\Lambda = \frac{2^{1/6} e^{1/3} g_s^{1/2}}{3^{3/2}}\, m_{\rm glueball} \;\approx\; 0.3 g_s^{1/2} m_{\rm glueball}\,. \tag{1.19}$$

Parallel to classification of the thermal equilibrium states, we now explain topological/symmetry considerations to classify de Sitter vacua of cascading gauge theory — the discussion is more intuitive for the closed spatial slicing in (1.17). To access AH (and thus to evaluate $s_{\rm ent}$), the dual gravitational bulk must be described in Eddington-Finkelstein (EF) coordinates. Fefferman-Graham (FG) coordinates cover only a patch of the former, which is outside of the EF frame AH [24], and thus is not suitable for the computation of the vacuum entanglement entropy. Still, FG frame is useful to implement analytical continuation to Euclidean (Bunch-Davies) vacuum

$$-d\tau^2 + \frac{1}{H^2}\cosh^2(H\tau)\left(dS^3\right)^2 \underbrace{\longrightarrow}_{\tau\to i\frac{\theta+\pi/2}{H}} \frac{1}{H^2}\left((d\theta)^2 + \sin^2(\theta)\,\left(dS^3\right)^2\right) = \frac{1}{H^2}\,\left(dS^4\right)^2\,. \tag{1.20}$$

Topologically, the compact directions of the Euclidean FG frame holographic dual are (compare with (1.12))

$$\begin{aligned} &\text{unbroken chiral symmetry}: && \underbrace{S^4}_{dS_4^{\rm Euclidean}} && \times && \underbrace{S^1\times S^2\times S^2}_{\mathrm{U}(1)-\text{symmetric } T^{1,1}}\;; \\ &\text{broken chiral symmetry}: && \underbrace{S^4}_{dS_4^{\rm Euclidean}} && \times && \underbrace{S^2\times S^3}_{\mathbb{Z}_2-\text{symmetric } T^{1,1}}\;. \end{aligned} \tag{1.21}$$

Parallel to (1.13), we can geometrically characterize different de Sitter vacua of the cascading gauge theory depending on which cycle shrinks to zero size in the interior of the

[6] We believe that restriction to homogeneity and isotropy is not relevant for the late-time dynamics, given the accelerated background space-time expansion.

[7] This procedure is implicit in all examples of holographic evolutions in Chesler-Yaffe framework [25]. Besides 'holographic quenches' of background space-time [26] (similar to de Sitter 'quenches' of interest here) it was successfully applied to quenches of the coupling constants of relevant operators in [27, 28].

JHEP05(2020)035

ten-dimensional Euclidean FG frame type IIB supergravity dual:

$$\begin{aligned}
&\text{TypeA}_s: && \underbrace{S^4}_{dS_4^{\text{Euclidean}}} \to 0 && \& && S^1\times S^2\times S^2 \text{ is finite}\,;\\
&\text{TypeA}_b: && \underbrace{S^4}_{dS_4^{\text{Euclidean}}} \to 0 && \& && S^2\times S^3 \text{ is finite}\,;\\
&\text{TypeB}: && \underbrace{S^4}_{dS_4^{\text{Euclidean}}} \text{ is finite} && \& && S^2\to 0 \quad \& \quad S^3 \text{ is finite}\,.
\end{aligned} \tag{1.22}$$

To evaluate s_{ent} we proceed in two steps:[8]

- first, we construct the FG frame vacua, subject to the 'boundary conditions' (1.22) (see appendix B.1 for the technical details);
- second, we use coordinate transformation to the EF frame for each of these vacua (see [24] and appendix B.2 for the technical details), and access the corresponding AH.

We summarize now our results:

- TypeA$_s$ de Sitter vacua were studied previously in [29–31]. These vacua share resemblance with the thermal deconfined chirally symmetric states of the cascading gauge theory, i.e., PhaseA$_s$. We find here that

$$s_{\text{ent}}(\Lambda,H)\Big|_{\text{TypeA}_s} \neq 0\,, \tag{1.23}$$

and vanishes as

$$s_{\text{ent}}(\Lambda,H)\Big|_{\text{TypeA}_s} \propto H^3\left(\ln\frac{H^2}{\Lambda^2}\right)^{-3/4} \qquad \text{as} \qquad H\gg\Lambda\,, \tag{1.24}$$

i.e., in the conformal limit. TypeA$_s$ de Sitter vacua exist only when

$$H \gtrsim H^s_{\text{min}}\,, \qquad H^s_{\text{min}} = 0.7\Lambda \approx 0.2\, g_s^{1/2} m_{\text{glueball}}\,. \tag{1.25}$$

As $\frac{H^2}{\Lambda^2}$ decreases, the Kretschmann scalar at the AH in the holographic dual increases, making supergravity approximation less reliable. H^s_{min} in (1.25) should be interpreted as the value of the Hubble constant at which the supergravity approximation breaks down. We identify the rapid growth of the curvature in the gravitational dual to TypeA$_s$ de Sitter vacua with collapsing of the compact manifold (a deformed $T^{1,1}$) at the location of the apparent horizon — as a result, s_{ent} vanishes in this limit as well.

[8] The same two-step procedure was also used in computation of the de Sitter vacuum entanglement entropy in $\mathcal{N}=2^*$ gauge theory in [20].

JHEP05(2020)035

- TypeA$_b$ de Sitter vacua are constructed here for the first time.[9] These vacua share resemblance with the thermal deconfined states of the cascading gauge theory with the spontaneously broken chiral symmetry, i.e., PhaseA$_b$. We find here that

$$s_{\rm ent}(\Lambda, H)\Big|_{\rm TypeA_b} \neq 0\,. \tag{1.26}$$

TypeA$_b$ de Sitter vacua exist only when

$$H \;\geq\; H^b_{\rm min}\,, \qquad H^b_{\rm min} = 0.92(1)\Lambda \approx 0.276\; g_s^{1/2} m_{\rm glueball}\,. \tag{1.27}$$

As $\frac{H^2}{\Lambda^2}$ increases, the Kretschmann scalar at the AH in the holographic dual increases, making the supergravity approximation less reliable.

- We find that while

$$s_{\rm ent}(\Lambda, H^b_{\rm min})\Big|_{\rm TypeA_s} = s_{\rm ent}(\Lambda, H^b_{\rm min})\Big|_{\rm TypeA_b}\,, \tag{1.28}$$

de Sitter vacua with the spontaneously broken chiral symmetry are entropically favored within a narrow window for the values of the Hubble constant

$$s_{\rm ent}(\Lambda, H)\Big|_{\rm TypeA_b} \;\geq\; s_{\rm ent}(\Lambda, H)\Big|_{\rm TypeA_s}\,, \qquad H_{\rm max} \geq H \geq H^b_{\rm min}\,, \tag{1.29}$$

where

$$H_{\rm max} = 0.92(5)\Lambda \approx 0.278\; g_s^{1/2} m_{\rm glueball}\,. \tag{1.30}$$

TypeA$_b$ de Sitter vacua continue to exist for $H > H_{\rm max}$, however they have smaller $s_{\rm ent}$ compare to the corresponding TypeA$_s$ de Sitter vacua.

- TypeB de Sitter vacua were studied previously in [31]. These vacua share resemblance with the thermal confined states of the cascading gauge theory with the spontaneously broken chiral symmetry, i.e., PhaseB. We find here that

$$s_{\rm ent}(\Lambda, H)\Big|_{\rm TypeB} = 0\,. \tag{1.31}$$

We emphasize that (1.31) does not mean that the coarse grained entropy of the cascading gauge theory vanishes — in fact, during de Sitter evolution the entropy production rate is always positive (see section 3.3). What (1.31) states is that the comoving entropy production rate in TypeB vacuum vanishes at late times (much like it does in conformal gauge theories [24]). As a result, TypeB vacuum is never realized as the late-time attractor of a dynamical evolution for a generic cascading gauge theory state in de Sitter, provided vacua TypeA$_s$ or TypeA$_b$ exist. Neither of the latter vacua exists for $H \lesssim H^s_{\rm min}$, see (1.25), thus[10]

$$\textit{TypeB de Sitter vacum is a late}-\textit{time attractor provided } H \lesssim H^s_{\rm min}\,. \tag{1.32}$$

[9] We introduce a novel technique used to identify phases/vacua with spontaneously broken symmetry.

[10] While this is likely to be true in general, the statement is strictly precise for the de Sitter evolution of spatially homogeneous and isotropic states of the cascading gauge theory.

JHEP05(2020)035

Of cause, (1.32) implies that TypeB vacua must exist at least for $H > H^s_{\rm min}$; in fact we find (see section 6.2) that TypeB vacua exist[11] for

$$H \lesssim H^B_{\rm max}\,, \qquad H^B_{\rm max} = 0.966(5)\Lambda \ > H^s_{\rm min} = 0.7\Lambda\,. \tag{1.33}$$

Eqs. (1.29) and (1.32) represents our main, and somewhat unexpected result:

> SU(N) × SU($N+M$) cascading gauge theory with a strong coupling scale Λ undergoes spontaneous chiral symmetry breaking in de Sitter space time with a Hubble constant H provided
>
> $$H \lesssim H^s_{\rm min} < H^b_{\rm min} \qquad \& \qquad H^b_{\rm min} \ \leq \ H \ \leq H_{\rm max}\,.$$
>
> The critical values $H^s_{\rm min}$, $H^b_{\rm min}$ and $H_{\rm max}$ are of order the strong coupling scale of the theory Λ.

The rest of the paper is organized as follows. In section 2 we discuss holographic dual effective action of cascading gauge theory. Section 2 contains a guide to set of appendices with technical details. Cascading gauge theory de Sitter vacuum entanglement entropy is identified with the Bekenstein entropy of the AH in the holographic dual at late times, see section 3. In section 3.1 we identify AH in ten dimensional holographic dual and compute its area density. In section 3.2 we establish that both the location of the AH and its associated entropy density is invariant upon Kaluza-Klein reduction on the warped-deformed $T^{1,1}$. In section 3.3 we prove a theorem that as long as the background geometry of the holographic dual is nonsingular, the area density of the AH does not decrease with time. In section 3.4 we show that whenever vacua of TypeB exist, their entanglement entropy vanishes, see (1.31). Section 4 devoted to TypeA$_s$ de Sitter vacua. Numerical results are presented in section 4.1: we construct first the dual holographic backgrounds in the FG frame, transform them to the EF frame, identify the location of the apparent horizon and compute the vacuum entanglement entropy, see figure 6. At each step we triple-check the numerical results by making use of distinct and independent computational schemes, see appendix C. Comparison of the results from the different computational schemes in the overlapping regions of the parameter space is shown in figures 2, 4, 7. In section 4.2 we make use of the computational SchemeII to discuss the conformal limit of TypeA$_s$ vacua, i.e., $H \gg \Lambda$, and establish (1.24). The validity of the supergravity approximation of the holographic dual to TypeA$_s$ de Sitter vacua is discussed in section 4.3. We establish a rapid growth of the Kretschmann scalar of the background geometry (2.13) evaluated at the AH for small values of $\frac{H^2}{\Lambda^2}$, and associate this growth with "collapsing" of the deformed $T^{1,1}$, see figures 11 and 12. Extrapolating the numerical data, we estimate the value of the Hubble constant $H^s_{\rm min}$, see (1.25), when the Kretschmann scalar diverges — we take this value as a limiting value of H below which TypeA$_s$ vacua stop existing. We study TypeA$_b$ vacua with the spontaneously broken chiral symmetry in section 5. We begin in section 5.1 with identification of the critical value $H^b_{\rm min}$, see (1.27), below which TypeA$_b$ vacua do not exist.

[11] This should be understood in the same sense as existence of TypeA$_s$ vacua: the supergravity approximation used to construct TypeB vacua is robust against higher-derivative α' corrections from the full string theory.

JHEP05(2020)035

This is done computing the linearized chiral symmetry breaking perturbations on top of TypeA$_s$ vacua with the explicit symmetric breaking parameter — the gaugino mass term. At this critical value $H = H^b_{\rm min}$ all the symmetry breaking expectation values diverge, see figure 13. We explain how TypeA$_b$ vacua, with the spontaneous symmetry breaking, can be constructed at values of the Hubble constant close to $H^b_{\rm min}$ using the linearized perturbations on top of TypeA$_s$ vacua with the explicit symmetry breaking. Numerical construction of TypeA$_b$ vacua in section 5.2 follows the discussion of section 4.1. Section 5.2 contains the central result of the paper — figure 21: it establishes that the chiral symmetry breaking of the cascading gauge theory in de Sitter space-time occurs in a narrow range of values of the Hubble constant, see (1.29). The validity of the supergravity approximation of the holographic dual to TypeA$_b$ de Sitter vacua is discussed in section 5.3. TypeB de Sitter vacua are discussed in section 6. These vacua have vanishing entanglement entropy (1.31); however, they exist for arbitrary small $\frac{H}{\Lambda}$, approaching the extremal Klebanov-Strassler solution [2] as $\frac{H}{\Lambda} \to 0$. We discuss TypeB vacua, first as a deformation of the extremal KS solution, and followed later by the numerical construction in two different computational schemes in section 6.1. In section 6.2 we present an indication that TypeB vacua exist only for $H \lesssim H^B_{\rm max}$ (1.33) — in this limit the 3-cycle of the dual geometry supporting the RR 3-form flux becomes vanishingly small in string units, making the supergravity approximation not reliable as indicated by the rapid growth of the Kretschmann scalar of the background geometry evaluated at the AH, see figure 26. Since both TypeA$_s$ and TypeA$_b$ vacua cease to exist below certain value of the Hubble constant, specifically for $H \lesssim H^s_{\rm min}$, and $H^B_{\rm max} > H^s_{\rm min}$, TypeB vacua become late-time attractors of the dynamical evolution of the cascading gauge theory in de Sitter for $H \lesssim H^s_{\rm min}$. We conclude in section 7 highlighting open questions and future directions.

2 Dual effective actions of the cascading gauge theory

Consider SU(2) × SU(2) × $\mathbb{Z}_2$ invariant states of the cascading gauge theory on a 4-dimensional manifold $\mathcal{M}_4 \equiv \partial\mathcal{M}_5$. In the planar limit and at large 't Hooft coupling, one can consistently truncate the theory to a finite number of operators [13]: a stress-energy tensor T_{ij}, a pair of dimension-3 operators $\mathcal{O}_3^{\alpha=\{1,2\}}$ (dual to gaugino condensates for each of the gauge group factors), a pair of dimension-4 operators $\mathcal{O}_4^{\beta=\{1,2\}}$, and dimension-6,7,8 operators $\mathcal{O}_6, \mathcal{O}_7, \mathcal{O}_8$. Effective gravitational action on a 5-dimensional manifold $\mathcal{M}_5$ describing holographic dual of such states was derived in [13]:

$$
\begin{aligned}
S_5\left[g_{\mu\nu} \leftrightarrow T_{ij}, \{\Omega_i, h_i, \Phi\} \leftrightarrow \{\mathcal{O}_3^\alpha, \mathcal{O}_4^\beta, \mathcal{O}_6, \mathcal{O}_7, \mathcal{O}_8\}\right] = \frac{108}{16\pi G_5}\int_{\mathcal{M}_5} \mathrm{vol}_{\mathcal{M}_5}\ \Omega_1\Omega_2^2\Omega_3^2 \times \\
\times \Bigg\{ R_{10} - \frac{1}{2}(\nabla\Phi)^2 - \frac{1}{2}e^{-\Phi}\left(\frac{(h_1-h_3)^2}{2\Omega_1^2\Omega_2^2\Omega_3^2} + \frac{1}{\Omega_3^4}(\nabla h_1)^2 + \frac{1}{\Omega_2^4}(\nabla h_3)^2\right) \\
- \frac{1}{2}e^{\Phi}\left(\frac{2}{\Omega_2^2\Omega_3^2}(\nabla h_2)^2 + \frac{1}{\Omega_1^2\Omega_2^4}\left(h_2 - \frac{P}{9}\right)^2 + \frac{1}{\Omega_1^2\Omega_3^4}h_2^2\right) \\
- \frac{1}{2\Omega_1^2\Omega_2^4\Omega_3^4}\left(4\Omega_0 + h_2(h_3-h_1) + \frac{1}{9}Ph_1\right)^2\Bigg\},
\end{aligned}
\tag{2.1}
$$

JHEP05(2020)035

where Ω_0 is a constant in the definition of the 5-form flux,[12] see (2.5), R_{10} is given by

$$\begin{aligned} R_{10} = R_5 + \left(\frac{1}{2\Omega_1^2} + \frac{2}{\Omega_2^2} + \frac{2}{\Omega_3^2} - \frac{\Omega_2^2}{4\Omega_1^2\Omega_3^2} - \frac{\Omega_3^2}{4\Omega_1^2\Omega_2^2} - \frac{\Omega_1^2}{\Omega_2^2\Omega_3^2}\right) - 2\Box \ln\left(\Omega_1\Omega_2^2\Omega_3^2\right) \\ - \left\{(\nabla \ln \Omega_1)^2 + 2\,(\nabla \ln \Omega_2)^2 + 2\,(\nabla \ln \Omega_3)^2 + \left(\nabla \ln\left(\Omega_1\Omega_2^2\Omega_3^2\right)\right)^2\right\}, \end{aligned} \tag{2.2}$$

and R_5 is the five-dimensional Ricci scalar of the metric

$$ds_5^2 = g_{\mu\nu}(y)dy^\mu dy^\nu\,, \tag{2.3}$$

that forms part of the ten dimensional full metric

$$ds_{10}^2 = ds_5^2 + ds_{T^{1,1}}^2\,, \qquad ds_{T^{1,1}}^2 = \Omega_1^2(y)g_5^2 + \Omega_2^2(y)(g_3^2+g_4^2) + \Omega_3^2(y)(g_1^2+g_2^2). \tag{2.4}$$

One-forms $\{g_i\}$ (for $i = 1, \cdots, 5$) are the usual forms defined in the warp-squashed $T^{1,1}$ and are given as in [13], for coordinates $0 \le \psi \le 4\pi$, $0 \le \theta_a \le \pi$ and $0 \le \phi_a \le 2\pi$ $(a = 1, 2)$. All the covariant derivatives ∇_λ are with respect to the metric (2.3). Fluxes (and dilaton Φ) are parameterized in such a way that functions $h_1(y), h_2(y), h_3(y)$ appear as

$$\begin{aligned} F_5 &= \mathcal{F}_5 + \star\mathcal{F}_5\,, \\ \mathcal{F}_5 &= \left(4\Omega_0 + h_2(y)(h_3(y) - h_1(y)) + \frac{P}{9}h_1(y)\right)\, g_1\wedge g_2\wedge g_3\wedge g_4\wedge g_5\,, \\ B_2 &= h_1(y)g_1\wedge g_2 + h_3(y)g_3\wedge g_4, \\ F_3 &= \frac{1}{9}P\; g_5\wedge g_3\wedge g_4 + h_2(y)\;\; (g_1\wedge g_2 - g_3\wedge g_4)\wedge g_5 \\ &\quad + (g_1\wedge g_3 + g_2\wedge g_4)\wedge d\left(h_2(y)\right)\,, \\ \Phi &= \Phi(y), \end{aligned} \tag{2.5}$$

Parameter P must be appropriately quantized [4, 12]:

$$\frac{1}{4\pi^2\alpha'}\int_{3-\text{cycle: }\theta_2=\phi_2=0} F_3 \quad = \quad \frac{2P}{9\alpha'} \in \mathbb{Z}\,, \tag{2.6}$$

thus

$$P = \frac{9}{2}M\alpha'\,, \tag{2.7}$$

corresponding to the number M of fractional branes (the difference of ranks of the cascading gauge theory gauge group factors) on the conifold. Finally, G_5 is the five dimensional effective gravitational constant

$$G_5 \equiv \frac{G_{10}}{\text{vol}_{T^{1,1}}} = \frac{27}{16\pi^3}\,G_{10}\,, \tag{2.8}$$

where $16\pi G_{10} = (2\pi)^7(\alpha')^4$ is 10-dimensional gravitational constant of type IIB supergravity.

[12] In the limit of vanishing 3-form fluxes, $\Omega_0 = \frac{L^4}{108}$, where L is the asymptotic AdS_5 radius.

JHEP05(2020)035

Chirally symmetric states of the cascading gauge theory correspond to enhancement of the global symmetry[13] $\mathrm{SU}(2)\times\mathrm{SU}(2)\times\mathbb{Z}_2\to\mathrm{SU}(2)\times\mathrm{SU}(2)\times\mathrm{U}(1)$, and are described by the gravitational configurations of (2.1) subject to constraints[14]

$$h_1=h_3\,,\qquad h_2=\frac{P}{18}\,,\qquad \Omega_2=\Omega_3\,, \tag{2.9}$$

or in the boundary QFT language [13],

$$\mathcal{O}_3^\alpha=0\,,\qquad \mathcal{O}_7=0\,. \tag{2.10}$$

We find it convenient to introduce

$$\begin{aligned} &h_1=\frac{1}{P}\left(\frac{K_1}{12}-36\Omega_0\right)\,,\quad h_2=\frac{P}{18}\,K_2\,,\qquad\quad h_3=\frac{1}{P}\left(\frac{K_3}{12}-36\Omega_0\right)\,,\\ &\Omega_1=\frac{1}{3}f_c^{1/2}h^{1/4}\,,\qquad\quad \Omega_2=\frac{1}{\sqrt{6}}f_a^{1/2}h^{1/4}\,,\quad \Omega_3=\frac{1}{\sqrt{6}}f_b^{1/2}h^{1/4}\,. \end{aligned} \tag{2.11}$$

The ultimate goal is to compute the entanglement entropy of the cascading gauge theory — using the dual holographic picture with the effective gravitational action (2.1) — in distinct vacua (see (1.22)) in four dimensional de Sitter space-time. As explained in the introduction, this is done in two steps:

- constructing de Sitter vacua in Fefferman-Graham coordinate frame

$$\begin{aligned} ds_{10}^2=&\frac{1}{h^{1/2}\rho^2}\left(-d\tau^2+e^{2H\tau}d\boldsymbol{x}^2\right)+\frac{h^{1/2}}{\rho^2}\,(d\rho)^2\\ &+\frac{f_ch^{1/2}}{9}g_5^2+\frac{f_ah^{1/2}}{6}(g_3^2+g_4^2)+\frac{f_bh^{1/2}}{6}(g_1^2+g_2^2)\,,\\ h=&h(\rho)\,,\qquad f_{a,b,c}=f_{a,b,c}(\rho)\,, \end{aligned} \tag{2.12}$$

subject to appropriate topological/symmetry restrictions (1.22);

- using diffeomorphism transformation to represent the FG frame vacua in Eddington-Finkelstein coordinate frame

$$\begin{aligned} &ds_{10}^2=2dt\ (dr-a\ dt)+\sigma^2e^{2Ht}\ d\boldsymbol{x}^2+\frac{1}{9}w_{c2}\ g_5^2+\frac{1}{6}\omega_{a2}\ (g_3^2+g_4^2)+\frac{1}{6}\omega_{b2}\ (g_1^2+g_2^2)\,,\\ &a=a(r)\,,\qquad \sigma=\sigma(r)\,,\qquad \omega_{a2,b2,c2}=\omega_{a2,b2,c2}(r)\,. \end{aligned} \tag{2.13}$$

It is important to keep in mind that EF frame vacua (2.13) are the late-time limits of the evolution in EF frame:

$$\begin{aligned} &ds_{10}^2=2dt\ (dr-A\ dt)+\Sigma^2\ d\boldsymbol{x}^2+\Omega_1^2\ g_5^2+\Omega_2^2\ (g_3^2+g_4^2)+\Omega_3^2\ (g_1^2+g_2^2)\,,\\ &A=A(t,r)\,,\qquad \Sigma=\Sigma(t,r)\,,\qquad \Omega_{1,2,3}=\Omega_{1,2,3}(t,r)\,. \end{aligned} \tag{2.14}$$

We now summarize technical details delegated to various appendices.

[13] In the planar limit.

[14] This is a consistent truncation of the cascading gauge theory to U(1) symmetric sector constructed in [15].

JHEP05(2020)035

- In appendix A we derive the equations of motion in the holographic bulk for the evolution of generic spatially homogeneous and isotropic state of the cascading gauge theory in de Sitter space-time, see (A.3)–(A.13). We explain how to take the late time limit $t \to \infty$ in (2.14) to obtain (2.13). The EF frame vacuum equations of motion are given by (A.16)–(A.26). The latter equations of motion have symmetries SEF1-SEF4 (A.27)–(A.30), which are used to set up and validate numerics (see appendix C).

- We begin appendix B presenting gravitational bulk equations of motion in FG frame (B.3)–(B.11). These equations of motion have (corresponding to SEF1-SEF4) symmetries SFG1-SFG4 (A.27)–(A.30), which are used to set up and validate numerics (see appendix C). In appendix B.1 we explain the near boundary (UV) $\rho \to 0$ and the interior (IR) $\rho \to \infty$ asymptotics. UV asymptotics are used to classify non-normalizable coefficients (defining parameters of the cascading gauge theory): the asymptotic string coupling g_s (1.4) and the strong coupling scale Λ of the theory (1.19), and the normalizable coefficients: the expectation values of boundary gauge theory operators:[15] $\{T_{ij}, \mathcal{O}_3^{\alpha=\{1,2\}}, \mathcal{O}_4^{\beta=\{1,2\}}, \mathcal{O}_6, \mathcal{O}_7, \mathcal{O}_8\}$. IR asymptotics are used to classify the distinct de Sitter vacua of the theory (1.22), as well to ensure that the bulk geometry is smooth as the corresponding cycles shrinks to zero size (S^4 for TypeA$_s$ and TypeA$_b$, and S^2 for TypeB vacua).

- TypeA$_s$ vacua enjoy unbroken chiral symmetry; appendix B.1.1 presents the UV and IR asymptotics in FG frame obtained in [31] and translates the coefficients governing the expansion to those used for the characterization of TypeA$_b$ vacua, see (B.47)–(B.51).

- Appendix B.2 establishes the map between EF and FG frame description for each type of the vacua: TypeA$_s$, TypeA$_b$ and TypeB.

- In the limit $H \to 0$, TypeB vacuum in FG frame represents the extremal KS solution [2]. We use this limit in appendix B.3 to related the strong coupling scale Λ of the cascading gauge theory to the complex structure conifold deformation parameter ϵ used in [2], see (B.80).

- Appendix C covers numerical procedures for construction of FG frame dual backgrounds (see C.1) and EF frame dual backgrounds (see C.2). We introduce three different computational schemes — SchemeI, SchemeII and SchemeIII (C.6) — explain how they are related and outline their computational advantages in accessing different regions of the parameter space of the model. We introduce the AH location function $\mathcal{L}_{AH}$ (C.8), used to identify the apparent horizon.

- Appendix D presents technical details for construction of TypeA$_s$ de Sitter vacua in computational scheme SchemeII in the conformal limit, i.e., $b \to 0$.

[15] Developing the precise holographic dictionary between these normalizable coefficients and the corresponding expectation values, while interesting, is not important for the results presented, and thus is outside the scope of the paper.

JHEP05(2020)035

- Appendix E collects the expression for the Kretschmann scalar (E.1) of the background geometry (2.13). It is used to test the validity of the supergravity approximation.

- Appendix F contains equations of motion and the asymptotic expansions for the chiral symmetry breaking perturbations about FG frame TypeA$_s$ de Sitter vacua with explicit symmetry breaking parameter — the gaugino mass term. These perturbations are used to identify TypeA$_b$ vacua "close" to TypeA$_s$ vacua.

3 Apparent horizon in de Sitter evolution of the cascading gauge theory

Apparent horizon[16] in holographic dual is crucial for identifying the attractor vacuum for the evolution of generic homogeneous and isotropic states of the cascading gauge theory in de Sitter: given competing trajectories for the evolution, dynamics proceeds along trajectory resulting in the maximum entropy at late times. We identify AH directly in ten-dimensional EF frame gravitational dual in section 3.1. We reproduce the same result in EF gravitational dual of the effective five-dimensional description in section 3.2. Both in ten-dimensions and upon Kaluza-Klein reduction to five dimensions the area of the AH stays the same. In section 3.3 we use equations of motion (A.3)–(A.13) to prove that the area of the AH is nondecreasing upon evolution. We identify the (dynamical) area density of the AH $\mathcal{A}_{10}(t)$ with the dynamical entropy density s of the boundary gauge theory as

$$a^3 s = e^{3Ht} s(t) = \frac{\mathcal{A}_{10}}{4G_{10}} = \frac{4\pi}{(2\pi)^7(\alpha')^4}\, \mathcal{A}_{10}(t)\,, \tag{3.1}$$

where $a = e^{Ht}$ is the boundary spatial metric scale factor, see (1.17). The entanglement entropy $s_{\rm ent}$ is related to the late-time limit of s as

$$\begin{aligned} \lim_{t\to\infty} \frac{1}{H^3 a^3}\frac{d}{dt}\left(a^3 s\right) &\equiv 3H \times \mathcal{R}\,, \\ \lim_{t\to\infty} s(t) \equiv s_{\rm ent} &= H^3 \mathcal{R}\,, \end{aligned} \tag{3.2}$$

where $\mathcal{R}$ is the comoving entropy production rate in de Sitter vacuum first introduced in [19]. Finally, in section 3.4 we show that

$$\mathcal{R}\Big|_{\rm TypeB} = 0 \qquad \Longrightarrow \qquad s_{\rm ent}\Big|_{\rm TypeB} = 0\,. \tag{3.3}$$

3.1 AH in ten dimensions

The apparent horizon of the bulk gravitational dual to the cascading gauge theory dynamics in de Sitter is located at the radius $r = r_{AH}$ where the expansion θ of a congruence of outward pointing null vectors vanishes (i.e., it stops expanding outwards). Working in

[16] In general AH is observer dependent. It is natural to define AH with respect to an observer reflecting the symmetries of the spatial slices — homogeneity and isotropy in $\boldsymbol{x}$ in (2.14), see [25]. Such an identification correctly reproduces the hydrodynamic limit [32] and can be proven to comply with the second law of thermodynamics [19, 24], thus serving as a useful definition of the dynamical (nonequilibrium) entropy.

JHEP05(2020)035

the coordinates of equation (2.14), we characterize such a congruence with the null vector $k = \partial_t + A\partial_r$. The null vector k points toward the boundary of the space-time outside of the initial black hole, and points inward inside the initial horizon.

Following [33], the expansion of a congruence of affine parameterized null vectors n is given by

$$\theta = \nabla_\alpha n^\alpha . \tag{3.4}$$

However, it turns out that $k^\beta \nabla_\beta k^\alpha = \partial_r A\, k^\alpha$, i.e., k is not affine. To remedy this, we rescale k by $\exp\{\int \partial_r A\, d\lambda\}$, where λ is the parameter along which the congruence k evolves. This ensures that the rescaled null vector satisfies the geodesic equation with λ as an affine parameter. Reference [33] then gives the expansion of k to be

$$\theta = \exp\left[\int \partial_r A\, d\lambda\right] (\nabla_\alpha k^\alpha - \partial_r A) . \tag{3.5}$$

Substituting in for $\nabla_\alpha k^\alpha$ computed in the metric (2.14)

$$\nabla_\alpha k^\alpha = \frac{1}{\sqrt{-g}} \partial_\alpha \left(\sqrt{-g} k^\alpha\right) = \partial_t \ln\left(\Sigma^3 \Omega_1 \Omega_2^2 \Omega_3^2\right) + A\ \partial_r \ln\left(\Sigma^3 \Omega_1 \Omega_2^2 \Omega_3^2\right) + \partial_r A . \tag{3.6}$$

We see that $\theta = 0$, when

$$\partial_t \left(\Sigma^3 \Omega_1 \Omega_2^2 \Omega_3^2\right) + A\ \partial_r \left(\Sigma^3 \Omega_1 \Omega_2^2 \Omega_3^2\right) \Big|_{r=r_{AH}} = 0 . \tag{3.7}$$

Eq. (3.7) determines the location of the AH, i.e., $r_{AH} = r_{AH}(t)$. The area density of the AH $\mathcal{A}_{10}$ is

$$\mathcal{A}_{10} = \Sigma^3 \Omega_1 \Omega_2^2 \Omega_3^2 \Big|_{r=r_{AH}} \int g_5 \wedge g_3 \wedge g_4 \wedge g_1 \wedge g_2 = 64\pi^3 \Sigma^3 \Omega_1 \Omega_2^2 \Omega_3^2 \Big|_{r=r_{AH}} , \tag{3.8}$$

leading to (see (3.1))

$$e^{3Ht} s = \frac{64\pi^3}{4G_{10}}\ \Sigma^3 \Omega_1 \Omega_2^2 \Omega_3^2 \Big|_{r=r_{AH}} = \frac{1}{4G_5}\ 108 \Sigma^3 \Omega_1 \Omega_2^2 \Omega_3^2 \Big|_{r=r_{AH}} . \tag{3.9}$$

3.2 AH in Kaluza-Klein reduction to five dimensions

We would like to reproduce (3.7) and (3.9) from the five-dimensional perspective.

While the effective action (2.1) is five dimensional, the metric frame used is not Einstein:

$$S_5 = \frac{108}{16\pi G_5} \int_{\mathcal{M}_5} \mathrm{vol}_{\mathcal{M}_5}\ \Omega_1 \Omega_2^2 \Omega_3^2 \times \left\{R_5 + \cdots\right\} . \tag{3.10}$$

This can be fixed with a simple conformal rescaling: introducing

$$d\tilde{s}_5^2 \equiv \tilde{g}_{\mu\nu} dy^\mu dy^\nu = \Omega^{10/3}\ ds_5^2 = \Omega^{10/3}\ g_{\mu\nu} dy^\mu dy^\nu , \qquad \Omega^5 = \Omega_1 \Omega_2^2 \Omega_3^2 , \tag{3.11}$$

and defining

$$\tilde{G}_5 = \frac{G_5}{108} , \tag{3.12}$$

JHEP05(2020)035

the effective action S_5 in (3.10) has now a standard Einstein-Hilbert term with respect to $\tilde{g}$

$$S_5 = \frac{1}{16\pi\tilde{G}_5}\int_{\mathcal{M}_5} \widetilde{\text{vol}}_{\mathcal{M}_5} \times \left\{\tilde{R}_5 + \cdots\right\}. \tag{3.13}$$

The new EF frame (compare with (2.14)) becomes

$$\begin{aligned} d\tilde{s}_5^2 &= \Omega^{10/3}\left[2dt\ (dr - A\ dt) + \Sigma^2\ d\boldsymbol{x}^2\right] = 2dtd\hat{r} - 2A\Omega^{10/3}\ dt^2 + \Omega^{10/3}\Sigma^2\ d\boldsymbol{x}^2\,, \\ d\hat{r} &= \Omega^{10/3}\ dr\,, \end{aligned} \tag{3.14}$$

where the second equality defines a new radial coordinate $\hat{r}$. The congruence of null geodesics is now characterized with

$$\tilde{k} = \partial_t + A\Omega^{10/3}\ \partial_{\hat{r}}\,, \tag{3.15}$$

so that

$$\tilde{k}^\beta\tilde{\nabla}_\beta\tilde{k}^\alpha = \partial_{\hat{r}}\left(A\Omega^{10/3}\right)\ \tilde{k}^\alpha\,. \tag{3.16}$$

Since

$$\sqrt{-\tilde{g}} = \Omega^5\Sigma^3\,, \tag{3.17}$$

we have

$$\tilde{\nabla}_\alpha\tilde{k}^\alpha = \partial_t \ln\left(\Omega^5\Sigma^3\right) + A\Omega^{10/3}\ \partial_{\hat{r}}\ln\left(\Omega^5\Sigma^3\right) + \partial_{\hat{r}}\left(A\Omega^{10/3}\right)\,. \tag{3.18}$$

For the expansion $\tilde{\theta}$ of the congruence of affine parameterized null vectors we have (compare with (3.5))

$$\begin{aligned} \tilde{\theta}\ &\propto\ \left(\tilde{\nabla}_\alpha\tilde{k}^\alpha - \partial_{\hat{r}}\left(A\Omega^{10/3}\right)\right) = \partial_t\ln\left(\Omega^5\Sigma^3\right) + A\Omega^{10/3}\ \partial_{\hat{r}}\ln\left(\Omega^5\Sigma^3\right) \\ &= \partial_t\ln\left(\Omega^5\Sigma^3\right) + A\ \partial_r\ln\left(\Omega^5\Sigma^3\right) = \partial_t\ln\left(\Sigma^3\Omega_1\Omega_2^2\Omega_3^2\right) + A\ \partial_r\ln\left(\Sigma^3\Omega_1\Omega_2^2\Omega_3^2\right)\,, \end{aligned} \tag{3.19}$$

where in the second line we used the definition of $\hat{r}$ (3.14) and Ω (3.11). Note that $\tilde{\theta} = 0$ in (3.19) is equivalent to $\theta = 0$ reproducing (3.7).

The five dimensional area density $\mathcal{A}_5$ of the AH in (3.14) is given by

$$\mathcal{A}_5 = \left(\Omega^{5/3}\Sigma\right)^3\Big|_{r=r_{AH}} = \Sigma^3\Omega_1\Omega_2^2\Omega_3^2\Big|_{r=r_{AH}}\,, \tag{3.20}$$

leading to the dynamical entropy density

$$e^{3Ht}s = \frac{\mathcal{A}_5}{4\tilde{G}_5} = \frac{1}{4G_5}\ 108\Sigma^3\Omega_1\Omega_2^2\Omega_3^2\Big|_{r=r_{AH}}\,, \tag{3.21}$$

reproducing (3.9).

JHEP05(2020)035

3.3 Area theorem for the AH

Following [19] and using the equations of motion (A.3)–(A.13) we prove now that the dynamical entropy density s defined as in (3.21) grows with time t, i.e.,

$$\frac{d\mathcal{A}_5}{dt} = \frac{d}{dt}\left(\Sigma^3\Omega_1\Omega_2^2\Omega_3^2\Big|_{r=r_{AH}}\right) \geq 0\,. \tag{3.22}$$

Note that the AH location is determined from (see (3.19))

$$0 = d_+(\Sigma^3\Omega_1\Omega_2^2\Omega_3^2)\Big|_{r=r_{AH}} \equiv \partial_t(\Sigma^3\Omega_1\Omega_2^2\Omega_3^2) + A\ \partial_r(\Sigma^3\Omega_1\Omega_2^2\Omega_3^2)\Big|_{r=r_{AH}}\,. \tag{3.23}$$

Taking $\frac{d}{dt}$ we have

$$\begin{aligned} 0 &= \frac{d}{dt}\left(\partial_t(\Sigma^3\Omega_1\Omega_2^2\Omega_3^2) + A\ \partial_r(\Sigma^3\Omega_1\Omega_2^2\Omega_3^2)\right) \\ &= \left\{\partial_t + \frac{dr_{AH}}{dt}\times\partial_r\right\}\left(\partial_t(\Sigma^3\Omega_1\Omega_2^2\Omega_3^2) + A\ \partial_r(\Sigma^3\Omega_1\Omega_2^2\Omega_3^2)\right)\Big|_{r=r_{AH}}\,, \end{aligned} \tag{3.24}$$

which is used to algebraically solve for $\frac{dr_{AH}}{dt}\Big|_{r=r_{AH}}$. The latter expression is then substituted in

$$\frac{d\mathcal{A}_5}{dt} = \left\{\partial_t + \frac{dr_{AH}}{dt}\times\partial_r\right\}\Sigma^3\Omega_1\Omega_2^2\Omega_3^2\Big|_{r=r_{AH}}\,. \tag{3.25}$$

We use equations of motion (A.3)–(A.13) to eliminate all second order derivative in (3.25); we further eliminate $\partial_t\Sigma$ using (3.23) to arrive at

$$\frac{dA_5}{dt} = \frac{\partial_r(\Sigma^3\Omega_1\Omega_2^2\Omega_3^2)}{\partial_r(d_+(\Sigma^3\Omega_1\Omega_2^2\Omega_3^2))}\times\mathcal{F}^2\Big|_{r=r_{AH}}\,, \tag{3.26}$$

where $\mathcal{F}^2$ is manifestly positive

$$\begin{aligned} \mathcal{F}^2 = \frac{\Sigma^3}{2592\Omega_2^2\Omega_3^2\Omega_1 g^2P^2}\times\Bigg(&\Omega_1^2\Big(8(d_+K_2)^2\Omega_2^2\Omega_3^2g^3P^4 + 1296(d_+g)^2\Omega_2^4\Omega_3^4P^2 \\ &+ 9(d_+K_3)^2\Omega_3^4g + 9(d_+K_1)^2\Omega_2^4g\Big) + 1728\Omega_1^2\Omega_2^4\Omega_3^4g^2P^2\Bigg(\left(\frac{2d_+\Omega_2}{\Omega_2} + \frac{d_+\Omega_3}{\Omega_3}\right)^2 \\ &+ \left(\frac{d_+\Omega_1}{\Omega_1} + \frac{d_+\Omega_2}{\Omega_2}\right)^2 + \left(\frac{d_+\Omega_1}{\Omega_1} + \frac{d_+\Omega_3}{\Omega_3}\right)^2 + \frac{3(d_+\Omega_3)^2}{\Omega_3^2}\Bigg)\Bigg)\,. \end{aligned} \tag{3.27}$$

Constraint (A.12) can be integrated (once) to obtain

$$\begin{aligned} \partial_r\left(\Sigma^3\Omega_1\Omega_2^2\Omega_3^2\right) &= \Sigma^3\Omega_1\Omega_2^2\Omega_3^2\int_r^\infty dr\ \mathcal{M}^2 \\ \mathcal{M}^2 &= \frac{2(\partial_r\Omega_2)^2}{\Omega_2^2} + \frac{2(\partial_r\Omega_3)^2}{\Omega_3^2} + \frac{(\partial_r\Omega_1)^2}{\Omega_1^2} + \frac{3(\partial_r\Sigma)^2}{\Sigma^2} + \frac{(\partial_r g)^2}{2g^2} + \frac{gP^2(\partial_r K_2)^2}{324\Omega_3^2\Omega_2^2} \\ &\quad + \frac{(\partial_r K_3)^2}{288gP^2\Omega_2^4} + \frac{(\partial_r K_1)^2}{288gP^2\Omega_3^4}\,, \end{aligned} \tag{3.28}$$

JHEP05(2020)035

which implies that

$$\partial_r \left(\Sigma^3 \Omega_1 \Omega_2^2 \Omega_3^2\right) \geq 0\,, \tag{3.29}$$

provided the integral in (3.28) is convergent and $\Sigma^3 \Omega_1 \Omega_2^2 \Omega_3^2 \geq 0$.

Note that (see appendix B.2)

$$\begin{aligned}
&\lim_{r\to\infty}\; d_+\left(\Sigma^3 \Omega_1 \Omega_2^2 \Omega_3^2\right) = \lim_{r\to\infty}\; A\partial_r \left(\Sigma^3 \Omega_1 \Omega_2^2 \Omega_3^2\right) \\
&= \lim_{\rho\to 0}\; \underbrace{\frac{1}{2h^{1/2}\rho^2}}_{A} \times \underbrace{(-\rho^2)\partial_\rho}_{\partial_r} \left(\underbrace{h^{-3/4}\rho^{-3}\exp(3H\int_0^\rho h^{1/2}(s)ds)}_{\Sigma^3} \times \underbrace{\frac{h^{5/4} f_c^{1/2} f_a f_b}{108}}_{\Omega_1\Omega_2^2\Omega_3^2} \right) \\
&= \lim_{\rho\to 0}\left(\frac{1}{72\rho^4} + \text{subleading}\right) \to +\infty\,,
\end{aligned} \tag{3.30}$$

where we transformed first to FG frame and used the boundary asymptotic expansions (B.17)–(B.20). Thus,

$$d_+\left(\Sigma^3 \Omega_1 \Omega_2^2 \Omega_3^2\right) > 0\,, \qquad r > r_{AH} \qquad \Longrightarrow \qquad \partial_r \left(d_+\left(\Sigma^3 \Omega_1 \Omega_2^2 \Omega_3^2\right)\right)\Big|_{r=r_{AH}} \geq 0\,, \tag{3.31}$$

since the quantity $d_+\left(\Sigma^3 \Omega_1 \Omega_2^2 \Omega_3^2\right)$ changes sign at $r = r_{AH}$, see (3.23). Combining (3.26), (3.29) and (3.31) we arrive at (3.22).

For future reference we present the expressions for the location of the AH and the entanglement entropy density in de Sitter vacua. Using (A.14) and (A.15) we find from (3.23) and (3.9)

$$\begin{aligned}
&\text{AH location}: \qquad \left(3H\ \sigma^3 \omega_{c2}^{1/2} \omega_{a2}\omega_{b2} + a\frac{d}{dr}\left\{\sigma^3 \omega_{c2}^{1/2} \omega_{a2}\omega_{b2}\right\}\right)\Big|_{r=r_{AH}} = 0\,; \\
&\text{vacum entanglement entropy}: \qquad s_{\rm ent} = \frac{1}{4G_5}\ \sigma^3 \omega_{c2}^{1/2} \omega_{a2}\omega_{b2}\Big|_{r=r_{AH}}\,.
\end{aligned} \tag{3.32}$$

3.4 Entanglement entropy of TypeB de Sitter vacua

We demonstrate here that entanglement entropy of TypeB de Sitter vacuum vanishes — this implies that the corresponding comoving entropy production rate vanishes. de Sitter comoving entropy production rate vanishes in conformal field theories as well [20]. In CFTs the reason is simple: de Sitter vacuum is a conformal transformation of a thermal equilibrium state and entropy production is invariant under conformal transformations [19]. We do not understand the physical reason why the same is true for a de Sitter vacuum in nonconformal gauge theory (TypeB vacuum in the cascading gauge theory).

JHEP05(2020)035

Using the asymptotic expansion (B.67) (recall that $z=-r$ (B.56)) we find for (3.32)

$$\text{AH location}: \quad \frac{3^{3/2}}{2}(h_0^h)^{3/4}(f_{a,0}^h)^{3/2}(s_0^h)^3\ r\left(1+3H(h_0^h)^{1/2}r+\mathcal{O}(r^2)\right)\Big|_{r=r_{AH}}=0$$
$$\Longrightarrow \qquad r_{AH}=0\,;$$
$$\text{vacum entanglement entropy}: \ s_{\rm ent}=\frac{1}{4G_5}\ \frac{3^{3/2}}{2}(h_0^h)^{5/4}(f_{a,0}^h)^{3/2}(s_0^h)^3\ r^2+\mathcal{O}(r^3)\Big|_{r=r_{AH}}$$
$$\Longrightarrow \qquad s_{\rm ent}\Big|_{\rm TypeB}=0\,. \tag{3.33}$$

The result (3.33) stands as long as vacua TypeB exist — we find in section 6.2 that this is true provided $H\lesssim H^B_{\rm max}$, see (1.33).

4 TypeA$_s$ de Sitter vacua

TypeA$_s$ vacua in FG frame were discussed in details in [31]. As emphasized in [19] and [20] this is not enough to access vacuum entanglement entropy — one needs the holographic construction in EF frame. In section 4.1 we present numerical results for TypeA$_s$ vacua for generic values of $\frac{H^2}{\Lambda^2}$, in particular the results for the entanglement entropy, see figure 6. We discuss TypeA$_s$ in the conformal limit $\Lambda\ll H$ in section 4.2. In section 4.3 we estimate $H^s_{\rm min}$ (see (1.25)) below which TypeA$_s$ vacua construction in type IIB supergravity becomes unreliable. We identify the source of breaking of the supergravity approximation.

4.1 Numerical results: TypeA$_s$

To begin, we numerically construct TypeA$_s$ de Sitter vacua in FG frame (2.12). This involves solving ODEs (B.3)–(B.11) in the chirally symmetric limit (B.38), subject to UV asymptotics (the radial coordinate $\rho\to 0$) (B.39)–(B.43) and IR asymptotics (the radial coordinate $\rho\to+\infty$) (B.45). There are 8 second order equations (B.3)–(B.10) and 1 first order equation (B.11). Imposing the chirally symmetric limit (B.38), this set of coupled ODEs is reduced to 5 second order equations for the three metric warp factors $f_2=f_c$, $f_3=f_a=f_b$ and h, the single 3-form flux function $K=K_1=K_3$ ($K_2=1$ in the chiral limit) and the string coupling g. The first order equation (B.11) involves (linearly) f_2' and can be used instead of one of the second order equations (namely, the one involving f_2''). Thus, altogether we have a coupled system of 4 second order ODEs (linear in $\{f_3'',h'',K'',g''\}$) and a single first order equation (linear in f_2'). As a result, a unique solution must be characterized by $9=2\times 4+1$ parameters; these are the UV/IR parameters

$$\begin{aligned}\text{UV}: &\quad \{f_{2,1,0}\,,\ g_{4,0}\,,\ f_{2,4,0}\,,\ f_{2,6,0}\,,\ f_{2,8,0}\}\,;\\ \text{IR}: &\quad \{f^h_{2,0}\,,\ f^h_{3,0}\,,\ K^h_0\,,\ g^h_0\}\,.\end{aligned} \tag{4.1}$$

The external parameters $\{P,K_0,H,g_s\}$ (the gauge group rank difference M of the cascading gauge theory (2.7), its strong coupling scale Λ (B.26), the Hubble constant (1.17), the renormalization group flow invariant sum of the gauge couplings (1.4)) labeling the vacuum are fixed with the choice of the computational scheme (C.6). Of cause, as emphasized in

JHEP05(2020)035

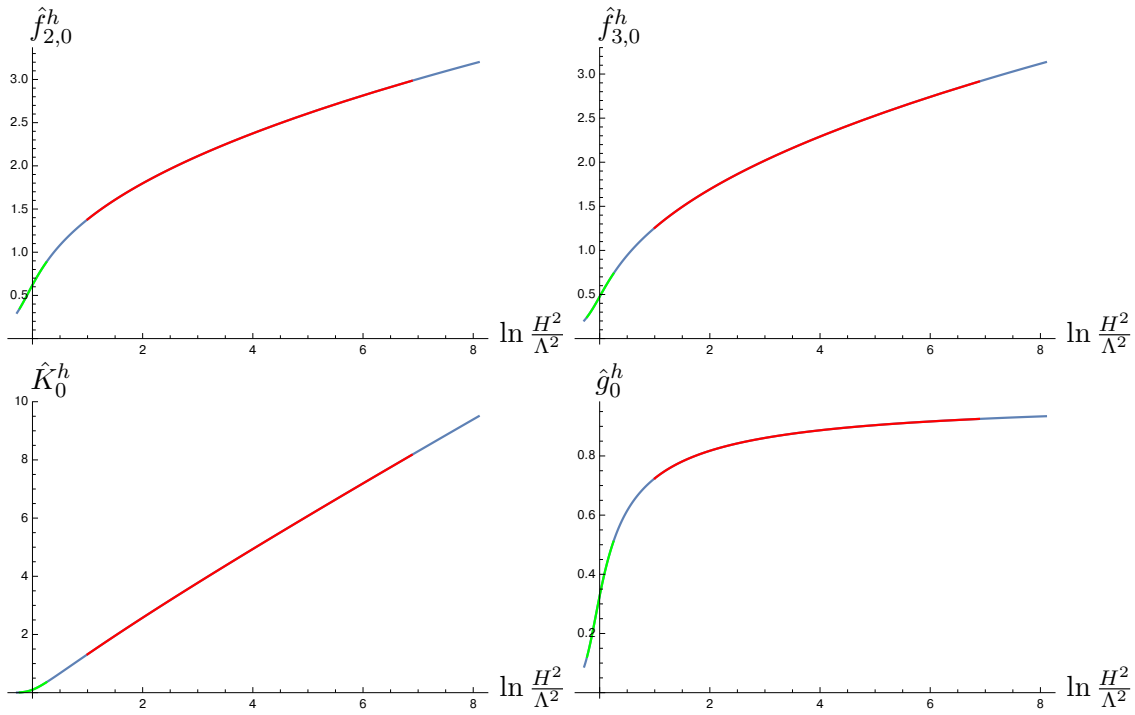

Figure 1. Infrared parameters $\{\hat{f}^h_{2,0}, \hat{f}^h_{3,0}, \hat{K}^h_0, \hat{g}^h_0\}$ of the Fefferman-Graham coordinate frame of TypeA$_s$ de Sitter vacua of the cascading gauge theory as functions of $\ln \frac{H^2}{\Lambda^2}$ in different computational schemes (C.6): SchemeI (blue), SchemeII (red) and Scheme III (green).

appendix C.1, the results must not depend on which computational scheme is adopted. We illustrate now that this is indeed the case using the IR parameters in (4.1) as an example.[17] Comparison of the different computational schemes is done using dimensionless and rescaled quantities: $\ln \frac{H^2}{\Lambda^2}$ (as a vacuum label) (C.2) and $\{\hat{f}^h_{2,3,0}\,,\, \hat{K}^h_0\,,\, \hat{g}^h_0\}$ (C.4). Explicitly:

$$\begin{aligned}
\text{SchemeI}: &\quad \ln\frac{H^2}{\Lambda^2} = k_s\,, && \hat{f}^h_{2,3,0} = f^h_{2,3,0}\,, && \hat{K}^h_0 = K^h_0\,, && \hat{g}^h_0 = g^h_0\,;\\
\text{SchemeII}: &\quad \ln\frac{H^2}{\Lambda^2} = \frac{1}{b} + \ln b\,, && \hat{f}^h_{2,3,0} = \frac{1}{b^{1/2}} f^h_{2,3,0}\,, && \hat{K}^h_0 = \frac{1}{b} K^h_0\,, && \hat{g}^h_0 = g^h_0\,;\\
\text{SchemeIII}: &\quad \ln\frac{H^2}{\Lambda^2} = \frac{1}{4} + \ln \alpha\,, && \hat{f}^h_{2,3,0} = \frac{1}{\alpha^{1/2}} f^h_{2,3,0}\,, && \hat{K}^h_0 = K^h_0\,, && \hat{g}^h_0 = g^h_0\,.
\end{aligned} \tag{4.2}$$

Following (4.2), we collect (subset of the) results of $\{\hat{f}^h_{2,0}, \hat{f}^h_{3,0}, \hat{K}^h_0, \hat{g}^h_0\}$ as functions of $\ln \frac{H^2}{\Lambda^2}$ in different computational schemes in figure 1: SchemeI (blue curves), SchemeII (red curves) and Scheme III (green curves). The accuracy of the collapsed results in different schemes is highlighted in figure 2 for $\hat{f}^h_{2,0}$ — the remaining parameters follow the same trend.

Next, FG frame TypeA$_s$ de Sitter vacua have to be reinterpreted in EF frame, see appendix B.2. The diffeomorphism transformation is performed at the radial location

$$\left\{\text{FG}: \quad \frac{1}{\rho} \equiv y = 0\right\} \quad \Longleftrightarrow \quad \left\{\text{EF}: \quad r \equiv -z = 0\right\}. \tag{4.3}$$

[17] The same is true for the UV parameters as well.

JHEP05(2020)035

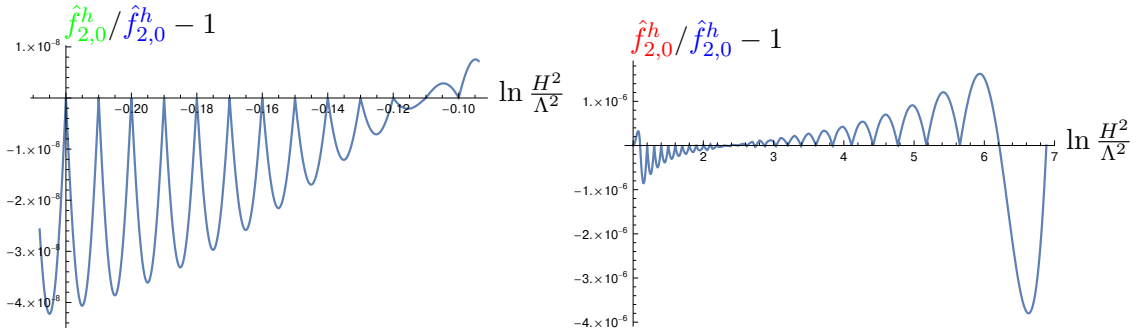

Figure 2. Left panel: comparison of $\hat{f}^h_{2,0}$ (the computational scheme SchemeIII) with $\hat{f}^h_{2,0}$ (the computational scheme SchemeI). Right panel: comparison of $\hat{f}^h_{2,0}$ (the computational scheme SchemeII) with $\hat{f}^h_{2,0}$ (the computational scheme SchemeI).

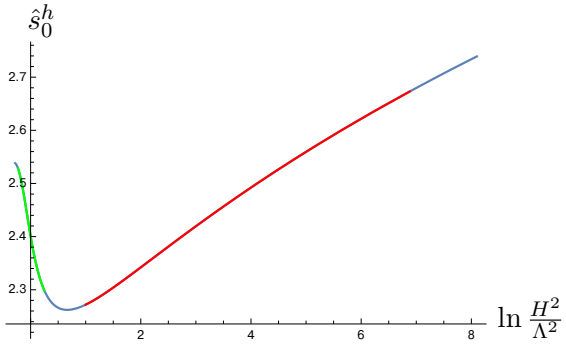

Figure 3. Parameters $\hat{s}^h_0$ of TypeA$_s$ de Sitter vacua of the cascading gauge theory as functions of $\ln \frac{H^2}{\Lambda^2}$ in different computational schemes (C.6): SchemeI (blue), SchemeII (red) and Scheme III (green).

Details of numerical construction of EF frame vacua from FG frame vacua are collected in appendix C.2. An important quantity is the parameter s^h_0, see (2.13),

$$s^h_0 = \sigma\Big|^{\text{FG frame}}_{y=0} = \sigma\Big|^{\text{EF frame}}_{z=0} \,. \tag{4.4}$$

As with FG frame UV/IR parameters (4.1), results for s^h_0 should not depend on the choice of the computational scheme, provided we compare properly dimensionless and rescaled quantities, i.e., $\ln \frac{H^2}{\Lambda^2}$ and $\hat{s}^h_0$ (C.15),

$$\begin{aligned}
\text{SchemeI}: &\quad \ln\frac{H^2}{\Lambda^2} = k_s\,, && \hat{s}^h_0 = s^h_0\,;\\
\text{SchemeII}: &\quad \ln\frac{H^2}{\Lambda^2} = \frac{1}{b} + \ln b\,, && \hat{s}^h_0 = \frac{1}{b^{1/4}} s^h_0\,;\\
\text{SchemeIII}: &\quad \ln\frac{H^2}{\Lambda^2} = \frac{1}{4} + \ln\alpha\,, && \hat{s}^h_0 = \frac{1}{\alpha^{1/2}} s^h_0\,.
\end{aligned} \tag{4.5}$$

Following (4.5), we collect (subset of the) results of $\hat{s}^h_0$ as functions of $\ln \frac{H^2}{\Lambda^2}$ in different computational schemes in figure 3: SchemeI (blue curve), SchemeII (red curve) and Scheme

JHEP05(2020)035

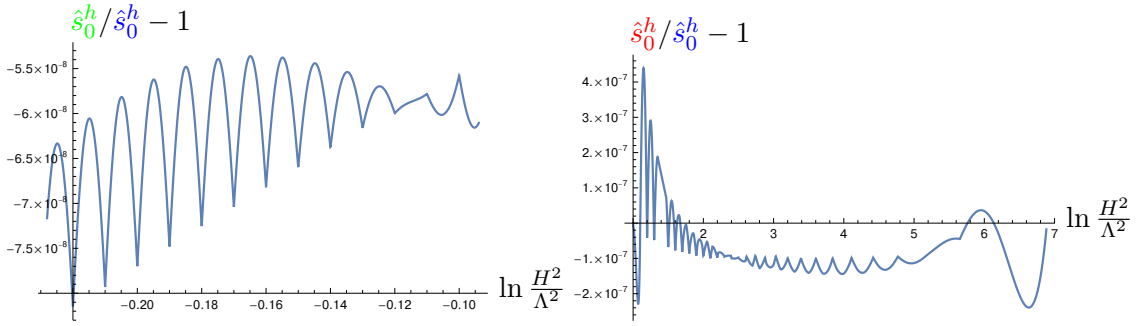

Figure 4. Left panel: comparison of $\hat{s}_0^h$ (the computational scheme SchemeIII) with $\hat{s}_0^h$ (the computational scheme SchemeI). Right panel: comparison of $\hat{s}_0^h$ (the computational scheme SchemeII) with $\hat{s}_0^h$ (the computational scheme SchemeI).

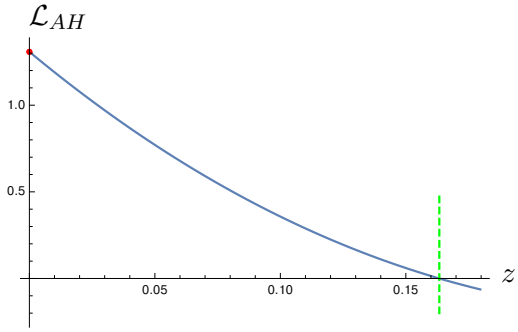

Figure 5. Apparent horizon location function $\mathcal{L}_{AH}(z)$ in computational scheme SchemeI at $k_s = 0$, i.e., at $H = \Lambda$, see (C.8). The red dot is $\mathcal{L}_{AH}(0)$, see (C.9). Notice that $\mathcal{L}'_{AH}(0) < 0$, see (C.10). The vertical green dashed line is the first zero of $\mathcal{L}_{AH}(z)$: $z_{AH} = 0.163346$.

III (green curve). The accuracy of the collapsed results in different schemes is highlighted in figure 4.

EF frame equations of motion (A.17)–(A.25) are solved subject to the initial conditions set by the asymptotic expansions (B.57) at $z = 0$. These equations have to be integrated on the interval

$$z \in [0, z_{AH}]\,, \tag{4.6}$$

where $z_{AH} = -r_{AH}$ is the location of the apparent horizon at asymptotically late times, see (3.32). To determine the location of the apparent horizon, along with integrating the gravitational background functions $\{a, \sigma, w_{c2}, w_{a2}, K_1, g\}$ (remember that $w_{b2} = w_{c2}$, $K_3 = K_1$ and $K_2 = 1$ when the chiral symmetry is unbroken), we evaluate the AH location function $\mathcal{L}_{AH}(z)$, see (C.8). AH is located at the first zero of this function for $z > 0$. A typical profile of the AH location function is shown in figure 5. Once the AH is identified, TypeA$_s$ vacua entanglement entropy is computed following (3.32):

$$s_{\rm ent} = \frac{H^3 P^4 g_s^2}{4G_5} \left\{\hat{\sigma}^3 \hat{w}_{c2}^{1/2} \hat{\omega}_{a2}^2\right\}\Big|_{\hat{z}=\hat{z}_{AH}} = \frac{3^5 M^4 g_s^2}{2^5 \pi^3}\, H^3 \left\{\hat{\sigma}^3 \hat{w}_{c2}^{1/2} \hat{\omega}_{a2}^2\right\}\Big|_{\hat{z}=\hat{z}_{AH}}, \tag{4.7}$$

where following (C.1) we introduced dimensionless and rescaled functions and the radial

JHEP05(2020)035

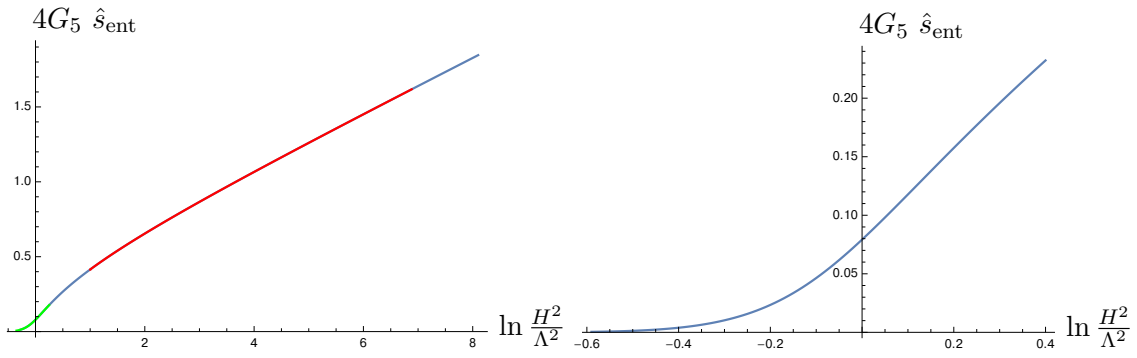

Figure 6. Left panel: entanglement entropy $\hat{s}_{\rm ent}$ (4.9) of TypeA$_s$ de Sitter vacua of the cascading gauge theory as functions of $\ln\frac{H^2}{\Lambda^2}$ in different computational schemes (C.6): SchemeI (blue), SchemeII (red) and Scheme III (green). Right panel: entanglement entropy $\hat{s}_{\rm ent}$ (4.9) for small values of $\frac{H^2}{\Lambda^2}$ — at the limit of validity of the supergravity approximation, see section 4.3.

coordinate:

$$\begin{aligned}
&\{z\,,\ a\,,\sigma\,,\ w_{c2}\,,\ w_{a2}\,,\ K_1\,,\ g\} \qquad \Longrightarrow \qquad \{\hat{z}\,,\ \hat{a}\,,\hat{\sigma}\,,\ \hat{\omega}_{c2}\,,\ \hat{\omega}_{a2}\,,\ \hat{K}_1\,,\ \hat{g}\}\,;\\
&\qquad z = HPg_s^{1/2}\ \hat{z}\,, \qquad a = H^2Pg_s^{1/2}\ \hat{a}\,, \qquad \sigma = HP^{1/2}g_s^{1/4}\ \hat{\sigma}\,,\\
&w_{c2,a2} = Pg_s^{1/2}\ \hat{\omega}_{c2,a2}\,, \qquad K_1 = P^2g_s\ \hat{K}_1\,, \qquad g = g_s\ \hat{g}\,.
\end{aligned} \tag{4.8}$$

In the last equality in (4.7) we used expressions for G_5 (2.8) and P (2.7). We compute entanglement entropy in different computational schemes; results must agree, provided we compare dimensionless and rescaled quantities,

$$s_{\rm ent} = H^3P^4g_s^2\ \hat{s}_{\rm ent}\,. \tag{4.9}$$

Explicitly,

$$\begin{aligned}
\text{SchemeI}: &\quad \ln\frac{H^2}{\Lambda^2} = k_s\,, &&\hat{s}_{\rm ent} = s_{\rm ent}\,;\\
\text{SchemeII}: &\quad \ln\frac{H^2}{\Lambda^2} = \frac{1}{b} + \ln b\,, &&\hat{s}_{\rm ent} = \frac{1}{b^2}s_{\rm ent}\,;\\
\text{SchemeIII}: &\quad \ln\frac{H^2}{\Lambda^2} = \frac{1}{4} + \ln\alpha\,, &&\hat{s}_{\rm ent} = \frac{1}{\alpha^{3/2}}s_{\rm ent}\,.
\end{aligned} \tag{4.10}$$

Following (4.10), we collect (subset of the) results of $(4G_5\ \hat{s}_{\rm ent})$ as functions of $\ln\frac{H^2}{\Lambda^2}$ in different computational schemes in figure 6: SchemeI (blue curves), SchemeII (red curves) and Scheme III (green curves). The accuracy of the collapsed results in different schemes is highlighted in figure 7.

4.2 TypeA$_s$ de Sitter vacua in the conformal limit

The cascading gauge theory is not conformal — it has a strong coupling scale Λ. Thermal states of the cascading gauge theory in Minkowski space-time at temperature $T \gg \Lambda$ enjoy conformal equation of state, $\mathcal{E} = 3\mathcal{P}$, up to $\mathcal{O}\left(\frac{1}{\ln(T/\Lambda)}\right)$ corrections, see [12]. On the gravity side the conformal limit is realized as $P \to 0$ (or Klebanov-Witten [3]) limit. We show here that exactly the same limit on the gravity side of TypeA$_s$ de Sitter vacua captures the

JHEP05(2020)035

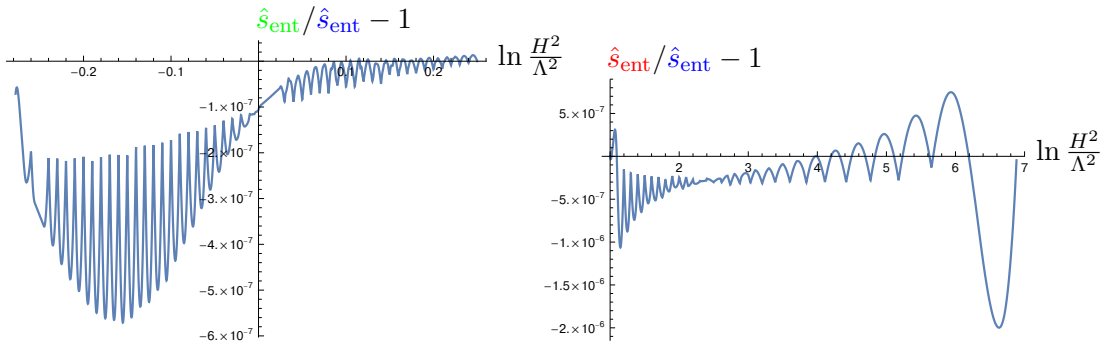

Figure 7. Left panel: comparison of $\hat{s}_{\rm ent}$ (the computational scheme SchemeIII) with $\hat{s}_{\rm ent}$ (the computational scheme SchemeI). Right panel: comparison of $\hat{s}_{\rm ent}$ (the computational scheme SchemeII) with $\hat{s}_{\rm ent}$ (the computational scheme SchemeI).

$H \gg \Lambda$ limit of the cascading gauge theory, resulting in de Sitter vacuum entanglement entropy density (1.24), vanishing, as appropriate, for the conformal gauge theory [19, 20].

To study the conformal limit it is convenient to use the computational scheme SchemeII (see (C.6)), i.e., we use the symmetry transformations SFG2-SFG4 of (B.13)–(B.15) to set $H = g_s = K_0 = 1$ and allow $b \equiv P^2$ to vary. The FG frame equations of motion (B.3)–(B.11) describing TypeA$_s$ vacua (see also (B.38)) can be solved perturbatively as a series expansion in b:

$$f_2 = (1+\rho)\,\left(1+\sum_{n=1}^{\infty} b^n\, f_{2n}(\rho)\right)\,, \qquad f_3 = (1+\rho)\,\left(1+\sum_{n=1}^{\infty} b^n\, f_{3n}(\rho)\right)\,, \tag{4.11}$$
$$h = \frac{1}{4(1+\rho)^2}\,\left(1+\sum_{n=1}^{\infty} b^n\, h_n(\rho)\right)\,, \quad K = 1+\sum_{n=1}^{\infty} b^n\, k_n(\rho)\,, \quad g = 1+\sum_{n=1}^{\infty} b^n\, g_n(\rho)\,.$$

Explicit equations for $\{f_{2n}, f_{3n}, h_n, k_n, g_n\}$ for $n = 1, 2$ along with the UV/IR asymptotics are presented in appendix D.1. Numerically solving these equations we find perturbative in b predictions for the UV/IR parameters (4.1). As explained in appendix C.2 we also need the FG frame parameter s_0^h, see (B.68). Given (4.11) we find from (C.15)

$$\begin{aligned} s_0^h &= \sqrt{2}\left(1+\frac{b}{4}\int_0^\infty ds\,\frac{h_1}{1+s}+\frac{b^2}{32}\int_0^\infty ds\,\frac{8(1+s)h_2-(1+2s)h_1^2}{(1+s)^2}+\mathcal{O}(b^3)\right) \\ &\equiv \sqrt{2}\left(1+s_{0;1}^h\, b+s_{0;2}^h\, b^2+\mathcal{O}(b^3)\right)\,. \end{aligned} \tag{4.12}$$

Using results of appendix 4.2 we evaluate the integrals in (4.12) to find

$$s_{0;1}^h = 0.828534\,, \qquad s_{0;2}^h = -0.284396\,. \tag{4.13}$$

Figures 8–9 present comparison of the results for the IR parameters $\{f_{2,0}^h\,,\ f_{3,0}^h\,,\ K_0^h\,,\ g_0^h\}$ and s_0^h in the computational SchemeII (blues curves), and independent perturbative $\mathcal{O}(b)$ (red curves) and $\mathcal{O}(b^2)$ (green curves) computations. The agreement is excellent.

JHEP05(2020)035

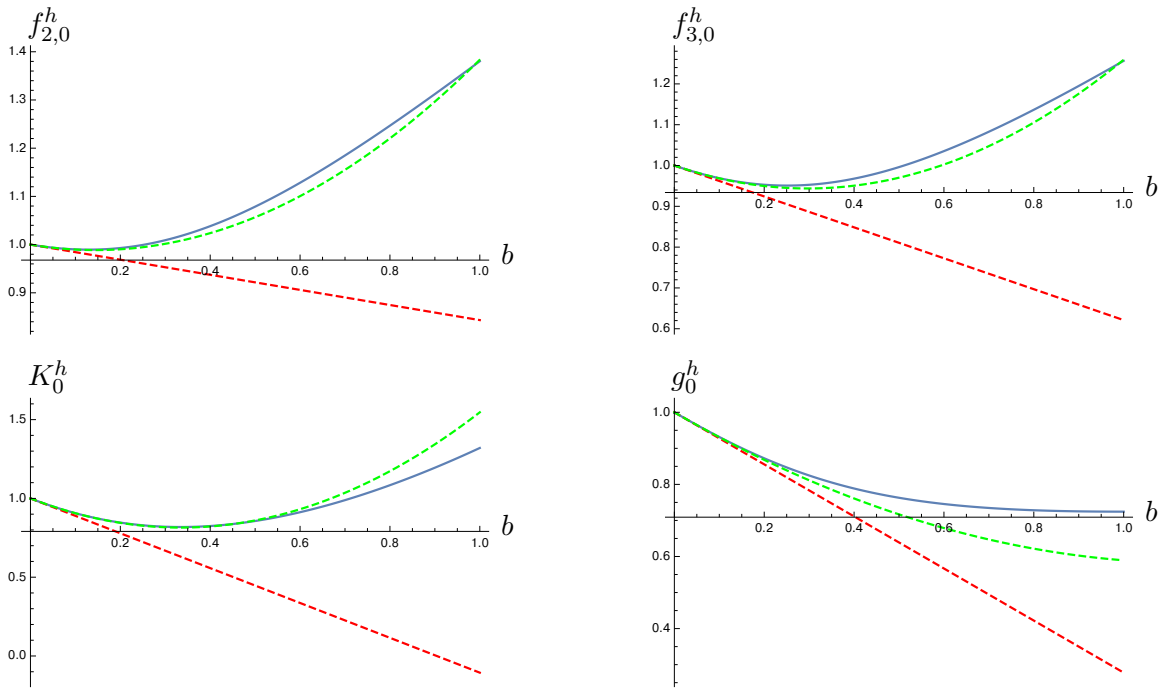

Figure 8. Infrared parameters $\{f^h_{2,0}, f^h_{3,0}, K^h_0, g^h_0\}$ in the conformal limit $b \to 0$. Blue curves: results in computational scheme SchemeII; red curves: perturbative approximation to order $\mathcal{O}(b)$; green curves: perturbative approximation to order $\mathcal{O}(b^2)$; see (D.11) with (D.17).

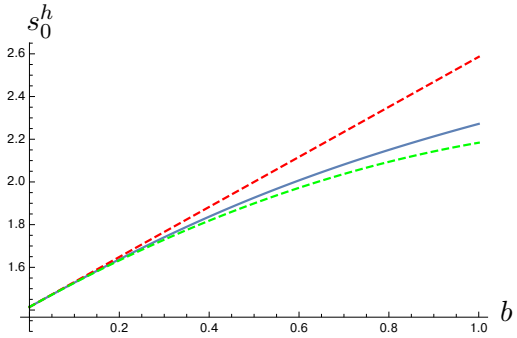

Figure 9. Infrared parameter s^h_0 in the conformal limit $b \to 0$. Blue curve: results in computational scheme SchemeII; red curve: perturbative approximation to order $\mathcal{O}(b)$; green curve: perturbative approximation to order $\mathcal{O}(b^2)$; see (4.12) with (4.13).

Following appendix B.2 we convert perturbative FG frame construction (4.11) to EF frame:

$$
\begin{aligned}
a &= -z(1-z)\left(1+\sum_{n=1}^{\infty} b^n\ a_n(z)\right), \qquad & \sigma &= \sqrt{2}(1-z)\left(1+\sum_{n=1}^{\infty} b^n\ s_n(z)\right), \\
w_{c2} &= \frac{1}{2}\left(1+\sum_{n=1}^{\infty} b^n\ w_{c2n}(z)\right), & w_{a2} &= \frac{1}{2}\left(1+\sum_{n=1}^{\infty} b^n\ w_{a2n}(z)\right), \\
K &= 1+\sum_{n=1}^{\infty} b^n\ k_n(z), & g &= 1+\sum_{n=1}^{\infty} b^n\ g_n(z).
\end{aligned}
\tag{4.14}
$$

JHEP05(2020)035

Explicit equations for $\{a_n, s_n, v_n \equiv w_{c2n} + 4w_{a2n}, w_{a2n}, k_n, g_n\}$ for $n = 1, 2$ along with the initial conditions are presented in appendix D.2. The equations for k_1 and g_1 ((D.18) and (D.23) correspondingly) can be solved analytically; in fact the solutions are just the FG $\to$ EF frame transformations of (D.13) and (D.15):

$$k_1 = \frac{z^2 - z + 1}{4z(z-1)} - \frac{1}{4} - 4\ln 2 + \frac{16z^3 - 24z^2 + 6z + 1}{4z^{3/2}(1-z)^{3/2}} \arctan\sqrt{\frac{z}{1-z}}\,, \tag{4.15}$$

$$g_1 = -\frac{13z^4 - 26z^3 + 29z^2 - 16z + 1}{32z^2(1-z)^2} + \frac{13}{32} - \frac{2z-1}{16z^{5/2}(1-z)^{5/2}} \arctan\sqrt{\frac{z}{1-z}} - \frac{12z^2 - 12z - 1}{32z^3(z-1)^3} \arctan^2\sqrt{\frac{z}{1-z}}\,. \tag{4.16}$$

We will show now that the location of the AH z_{AH}, as determined from the zero of the AH location function $\mathcal{L}_{AH}$ (C.8), is

$$1 - z_{AH} = \mathcal{O}\left(b^{1/4}\right)\,, \tag{4.17}$$

and can be determined analytically (in perturbative expansion in b) as it is controlled by the singularities of the EOMs (D.19)–(D.22) and (D.25)–(D.29) as $u \equiv 1 - z \to 0_+$, provided we use (4.15) and (4.16). From (4.15), (4.16):

$$k_1 = -\frac{\pi}{8}u^{-3/2} - \frac{15\pi}{16}u^{-1/2} + \mathcal{O}(u^{0/2})\,, \qquad g_1 = -\frac{\pi^2}{128}u^{-3} - \frac{15\pi^2}{128}u^{-2} + \mathcal{O}(u^{-3/2})\,, \tag{4.18}$$

leading to[18] (from direct asymptotic analysis of (D.19)–(D.22) and (D.25)–(D.29))

$$\begin{aligned} v_1 &= -\frac{3\pi^2}{256}u^{-3} + \frac{51\pi^2}{256}u^{-2} + \mathcal{O}(u^{-3/2})\,, & a_1 &= \frac{3\pi^2}{1024}u^{-3} - \frac{177\pi^2}{1024}u^{-2} + \mathcal{O}(u^{-3/2})\,, \\ s_1 &= \frac{\pi^2}{512}u^{-3} - \frac{33\pi^2}{256}u^{-2} + \mathcal{O}(u^{-3/2})\,, & w_{a21} &= -\frac{\pi^2}{256}u^{-3} + \frac{9\pi^2}{256}u^{-2} + \mathcal{O}(u^{-3/2})\,, \end{aligned} \tag{4.19}$$

$$\begin{aligned} k_2 &= \frac{35\pi^3}{49152}u^{-9/2} - \frac{2985\pi^3}{229376}u^{-7/2} + \mathcal{O}(u^{-6/2})\,, \\ g_2 &= \frac{23\pi^4}{393216}u^{-6} - \frac{571\pi^4}{573440}u^{-5} + \mathcal{O}(u^{-9/2})\,, \\ v_2 &= \frac{21\pi^4}{262144}u^{-6} - \frac{1097\pi^4}{327680}u^{-5} + \mathcal{O}(u^{-9/2})\,, \\ a_2 &= -\frac{13\pi^4}{1310720}u^{-6} + \frac{751\pi^4}{2621440}u^{-5} + \mathcal{O}(u^{-9/2})\,, \\ s_2 &= -\frac{53\pi^4}{7864320}u^{-6} + \frac{143\pi^4}{524288}u^{-5} + \mathcal{O}(u^{-9/2})\,, \\ w_{a22} &= \frac{17\pi^4}{786432}u^{-6} - \frac{2599\pi^4}{2293760}u^{-5} + \mathcal{O}(u^{-9/2})\,. \end{aligned} \tag{4.20}$$

In fact, from the general structure of the perturbative equations we expect

$$k_n = \mathcal{O}(u^{-3n+3/2})\,, \qquad \{a, s, v, w_{a2}, g\}_n = \mathcal{O}(u^{-3n})\,, \tag{4.21}$$

[18] Subleading terms depend on coefficients that have to be determined numerically.

JHEP05(2020)035

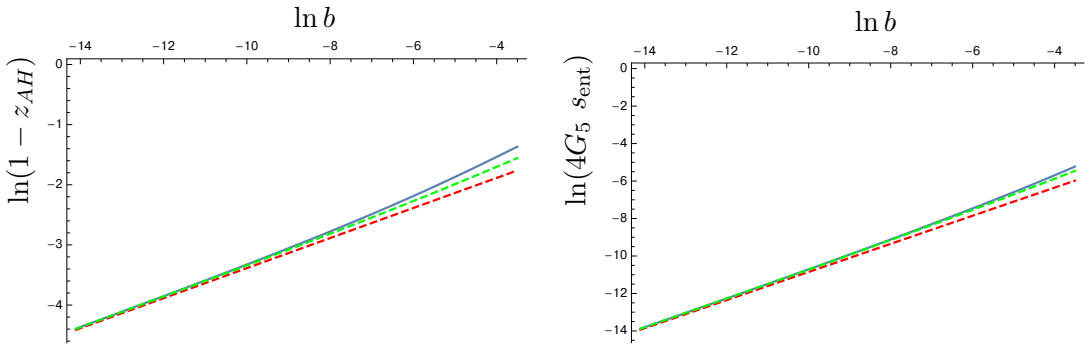

Figure 10. Location of the apparent horizon z_{AH} (left panel) and the entanglement entropy $s_{\rm ent}$ (right panel) of TypeA$_s$ de Sitter vacua in the conformal limit $b \to 0$. Blue curves: results in computational scheme SchemeII; red curves: leading perturbative approximation; green curves: next-to-leading perturbative approximation, see (4.24) and (4.25).

so that

$$b^n\ k_n\Big|_{u=u_{AH}=\mathcal{O}(b^{1/4})} = \mathcal{O}(b^{n/4+3/8})\,, \qquad b^n\ \{a,s,v,w_{a2},g\}_n\Big|_{u=u_{AH}=\mathcal{O}(b^{1/4})} = \mathcal{O}(b^{n/4})\,, \tag{4.22}$$

rendering successive higher order perturbative corrections in (4.14) at $z = z_{AH}$ small despite the singular behavior of $\{a_n, s_n, w_{c2n}, w_{a2n}, k_n, g_n\}$ in this limit.[19]

Given (4.19) and (4.20) we find from (C.8):

$$\begin{aligned}\mathcal{L}_{AH}(u \equiv 1-z) = \frac{3}{2}u^3\Bigg(u + b\left(-\frac{3\pi^2}{1024}u^{-3} - \frac{\pi^2}{64}u^{-2} + \mathcal{O}(u^{-3/2})\right)\\ + b^2\left(0\cdot u^{-6} + \frac{349\pi^4}{3932160}u^{-5} + \mathcal{O}(u^{-9/2})\right) + \mathcal{O}\left(b^3\ u^{-9}\right)\Bigg)\,,\end{aligned} \tag{4.23}$$

so that the first zero of the apparent horizon location function occurs at

$$1 - z_{AH} = u_{AH} = \frac{1}{8}3^{1/4}(2\pi)^{1/2}\ b^{1/4}\ \left(1 + \frac{1}{6}3^{1/4}(2\pi)^{1/2}\ b^{1/4} + \mathcal{O}(b^{1/2})\right). \tag{4.24}$$

From (3.32) we find perturbative predictions in the conformal limit for the TypeA$_s$ de Sitter vacua entanglement entropy:

$$4G_5\ s_{\rm ent} = \frac{1}{1024}3^{3/4}(2\pi)^{3/2}\ b^{3/4}\ \left(1 + \frac{1}{2}3^{1/4}(2\pi)^{1/2}\ b^{1/4} + \mathcal{O}(b^{1/2})\right). \tag{4.25}$$

In figure 10 we compare numerical results for z_{AH} and $s_{\rm ent}$ in computational scheme SchemeII (blue curves) with the perturbative predictions (4.24) and (4.25) at leading (red curves) and next-to-leading (green curves) orders in the conformal limit: $b \to 0$. Restoring dimensional parameters, from (4.25),

$$s_{\rm ent}\Big|_{\rm TypeA_s} \propto H^3\ \left(\ln\frac{H^2}{\Lambda^2}\right)^{-3/4} \qquad \text{as} \qquad H \gg \Lambda\,. \tag{4.26}$$

[19] This is similar to the behavior of the phenomenological model [24] in the conformal limit.

JHEP05(2020)035

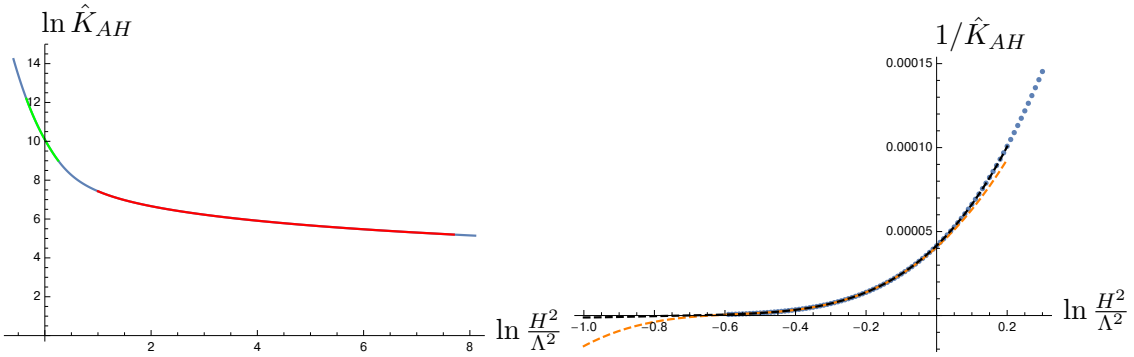

Figure 11. Left panel: Kretschmann scalar of (2.13) evaluated at the apparent horizon as functions of $\ln \frac{H^2}{\Lambda^2}$ in different computation schemes (C.6): SchemeI (blue), SchemeII (red) and Scheme III (green). Right panel: we use order-3 polynomial fit (orange dashed curve) and order-4 polynomial fit (black dashed curve) to $\frac{1}{\hat{K}_{AH}}$, see (4.29).

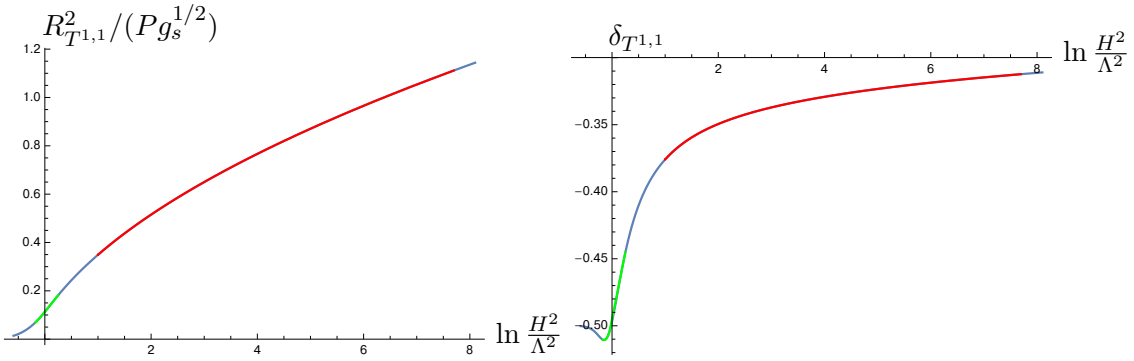

Figure 12. The curvature growth at the apparent horizon of the TypeA$_s$ de Sitter vacua gravitational dual for small $\frac{H^2}{\Lambda^2}$ is due to collapsing the compact manifold: the size of deformed $T^{1,1}$, see (4.31) (left panel). Right panel: the $T^{1,1}$ deformation parameter $\delta_{T^{1,1}}$, see (4.32). Results are presented in different computation schemes (C.6): SchemeI (blue), SchemeII (red) and Scheme III (green).

4.3 Validity of supergravity approximation for TypeA$_s$ vacua

Results for the entanglement entropy $s_{\rm ent}$ of TypeA$_s$ de Sitter vacua of the cascading gauge theory are presented in section 4.1, see figure 6. Notice that it is a monotonically decreasing function of $\frac{H^2}{\Lambda^2}$. We have been able to obtain reliable numerical results for

$$\ln \frac{H^2}{\Lambda^2} \geq -0.59 \qquad \Longrightarrow \qquad 4G_5\ \hat{s}_{\rm ent} \gtrsim 4.1 \times 10^{-4}\,. \tag{4.27}$$

Besides numerical (technical) difficulties associated with construction of these vacua, there are conceptual ones, associated with the breakdown of the supergravity approximation — the effective action (2.1) becomes less reliable as the background space-time curvature of (2.13) grows. In figure 11 (left panel) we present the Kretschmann scalar of (2.13)

JHEP05(2020)035

evaluated at the apparent horizon in different computations schemes, see appendix E:

$$\begin{aligned} \text{SchemeI}: &\quad \ln\frac{H^2}{\Lambda^2} = k_s\,, &&\hat{K} = K\,;\\ \text{SchemeII}: &\quad \ln\frac{H^2}{\Lambda^2} = \frac{1}{b} + \ln b\,, &&\hat{K} = bK\,;\\ \text{SchemeIII}: &\quad \ln\frac{H^2}{\Lambda^2} = \frac{1}{4} + \ln\alpha\,, &&\hat{K} = K\,. \end{aligned} \tag{4.28}$$

Notice the fast growth of K_{AH} for small values of $\frac{H^2}{\Lambda^2}$ — in figure 11 (right panel) we fit the values of $\frac{1}{\hat{K}_{AH}}$ with order-3 (orange dashed curve) and order-4 (black dashed curve) polynomials. The fits suggest that the curvature is divergent at

$$\ln\frac{H^2}{\Lambda^2}\bigg|_{\text{orange fit}} \approx -0.64\,, \qquad \ln\frac{H^2}{\Lambda^2}\bigg|_{\text{black fit}} \approx -0.72\,. \tag{4.29}$$

We take (4.29) as an indication that TypeA$_s$ vacua do not exist[20] for

$$\ln\frac{(H^s_{\text{min}})^2}{\Lambda^2} \lesssim -0.8 \qquad \Longrightarrow \qquad H^s_{\text{min}} \lesssim 0.7\Lambda\,. \tag{4.30}$$

In figure 12 (left panel) we identify the rapid curvature growth with the fact that the size of (deformed) $T^{1,1}$, $R^2_{T^{1,1}}$, evaluated at the apparent horizon

$$R^2_{T^{1,1}} \equiv w_{a2}\Big|_{AH} = P g_s^{1/2}\,\hat{\omega}_{a2}\Big|_{AH}\,, \tag{4.31}$$

becomes vanishingly small in string units, $P \propto M\alpha' = M\,\ell_s^2$. Note that in the limit $R^2_{T^{1,1}} \to 0$ TypeA$_s$ vacua entanglement entropy vanishes, see (4.7). Right panel shows the deformation parameter $\delta_{T^{1,1}}$ of the $T^{1,1}$: the size of the U(1) fiber compare to the $S^2 \times S^2$ base,

$$\delta_{T^{1,1}} \equiv 1 - \frac{w^2_{c2}}{w^2_{a2}}\bigg|_{AH} = 1 - \frac{\hat{\omega}^2_{c2}}{\hat{\omega}^2_{a2}}\bigg|_{AH}\,. \tag{4.32}$$

5 TypeA$_b$ de Sitter vacua

TypeA$_b$ vacua have the same topology in Euclidean FG frame as TypeA$_s$ vacua (1.22); they differ in global symmetry: TypeA$_s$ vacua have unbroken U(1) chiral symmetry (in the supergravity approximation), while the latter symmetry is broken *spontaneously* to $\mathbb{Z}_2$ in TypeA$_b$ vacua. The following table highlights the differences between the dual backgrounds in FG frame and EF frame:

Unlike TypeA$_s$ vacua, TypeA$_b$ vacua have never been constructed in the literature before — morally, they are similar to Klebanov-Strassler black holes, constructed only recently [14]. We begin in section 5.1 with perturbative construction of TypeA$_b$ vacua. Specifically, we study static linearized perturbations about TypeA$_s$ vacua responsible for the chiral symmetry breaking U(1) $\to \mathbb{Z}_2$. The symmetry breaking is associated with three

[20] It would be interesting to rigorously establish this.

JHEP05(2020)035

	chiral symmetry	FG frame (2.12)	EF frame (2.13)	fluxes (2.11)
TypeA$_s$	U(1)	$f_a = f_b$	$w_{a2} = w_{b2}$	$K_1 = K_3$ & $K_2 = 1$
TypeA$_b$	$\mathbb{Z}_2$	$f_a \neq f_b$	$w_{a2} \neq w_{b2}$	$K_1 \neq K_3$ & $K_2 \neq 1$

Table 1. TypeA de Sitter vacua with broken/unbroken ($_b$ / $_s$) chiral symmetry.

operators $\mathcal{O}_3^{\alpha=1,2}$ and $\mathcal{O}_7$ (see section 2) developing nonzero expectation values. We break the chiral symmetry *explicitly*, by turning on a non-normalizable component for one of the dim-3 operators[21] (a mass term for one of the gaugino bilinears). We vary $\frac{H^2}{\Lambda^2}$ keeping the gaugino mass parameter fixed and nonzero — the signature of the *spontaneous* chiral symmetry breaking is the divergence of all the condensates $\mathcal{O}_3^{\alpha=1,2}$ and $\mathcal{O}_7$ for a particular value of $\frac{H^2}{\Lambda^2}$, see figure 13. Once the bifurcation point of TypeA$_b$ vacua off TypeA$_s$ vacua is identified as a function of $\frac{H^2}{\Lambda^2}$, we construct fully nonlinear solution with spontaneous symmetry breaking slowing increasing the amplitudes of the symmetry breaking expectation values, using the linearized solution as a seed. Numerical results for TypeA$_b$ vacua are presented in section 5.2, in particular the results for the entanglement entropy $s_{\rm ent}\Big|_{\rm TypeA_b}$ compare to the entanglement entropy $s_{\rm ent}\Big|_{\rm TypeA_s}$ at corresponding values of $\frac{H^2}{\Lambda^2}$ are presented in figure 21. Validity of supergravity approximation for TypeA$_b$ vacua is a subject of section 5.3.

5.1 TypeA$_b$ vacua from perturbative chiral symmetry breaking of TypeA$_s$ vacua

We will use computational scheme SchemeI (C.6). Consider static, linearized chiral symmetry breaking fluctuation about TypeA$_s$ in FG frame, see table 1:

$$f_a = f_3 + \delta f\,,\ f_b = f_3 - \delta f\,,\ K_1 = K + \delta k_1\,,\ K_2 = 1 + \delta k_2\,,\ K_1 = K - \delta k_1\,, \tag{5.1}$$

with the remaining metric functions and the string coupling as in TypeA$_s$ vacua, i.e., $\{f_c = f_2, h, g\}$. It is straightforward to verify that truncation to $\{\delta f, \delta k_{1,2}\}$ is consistent (at the linearized level). Equations of motion for the fluctuations and their asymptotic expansions in the UV ($\rho \to 0$) and the IR ($y = \frac{1}{\rho}$) are collected in appendix F. Once the non-normalizable coefficient (the explicit chiral symmetry breaking parameter, i.e., the gaugino mass term) is fixed to $\delta f_{1,0} = 1$, the expansions are characterized by 6 UV/IR parameters

$$\begin{aligned} \text{UV}: &\quad \{\delta f_{3,0}\,,\ \delta k_{1,3,0}\,,\ \delta f_{7,0}\}\,; \\ \text{IR}: &\quad \{\delta f_0^h\,,\ \delta k_{1,0}^h\,,\ \delta k_{2,0}^h\}\,, \end{aligned} \tag{5.2}$$

which is the correct number of parameters to find a unique solution of 3 second-order differential equations (F.1)–(F.3) for $\{\delta f, \delta k_{1,2}\}$ on the TypeA$_s$ background parameterized by k_s.

In figure 13 we assemble results for the fluctuation parameters (5.2) as k_s label of TypeA$_s$ vacua is varied. A signature of the spontaneous symmetry breaking is the divergence of all the parameters, once the scale of the explicit chiral symmetry breaking, i.e.,

[21] This was discussed earlier in [13].

JHEP05(2020)035

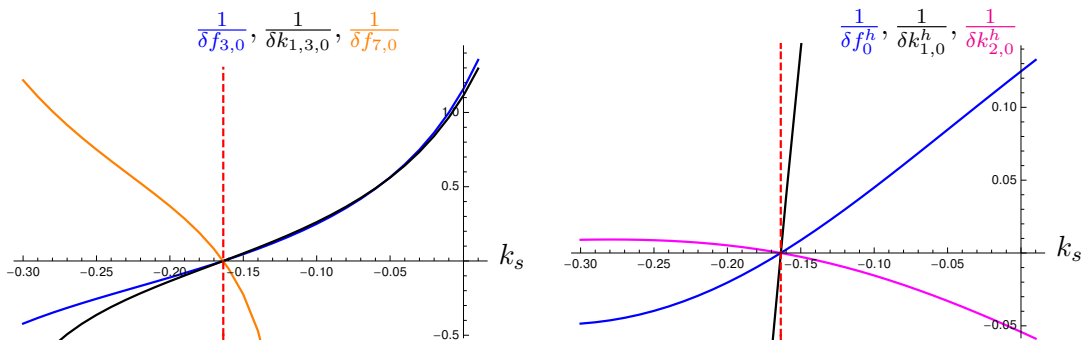

Figure 13. Parameters $\{\delta f_{3,0}\,,\, \delta k_{1,3,0}\,,\, \delta f_{7,0}\,,\, \delta f_0^h\,,\, \delta k_{1,0}^h\,,\, \delta k_{2,0}^h\}$ of the chiral symmetry breaking fluctuations over TypeA$_s$ vacua parameterized by k_s, evaluated at fixed explicit chiral symmetry breaking scale $\delta f_{1,0} = 1$, diverge at $k_s^{\rm crit}$ (5.3), indicated by a vertical red dashed line. $k_s^{\rm crit}$ identifies the bifurcation point of spontaneous symmetry broken TypeA$_b$ de Sitter vacua off chirally symmetric TypeA$_s$ de Sitter vacua parameterized by $\ln \frac{H^2}{\Lambda^2}$.

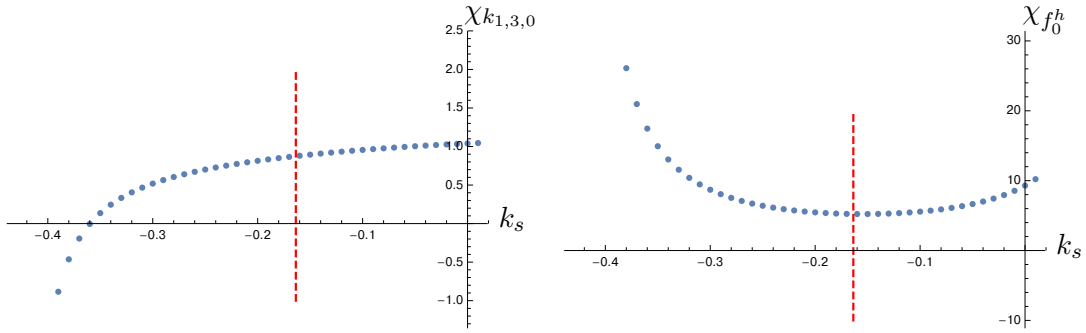

Figure 14. Sample susceptibilities, see (5.5), of the linearized chiral symmetry breaking fluctuations. The red dashed vertical line denotes $k_s^{\rm crit}$, see (5.3).

the non-normalizable parameter $\delta f_{1,0}$, is kept fixed. This occurs at

$$\ln \frac{(H^b_{\rm min})^2}{\Lambda^2} = k_s^{\rm crit} = -16363(2) \qquad \Longrightarrow \qquad H^b_{\rm min} = 0.92(1)\Lambda\,, \tag{5.3}$$

represented by vertical dashed red lines. We denote the critical value of H corresponding to $k_s^{\rm crit}$ as $H^b_{\rm min}$ — we will see in section 5.2 that TypeA$_b$ vacua exist only for $H \geq H^b_{\rm min}$, hence the name. The value of $k_s^{\rm crit}$ can be computed separately of each of the parameters — the fractional differences are of order $\propto 10^{-6}$, excepts for

$$\left(\frac{k_s^{\rm crit}\Big|_{\delta f_{7,0}}}{k_s^{\rm crit}\Big|_{\delta f_{3,0}}} - 1 \right) \;\propto\; 10^{-4}\,. \tag{5.4}$$

To use the critical fluctuations as a seed for TypeA$_b$ vacua, we need to know the 'susceptibilities'

$$\left\{ \chi_{k_{1,3,0}}\,,\, \chi_{f_{7,0}}\,,\, \chi_{f_0^h}\,,\, \chi_{k_{1,0}^h}\,,\, \chi_{k_{2,0}^h} \right\} \;\equiv\; \lim_{k_s \to k_s^{\rm crit}} \left\{ \frac{\delta k_{1,3,0}}{\delta f_{3,0}}\,,\, \frac{\delta f_{7,0}}{\delta f_{3,0}}\,,\, \frac{\delta f_0^h}{\delta f_{3,0}}\,,\, \frac{\delta k_{1,0}^h}{\delta f_{3,0}}\,,\, \frac{\delta k_{2,0}^h}{\delta f_{3,0}} \right\}. \tag{5.5}$$

JHEP05(2020)035

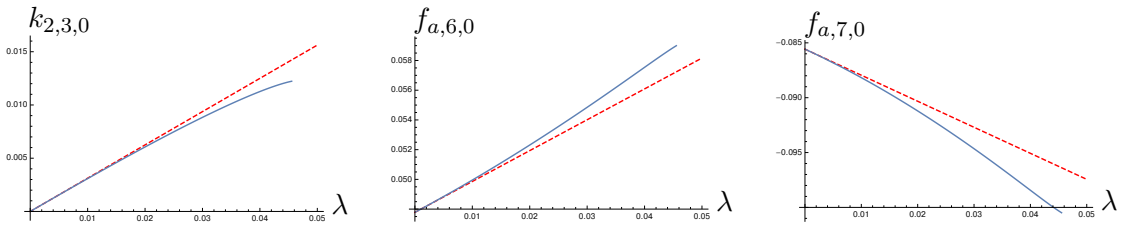

Figure 15. Sample of the UV parameters of TypeA$_b$ de Sitter vacua constructed from the 'seed' (5.11). The linearized approximations in λ are represented by dashed red lines.

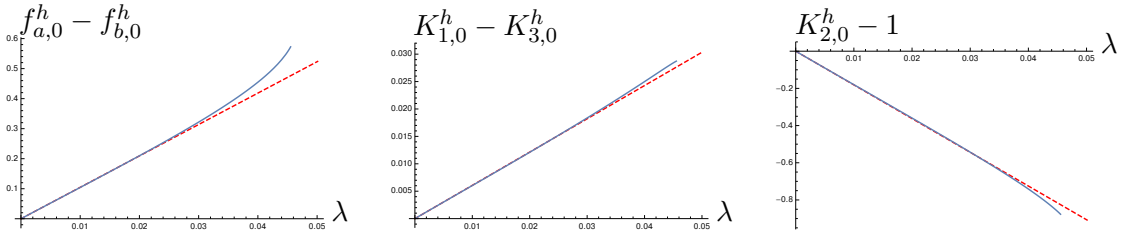

Figure 16. Sample of the IR parameters of TypeA$_b$ de Sitter vacua constructed from the 'seed' (5.11). The linearized approximations in λ are represented by dashed red lines.

In figure 14 we present susceptibilities $\chi_{k_{1,3,0}}$ and $\chi_{f^h_0}$ — notice that they are finite at $k_s^{\rm crit}$, represented by vertical dashed red lines. The other susceptibilities are finite as well; we find:

$$\begin{aligned} \chi_{k_{1,3,0}} &= 0.8749(7)\,, \quad \chi_{f_{7,0}} = -0.2373(6)\,, \quad \chi_{f^h_0} = 5.230(0)\,, \\ \chi_{k^h_{1,0}} &= 0.3034(2)\,, \quad \chi_{k^h_{2,0}} = -18.12(6)\,. \end{aligned} \tag{5.6}$$

Given (5.6), fully nonlinear TypeA$_b$ vacua, with k_s close to $k_s^{\rm crit}$, can be constructed following the same procedure as the one employed in construction of Klebanov-Strassler black hole in [14]. We highlight the main steps:

- We set $k_s = k_s^{\rm crit}$ and compute the corresponding TypeA$_s$ vacuum. This vacuum is characterized by (see (B.44) and (B.46))

$$\begin{aligned} &\text{UV}: \quad \{K_0 = k_s^{\rm crit}\,,\, H=1\,,\, g_s=1\,,\, f^{\rm crit}_{2,1,0}\,,\, g^{\rm crit}_{4,0}\,,\, f^{\rm crit}_{2,4,0}\,,\, f^{\rm crit}_{2,6,0}\,,\, f^{\rm crit}_{2,8,0}\}\,; \\ &\text{IR}: \quad \{f^{h,{\rm crit}}_{2,0}\,,\, f^{h,{\rm crit}}_{3,0}\,,\, K^{h,{\rm crit}}_0\,,\, g^{h,{\rm crit}}_0\}\,. \end{aligned} \tag{5.7}$$

  Next, we use (B.47)–(B.51) to compute the corresponding

$$\begin{aligned} &\text{UV}: \quad \{f^{s,{\rm crit}}_{a,1,0}\,,\, f^{s,{\rm crit}}_{a,3,0}\,,\, k^{s,{\rm crit}}_{2,3,0}\,,\, g^{s,{\rm crit}}_{4,0}\,,\, f^{s,{\rm crit}}_{c,4,0}\,,\, f^{s,{\rm crit}}_{a,6,0}\,,\, f^{s,{\rm crit}}_{a,7,0}\,,\, f^{s,{\rm crit}}_{a,8,0}\}\,; \\ &\text{IR}: \quad \{f^{h,s,{\rm crit}}_{a,0}\,,\, f^{h,s,{\rm crit}}_{b,0}\,,\, f^{h,s,{\rm crit}}_{c,0}\,,\, K^{h,s,{\rm crit}}_{1,0}\,,\, K^{h,s,{\rm crit}}_{2,0}\,,\, K^{h,s,{\rm crit}}_{3,0}\,,\, g^{h,s,{\rm crit}}_0\}\,. \end{aligned} \tag{5.8}$$

  We use superscript ^{s} to indicate that UV/IR parameters of TypeA$_b$ vacua (B.25) and (B.30) are obtained from the critical TypeA$_s$ vacuum.

- Let's denote the amplitude of the symmetry breaking condensate (see (5.1))

$$\delta f_{3,0} \equiv \frac{1}{2}\,(f_{a,3,0} - f_{b,3,0}) = \lambda\,. \tag{5.9}$$

JHEP05(2020)035

Then,

$$\left\{\delta k_{1,3,0}\,,\,\delta f_{7,0}\,,\,\delta f_0^h\,,\,\delta k_{1,0}^h\,,\,\delta k_{2,0}^h\right\} = \lambda\,\{\chi_{k_{1,3,0}}\,,\,\chi_{f_{7,0}}\,,\,\chi_{f_0^h}\,,\,\chi_{k_{1,0}^h}\,,\,\chi_{k_{2,0}^h}\} + \mathcal{O}(\lambda^2)\,. \tag{5.10}$$

- Using (5.1) and (F.4)–(F.6), (F.8), with $\delta f_{1,0} = 0$, in asymptotic expansions (B.17)–(B.24) and (B.30) we find

$$\begin{aligned}
&k_s = k_s^{\rm crit} + \mathcal{O}(\lambda^2)\,, \qquad f_{a,1,0} = f_{a,1,0}^{s,\rm crit} + \mathcal{O}(\lambda^2)\,, \qquad f_{a,3,0} = f_{a,3,0}^{s,\rm crit} + \lambda + \mathcal{O}(\lambda^2)\,,\\
&k_{2,3,0} = k_{2,3,0}^{s,\rm crit} - \lambda\left(1 - \frac{3}{2}\chi_{k_{1,3,0}}\right) + \mathcal{O}(\lambda^2)\,, \qquad g_{4,0} = g_{4,0}^{s,\rm crit} + \mathcal{O}(\lambda^2)\,,\\
&f_{c,4,0} = f_{c,4,0}^{s,\rm crit} + \mathcal{O}(\lambda^2)\,,\\
&f_{a,6,0} = f_{a,6,0}^{s,\rm crit} - \frac{f_{2,1,0}^{\rm crit}}{64}\left(8(f_{2,1,0}^{\rm crit})^2 + 18\chi_{k_{1,3,0}} + 12k_s^{\rm crit} - 35\right)\lambda + \mathcal{O}(\lambda^2)\,,\\
&f_{a,7,0} = f_{a,7,0}^{s,\rm crit} + \lambda\,\chi_{f_{7,0}} + \mathcal{O}(\lambda^2)\,,\\
&f_{a,8,0} = f_{a,8,0}^{s,\rm crit} - \frac{f_{2,1,0}^{\rm crit}}{1536}\Big(550 - 192(f_{2,1,0}^{\rm crit})^4 - 720\chi_{k_{1,3,0}}(f_{2,1,0}^{\rm crit})^2 - 480(f_{2,1,0}^{\rm crit})^2 k_s^{\rm crit}\\
&\qquad + 36\chi_{k_{1,3,0}}k_s^{\rm crit} + 1184(f_{2,1,0}^{\rm crit})^2 + 3840\chi_{f_{7,0}} - 45\chi_{k_{1,3,0}} + 2304 f_{2,4,0}^{\rm crit} + 21 k_s^{\rm crit}\Big)\,\lambda\\
&\qquad + \mathcal{O}(\lambda^2)\,,\\
&f_{a,0}^h = f_{a,0}^{h,s,\rm crit} + \chi_{f_0^h}\,\lambda + \mathcal{O}(\lambda^2)\,, \qquad f_{b,0}^h = f_{b,0}^{h,s,\rm crit} - \chi_{f_0^h}\,\lambda + \mathcal{O}(\lambda^2)\,,\\
&f_{c,0}^h = f_{c,0}^{h,s,\rm crit} + \mathcal{O}(\lambda^2)\,, \qquad K_{1,0}^h = K_{1,0}^{h,s,\rm crit} + \chi_{k_{1,0}^h}\,\lambda + \mathcal{O}(\lambda^2)\,,\\
&K_{2,0}^h = K_{2,0}^{h,s,\rm crit} + \chi_{k_{2,0}^h}\,\lambda + \mathcal{O}(\lambda^2)\,, \qquad K_{3,0}^h = K_{3,0}^{h,s,\rm crit} - \chi_{k_{1,0}^h}\,\lambda + \mathcal{O}(\lambda^2)\,,\\
&g_0^h = g_0^{h,s,\rm crit} + \mathcal{O}(\lambda^2)\,.
\end{aligned} \tag{5.11}$$

- We construct fully nonlinear in λ TypeA$_b$ vacua using the linearized approximation (5.11) as a seed. Select UV/IR parameters, along with the corresponding linearized approximations (dashed red lines) are shown in figures 15–16.

5.2 Numerical results: TypeA$_b$

Numerical construction of TypeA$_b$ vacua follows the steps of section 4.1. In FG frame, there are 8 second order equations (B.3)–(B.10) and 1 first order equation (B.11). The first order equation (B.11) involves (linearly) f_c' and can be used instead of one of the second order equations (namely, the one involving f_c''). Thus, altogether we have a coupled system of 7 second order ODEs (linear in $\{f_a'', f_b'', h'', K_1'', K_2'', K_3'', g''\}$) and a single first order equation (linear in f_c'). As a result, a unique solution must be characterized by $15 = 2\times 7 + 1$ parameters; these are the UV/IR parameters

$$\begin{aligned}
&\text{UV}: \quad \{f_{a,1,0}\,,\,f_{a,3,0}\,,\,k_{2,3,0}\,,\,g_{4,0}\,,\,f_{c,4,0}\,,\,f_{a,6,0}\,,\,f_{a,7,0}\,,\,f_{a,8,0}\}\,;\\
&\text{IR}: \quad \{f_{a,0}^h\,,\,f_{b,0}^h\,,\,f_{c,0}^h\,,\,K_{1,0}^h\,,\,K_{2,0}^h\,,\,K_{3,0}^h\,,\,g_0^h\}\,.
\end{aligned} \tag{5.12}$$

JHEP05(2020)035

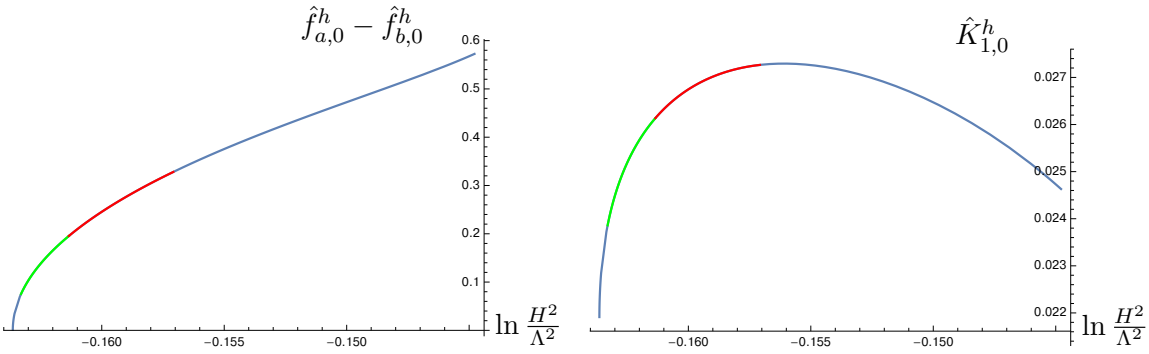

Figure 17. Infrared parameters $\{\hat{f}^h_{a,0} - \hat{f}^h_{b,0}, \hat{K}^h_{1,0}\}$ of the Fefferman-Graham coordinate frame of TypeA$_b$ de Sitter vacua of the cascading gauge theory as functions of $\ln \frac{H^2}{\Lambda^2}$ in different computational schemes (5.14): SchemeI (blue), SchemeII (red) and Scheme III (green).

It is rather challenging to find the solutions of the corresponding system of ODEs in 15-dimensional parameter space by brute force — fortunately, we already know some solutions which are close to $k_s^{\rm crit}$, see section 5.1.

As for the construction of TypeA$_s$ we use three different computation schemes, see appendix C.1. There are some differences though: both in SchemeII and SchemeIII we use as a pivot value[22]

$$K_0^\star = -0.161344\,. \tag{5.13}$$

Numerical results must not depend on which computational scheme is adopted. We illustrate now that this is indeed the case using a sample of IR parameters in (5.12) as an example.[23] Comparison of the different computational schemes is done using dimensionless and rescaled quantities: $\ln \frac{H^2}{\Lambda^2}$ (as a vacuum label) (C.2) and $\{\hat{f}^h_{a,b,c,0}\,,\, \hat{K}^h_{1,2,3,0}\,,\, \hat{g}^h_0\}$ (C.4). Explicitly:

$$\begin{aligned}
&\text{SchemeI}: && \ln\frac{H^2}{\Lambda^2} = k_s\,, && \hat{f}^h_{a,b,c,0} = f^h_{a,b,c,0}\,, && \hat{K}^h_{1,2,3,0} = K^h_{1,2,3,0}\,, && \hat{g}^h_0 = g^h_0\,;\\
&\text{SchemeII}: && \ln\frac{H^2}{\Lambda^2} = \frac{K_0^\star}{b} + \ln b\,, && \hat{f}^h_{a,b,c,0} = \frac{1}{b^{1/2}} f^h_{a,b,c,0}\,, && \hat{K}^h_{1,2,3,0} = \frac{1}{b} K^h_{1,2,3,0}\,, && \hat{g}^h_0 = g^h_0\,;\\
&\text{SchemeIII}: && \ln\frac{H^2}{\Lambda^2} = K_0^\star + \ln\alpha\,, && \hat{f}^h_{a,b,c,0} = \frac{1}{\alpha^{1/2}} f^h_{a,b,c,0}\,, && \hat{K}^h_{1,2,3,0} = K^h_{1,2,3,0}\,, && \hat{g}^h_0 = g^h_0\,.
\end{aligned} \tag{5.14}$$

Following (5.14), we collect results of $\{\hat{f}^h_{a,0} - \hat{f}^h_{b,0}, \hat{K}^h_{1,0}\}$ as functions of $\ln \frac{H^2}{\Lambda^2}$ in different computational schemes in figure 17: SchemeI (blue curves), SchemeII (red curves) and Scheme III (green curves). The accuracy of the collapsed results in different schemes is highlighted in figure 18 for $\hat{K}^h_{1,0}$ — the remaining parameters follow the same trend. Notice that TypeA$_b$ vacua exist only for $H \geq H^b_{\rm min}$ (5.3); furthermore, in the limit $H \to H^b_{\rm min} + 0$, all the chiral symmetry breaking condensates (5.2) vanish as $\propto (H - H^b_{\rm min})^{1/2}$, typical for a spontaneous symmetry breaking with a mean-field exponent $\frac{1}{2}$.

[22] As will be clear from the presented results this is a convenient value.

[23] The same is true for the rest of IR parameters and the UV parameters as well.

JHEP05(2020)035

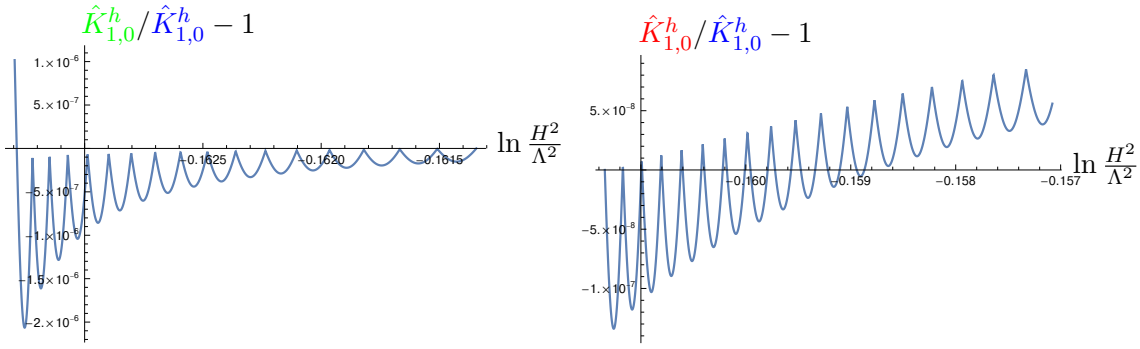

Figure 18. Left panel: comparison of $\hat{K}^h_{1,0}$ (the computational scheme SchemeIII) with $\hat{K}^h_{1,0}$ (the computational scheme SchemeI). Right panel: comparison of $\hat{K}^h_{1,0}$ (the computational scheme SchemeII) with $\hat{K}^h_{1,0}$ (the computational scheme SchemeI).

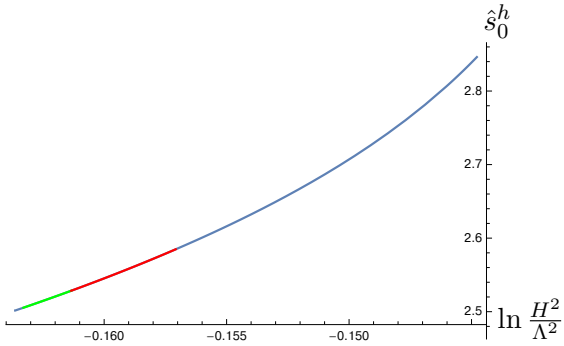

Figure 19. Parameters $\hat{s}^h_0$ of TypeA$_s$ de Sitter vacua of the cascading gauge theory as functions of $\ln\frac{H^2}{\Lambda^2}$ in different computational schemes (5.14): SchemeI (blue), SchemeII (red) and Scheme III (green).

Next, FG frame TypeA$_b$ de Sitter vacua have to be reinterpreted in EF frame, see appendix B.2. The diffeomorphism transformation is performed at the radial location as in (4.3). Details of numerical construction of EF frame vacua from FG frame vacua are collected in appendix C.2. An important quantity is the parameter s^h_0, see (2.13), and (4.4). As with FG frame UV/IR parameters (5.12), results for s^h_0 should not depend on the choice of the computational scheme, provided we compare properly dimensionless and rescaled quantities, i.e., $\ln\frac{H^2}{\Lambda^2}$ and $\hat{s}^h_0$ (C.15),

$$\begin{aligned}
\text{SchemeI}: &\quad \ln\frac{H^2}{\Lambda^2}=k_s\,, && \hat{s}^h_0=s^h_0\,;\\
\text{SchemeII}: &\quad \ln\frac{H^2}{\Lambda^2}=\frac{K^\star_0}{b}+\ln b\,, && \hat{s}^h_0=\frac{1}{b^{1/4}}s^h_0\,;\\
\text{SchemeIII}: &\quad \ln\frac{H^2}{\Lambda^2}=K^\star_0+\ln\alpha\,, && \hat{s}^h_0=\frac{1}{\alpha^{1/2}}s^h_0\,.
\end{aligned} \tag{5.15}$$

Following (5.15), we collect (subset of the) results of $\hat{s}^h_0$ as functions of $\ln\frac{H^2}{\Lambda^2}$ in different computational schemes in figure 19: SchemeI (blue curves), SchemeII (red curves) and Scheme III (green curves). The accuracy of the collapsed results in different schemes is highlighted in figure 20.

JHEP05(2020)035

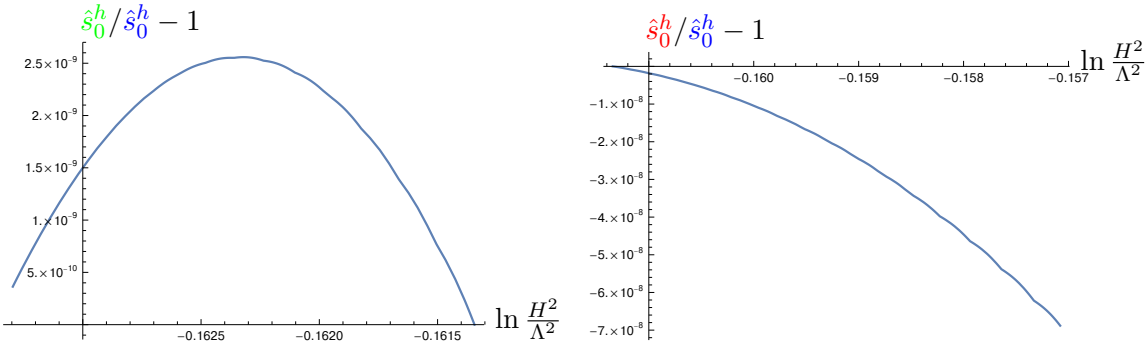

Figure 20. Left panel: comparison of $\hat{s}_0^h$ (the computational scheme SchemeIII) with $\hat{s}_0^h$ (the computational scheme SchemeI). Right panel: comparison of $\hat{s}_0^h$ (the computational scheme SchemeII) with $\hat{s}_0^h$ (the computational scheme SchemeI).

EF frame equations of motion (A.17)–(A.25) are solved subject to the initial conditions set by the asymptotic expansions (B.58)–(B.66) at $z = 0$. These equations have to be integrated on the interval

$$z \in [0, z_{AH}] \,, \tag{5.16}$$

where $z_{AH} = -r_{AH}$ is the location of the apparent horizon at asymptotically late times, see (3.32). To determine the location of the apparent horizon, along with integrating the gravitational background functions $\{a, \sigma, w_{a,b,c,2}, K_{1,2,3}, g\}$, we evaluate the AH location function $\mathcal{L}_{AH}(z)$, see (C.8). AH is located at the first zero of this function for $z > 0$. Once the AH is identified, TypeA$_b$ vacua entanglement entropy is computed following (3.32):

$$s_{\rm ent} = \frac{H^3 P^4 g_s^2}{4 G_5} \left\{ \hat{\sigma}^3 \hat{w}_{c2}^{1/2} \hat{\omega}_{a2} \hat{\omega}_{b2} \right\} \Big|_{\hat{z}=\hat{z}_{AH}} = \frac{3^5 M^4 g_s^2}{2^5 \pi^3} \, H^3 \left\{ \hat{\sigma}^3 \hat{w}_{c2}^{1/2} \hat{\omega}_{a2} \hat{\omega}_{b2} \right\} \Big|_{\hat{z}=\hat{z}_{AH}} , \tag{5.17}$$

where following (C.1) we introduced dimensionless and rescaled functions and the radial coordinate:

$$\begin{aligned} &\{z \,,\; a \,,\, \sigma \,,\, w_{a2,b2,c2} \,,\, K_{1,2,3} \,,\; g\} \qquad \Longrightarrow \qquad \{\hat{z} \,,\; \hat{a} \,,\, \hat{\sigma} \,,\, \hat{\omega}_{a2,b2,c2} \,,\, \hat{K}_{1,2,3} \,,\; \hat{g}\} \,; \\ &\qquad z = H P g_s^{1/2} \; \hat{z} \,, \qquad\qquad a = H^2 P g_s^{1/2} \; \hat{a} \,, \qquad\quad \sigma = H P^{1/2} g_s^{1/4} \; \hat{\sigma} \,, \\ &w_{a2,b2,c2} = P g_s^{1/2} \; \hat{\omega}_{a2,b2,c2} \,, \qquad K_{1,3} = P^2 g_s \; \hat{K}_{1,3} \,, \qquad K_2 = \hat{K}_2 \,, \qquad g = g_s \; \hat{g} \,. \end{aligned} \tag{5.18}$$

In the last equality in (5.17) we used expressions for G_5 (2.8) and P (2.7). We compute entanglement entropy in different computational schemes; results must agree, provided we compare dimensionless and rescaled quantities, see (4.9). Explicitly,

$$\begin{aligned} \text{SchemeI}: \quad & \ln \frac{H^2}{\Lambda^2} = k_s \,, && \hat{s}_{\rm ent} = s_{\rm ent} \,; \\ \text{SchemeII}: \quad & \ln \frac{H^2}{\Lambda^2} = \frac{K_0^\star}{b} + \ln b \,, && \hat{s}_{\rm ent} = \frac{1}{b^2} s_{\rm ent} \,; \\ \text{SchemeIII}: \quad & \ln \frac{H^2}{\Lambda^2} = K_0^\star + \ln \alpha \,, && \hat{s}_{\rm ent} = \frac{1}{\alpha^{3/2}} s_{\rm ent} \,. \end{aligned} \tag{5.19}$$

JHEP05(2020)035

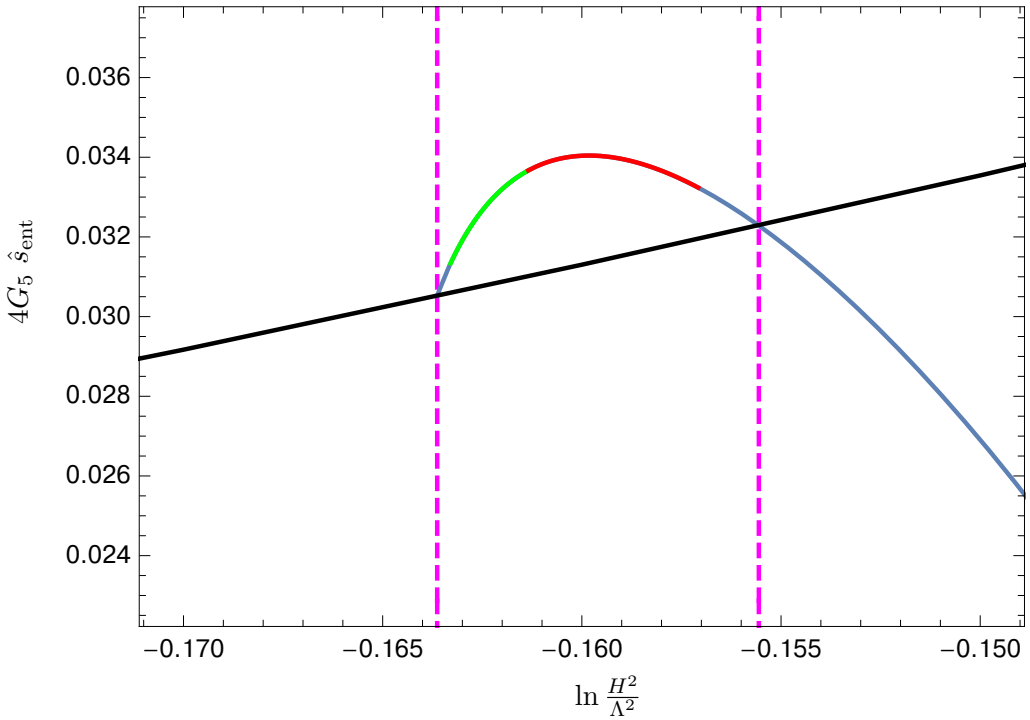

Figure 21. Entanglement entropy $\hat{s}_{\rm ent}$ (4.9) of TypeA$_s$ (black curve) and TypeA$_b$ (different computational schemes (5.19): SchemeI (blue), SchemeII (red) and Scheme III (green)) de Sitter vacua of the cascading gauge theory as functions of $\ln \frac{H^2}{\Lambda^2}$. Dashed vertical magenta lines indicate the range of the Hubble constant H such that $s_{\rm ent}\Big|_{\rm TypeA_b} \geq s_{\rm ent}\Big|_{\rm TypeA_s}$, see (5.20).

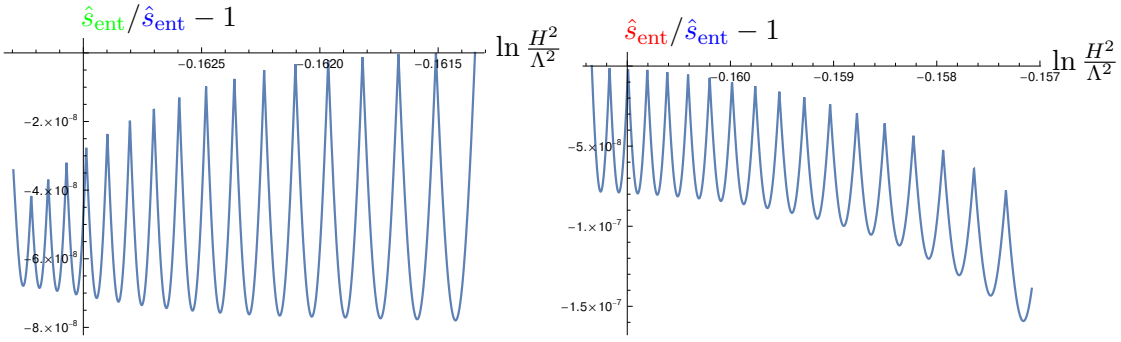

Figure 22. Left panel: comparison of $\hat{s}_{\rm ent}$ (the computational scheme SchemeIII) with $\hat{s}_{\rm ent}$ (the computational scheme SchemeI). Right panel: comparison of $\hat{s}_{\rm ent}$ (the computational scheme SchemeII) with $\hat{s}_{\rm ent}$ (the computational scheme SchemeI).

JHEP05(2020)035

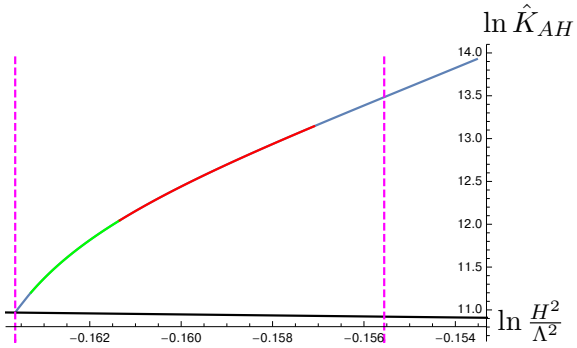

Figure 23. Kretschmann scalar of (2.13) evaluated at the apparent horizon as functions of $\ln \frac{H^2}{\Lambda^2}$ for TypeA$_b$ vacua in different computation schemes (5.22): SchemeI (blue), SchemeII (red) and Scheme III (green). The black curve is the Kretschmann scalar of (2.13) evaluated at the apparent horizon as a function of $\ln \frac{H^2}{\Lambda^2}$ for TypeA$_s$ vacua. Vertical dashed magenta lines indicate the range of dominance of TypeA$_b$ vacua over TypeA$_s$, see (5.20).

Following (5.19), we collect (subset of the) results of $(4G_5\ \hat{s}_{\rm ent})$ as functions of $\ln \frac{H^2}{\Lambda^2}$ in different computational schemes in figure 21: SchemeI (blue curves), SchemeII (red curves) and Scheme III (green curves). Additionally, we replot the results for the entanglement entropy of TypeA$_s$ vacua (black curve). Figure 21 is the main result of the paper: it demonstrates that the entanglement entropy of TypeA$_b$ vacua is larger than that of TypeA$_s$ vacua provided (the values $H^b_{\rm min}$ and $H_{\rm max}$ are denoted by vertical dashed magenta lines)

$$H^b_{\rm min} \leq H \leq H_{\rm max}\,, \tag{5.20}$$

where

$$\frac{H^b_{\rm min}}{\Lambda} = 0.92(1)\,, \qquad \frac{H_{\rm max}}{\Lambda} = 0.92(5)\,. \tag{5.21}$$

This is an unexpected result, as it implies that SU(N) × SU($N+M$) cascading gauge theory with a strong coupling scale Λ undergoes spontaneous chiral symmetry breaking in de Sitter space time with a Hubble constant H in the interval (5.20).

The accuracy of the collapsed results for TypeA$_b$ vacua in different schemes is highlighted in figure 22.

5.3 Validity of supergravity approximation for TypeA$_b$ vacua

In this section we briefly comment on the validity of the supergravity approximation in construction of TypeA$_b$ vacua. In figure 23 we present the Kretschmann scalar of (2.13) evaluated at the apparent horizon in different computations schemes for the TypeA$_b$ vacua, see appendix E:

$$\begin{aligned}
\text{SchemeI}: &\quad \ln\frac{H^2}{\Lambda^2} = k_s\,, && \hat{K} = K\,;\\
\text{SchemeII}: &\quad \ln\frac{H^2}{\Lambda^2} = \frac{K_0^\star}{b} + \ln b\,, && \hat{K} = bK\,;\\
\text{SchemeIII}: &\quad \ln\frac{H^2}{\Lambda^2} = K_0^\star + \ln\alpha\,, && \hat{K} = K\,.
\end{aligned} \tag{5.22}$$

JHEP05(2020)035

Vertical dashed magenta lines indicate the range of dominance of TypeA$_b$ vacua over TypeA$_s$, see (5.20). Additionally, we replot the Kretschmann scalar of (2.13) evaluated at the apparent horizon for TypeA$_s$ vacua (black curve). K_{AH} is the same for TypeA$_b$ and TypeA$_s$ vacua at $H = H^b_{\rm min}$; the former is about 13 times larger for TypeA$_b$ vacuum at $H = H_{\rm max}$ and continues to increase as $\frac{H}{\Lambda}$ increases. We do not study the breakdown of the supergravity approximation for TypeA$_b$ vacua for $H > H_{\rm max}$, as these vacua are irrelevant.

6 TypeB de Sitter vacua

TypeB de Sitter vacua were studied previously in [31]. We showed in section 3.4 that the entanglement entropy of these vacua vanishes. Thus, these vacua can arise as late-time dynamical attractors of the cascading gauge theory in de Sitter only when neither TypeA$_s$ nor TypeA$_b$ vacua exist (for the corresponding values $\frac{H}{\Lambda}$). Recall that TypeA$_s$ vacua exist only for $H \gtrsim H^s_{\rm min}$ (4.30), and TypeA$_b$ vacua exist only when $H \geq H^b_{\rm min}$ (5.21). In this section we establish that TypeB vacua do exist for $H \lesssim H^B_{\rm max}$ with $H^B_{\rm max} > \{H^s_{\rm min}, H^b_{\rm min}\}$, see (1.33). In section 6.1 we present numerical results for TypeB vacua for generic values of $\frac{H^2}{\Lambda^2}$. In section 6.2 we estimate $H^B_{\rm max}$ above which TypeB vacua construction in type IIB supergravity becomes unreliable/does not exist. We identify the source of breaking of the supergravity approximation.

6.1 Numerical results: TypeB

To establish the existence of TypeB vacua it is sufficient to construct them in FG frame (2.12). The construction follows the steps implemented for TypeA$_s$ vacua in section 4.1. There are 8 second order equations (B.3)–(B.10) and 1 first order equation (B.11). The first order equation (B.11) involves (linearly) f_c' and can be used instead of one of the second order equations (namely, the one involving f_c''). Thus, altogether we have a coupled system of 7 second order ODEs (linear in $\{f_a'', f_b'', h'', K_1'', K_2'', K_3'', g''\}$) and a single first order equation (linear in f_c'). As a result, a unique solution must be characterized by $15 = 2 \times 7 + 1$ parameters; these are the UV/IR parameters

$$\begin{aligned} &\text{UV}: \quad \{f_{a,1,0}\,,\ f_{a,3,0}\,,\ k_{2,3,0}\,,\ g_{4,0}\,,\ f_{c,4,0}\,,\ f_{a,6,0}\,,\ f_{a,7,0}\,,\ f_{a,8,0}\}\,; \\ &\text{IR}: \quad \{f^h_{a,0}\,,\ h^h_0\,,\ k^h_{1,3}\,,\ k^h_{2,2}\,,\ k^h_{2,4}\,,\ k^h_{3,1}\,,\ g^h_0\}\,. \end{aligned} \tag{6.1}$$

It is rather challenging to find the solutions of the corresponding system of ODEs in 15-dimensional parameter space by brute force — fortunately, a special case of TypeB vacua, namely, the limit $H \to 0$, is the supersymmetric Minkowski space-time Klebanov-Strassler solution [2], see appendix B.3. Using this extremal KS solution as a seed, we can construct TypeB vacua turning on the deformation parameter $\alpha \equiv H^2$ in the ODEs (B.3)–(B.11).

To validate our results, we use two different computation schemes: SchemeI and SchemeIII, see (C.6). Numerical results must not depend on which computational scheme is adopted. We illustrate now that this is indeed the case using a sample of IR parameters in (6.1) as an example.[24] Comparison of the different computational schemes is

[24]The same is true for the rest of IR parameters and the UV parameters as well.

JHEP05(2020)035

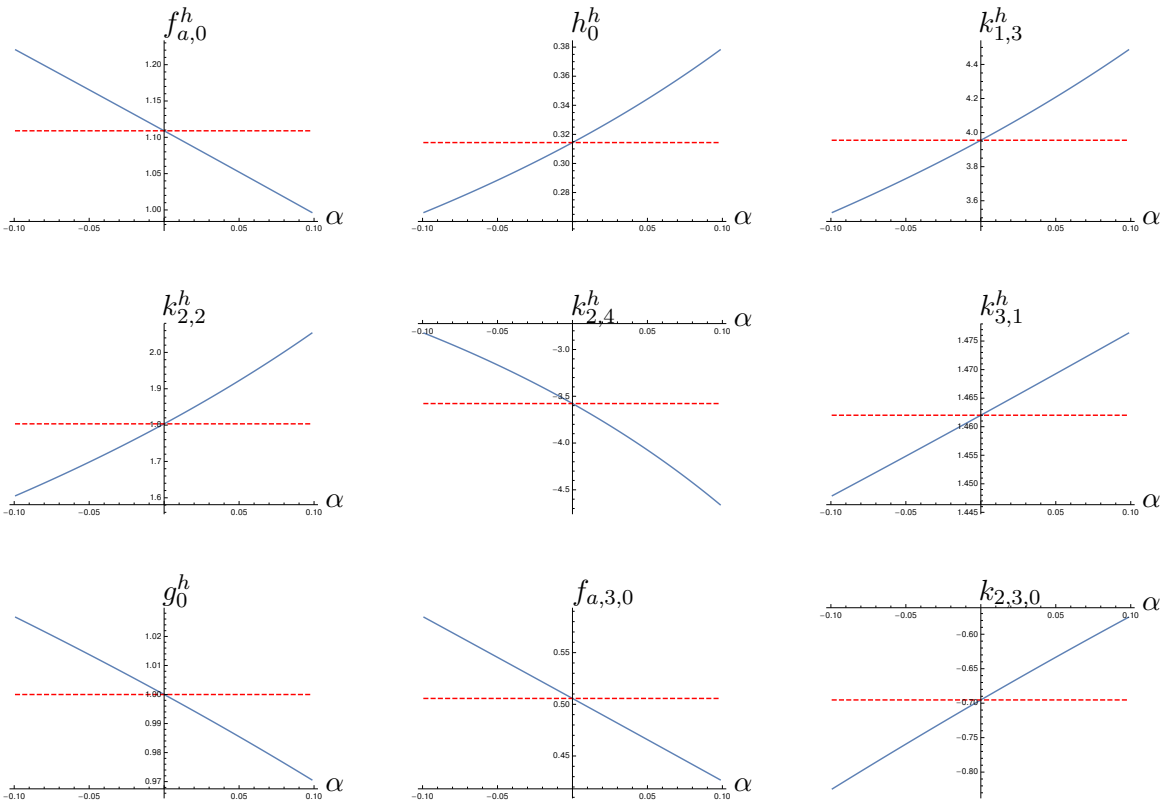

Figure 24. TypeB vacua IR parameters and select UV parameters (6.1) in computational SchemeIII as functions of $\alpha \equiv H^2$ (solid blue curves). Red dashed horizontal lines represent comparison with extremal KS solution, see (6.3), at $\alpha = 0$.

done using dimensionless and rescaled quantities: $\ln \frac{H^2}{\Lambda^2}$ (as a vacuum label) (C.2) and $\{\hat{f}^h_a\,,\, \hat{h}^h_0\,,\, \hat{k}^h_{1,3}\,,\, \hat{k}^h_{2,2}\,,\, \hat{k}^h_{2,4}\,,\, \hat{k}^h_{3,1}\,,\, \hat{g}^h_0\}$ (C.5). Explicitly:

$$\begin{aligned}
\text{SchemeI}: \quad & \ln\frac{H^2}{\Lambda^2} = k_s\,, && \hat{f}^h_a = f^h_a\,,\ \hat{h}^h_0 = h^h_0\,,\ \hat{k}^h_{1,3} = k^h_{1,3}\,,\ \hat{k}^h_{2,2} = k^h_{2,2}\,,\ \hat{k}^h_{2,4} = k^h_{2,4}\,,\\
& \hat{k}^h_{3,1} = k^h_{3,1}\,, && \hat{g}^h_0 = g^h_0\,;\\
\text{SchemeIII}: \quad & \ln\frac{H^2}{\Lambda^2} = \frac{1}{4} + \ln\alpha\,, && \hat{f}^h_a = \frac{1}{\alpha} f^h_a\,,\ \hat{h}^h_0 = \alpha^2 h^h_0\,,\ \hat{k}^h_{1,3} = \alpha^{3/2} k^h_{1,3}\,,\\
& \hat{k}^h_{2,2} = \alpha k^h_{2,2}\,, && \hat{k}^h_{2,4} = \alpha^2 k^h_{2,4}\,,\ \hat{k}^h_{3,1} = \alpha^{1/2} k^h_{3,1}\,,\ \hat{g}^h_0 = g^h_0\,.
\end{aligned} \tag{6.2}$$

Figure 24 presents all the IR parameters and select UV parameters ($f_{a,3,0}$ and $k_{2,3,0}$), see (6.1), of TypeB vacua in computational SchemeIII as functions of α. Extremal KS parameters are represented by dashed horizontal red lines and must agree with the corresponding TypeB parameters at $\alpha = 0$. While negative values of α are not physical, we run numerical codes for $\alpha < 0$ to extract more precisely this comparison at $\alpha = 0$. Extremal KS parameters in computational SchemeIII can be determined from (B.78) and (B.79)

JHEP05(2020)035

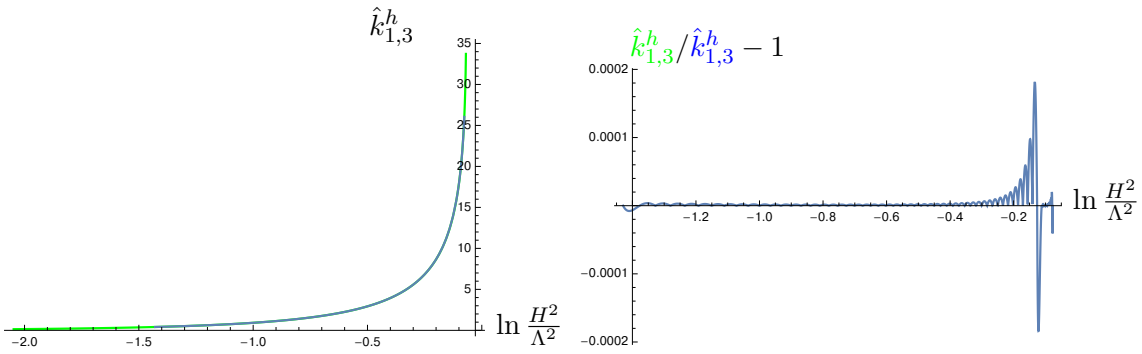

Figure 25. Left panel: infrared parameter $\hat{k}^h_{1,3}$ of the Fefferman-Graham coordinate frame of TypeB de Sitter vacua of the cascading gauge theory as functions of $\ln \frac{H^2}{\Lambda^2}$ in different computational schemes (6.2): SchemeI (blue) and Scheme III (green). Right panel: comparison of $\hat{k}^h_{1,3}$ (the computational scheme SchemeIII) with $\hat{k}^h_{1,3}$ (the computational scheme SchemeI).

provided we set

$$\begin{aligned} & K_0 = P^2 g_s \left(-\ln 3 + \frac{5}{3}\ \ln 2 - \frac{4}{3}\ \ln \epsilon - \frac{2}{3} \right) \Big|_{\text{SchemeIII}} = \frac{1}{4} \\ \Longrightarrow & \\ & \epsilon \Big|_{\text{SchemeIII}} = \frac{2}{3}\ 6^{1/4}\ e^{-11/16}\,. \end{aligned} \tag{6.3}$$

We find remarkable agreements, e.g.,

$$\frac{f^h_{a,0}(\alpha=0)}{f^h_{a,0}(KS)} - 1 \sim 5 \times 10^{-10}\,, \qquad \frac{k^h_{2,4}(\alpha=0)}{k^h_{2,4}(KS)} - 1 \sim 2 \times 10^{-10}\,. \tag{6.4}$$

The remaining parameters are validated at $\sim 10^{-6}$ level or better.

Following (6.2), we collect results of $\hat{k}^h_{1,3}$ as functions of $\ln \frac{H^2}{\Lambda^2}$ in different computational schemes in figure 25: SchemeI (blue curves) and Scheme III (green curves) (left panel); the accuracy of the collapsed results in different schemes is highlighted in right panel. Comparison of the remaining parameters follows the same trend. Note the degradation in accuracy as $\frac{H}{\Lambda}$ increases — in section 6.2 we relate this to the breakdown of the supergravity approximation.

6.2 Validity of supergravity approximation for TypeB vacua

As clear from figure 25 the accuracy in constructing TypeB vacua deteriorates as H increases; we have been able to construct TypeB vacua for

$$\ln \frac{H^2}{\Lambda^2} \leq -0.06(8) \qquad \Longrightarrow \qquad H \leq H^B_{\text{max}} = 0.966(5)\Lambda\,. \tag{6.5}$$

Besides numerical (technical) difficulties associated with construction of these vacua, there are conceptual ones, associated with the breakdown of the supergravity approximation — the effective action (2.1) becomes less reliable as the background space-time curvature

JHEP05(2020)035

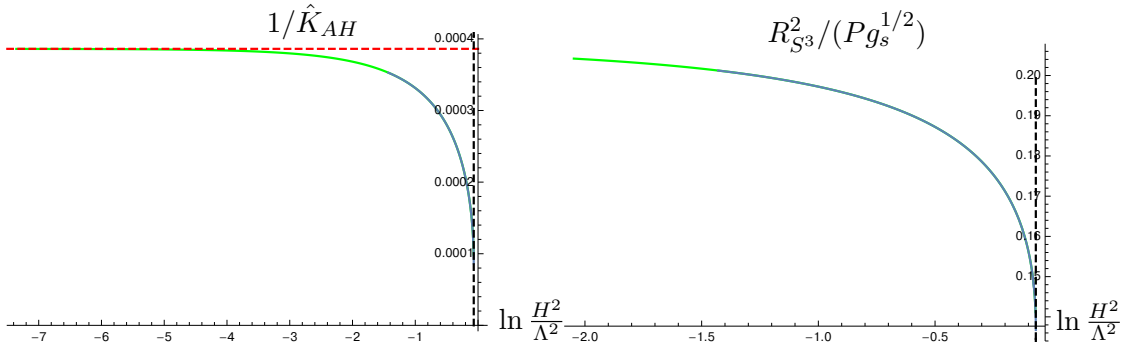

Figure 26. Left panel: inverse Kretschmann scalar of (2.13) evaluated at the apparent horizon for TypeB vacua as functions of $\ln \frac{H^2}{\Lambda^2}$ in different computation schemes (C.6): SchemeI (blue) and Scheme III (green). Horizontal red dashed line represents $\frac{1}{\hat{K}_{AH}}$ for the extremal KS solution, which is recovered in the limit $\frac{H}{\Lambda} \to 0$. Right panel: the divergence of the Kretschmann scalar as $H \to H^B_{\rm max}$ is associated with the collapse of the 3-cycle, see (6.7). Vertical black dashed lines represent $\frac{H^B_{\rm max}}{\Lambda}$.

of (2.13) grows. In figure 26 (left panel) we present the inverse Kretschmann scalar of (2.13) evaluated at the apparent horizon in different computations schemes, see appendix E, specifically (E.4):

$$\begin{aligned} \text{SchemeI}: \quad & \ln \frac{H^2}{\Lambda^2} = k_s\,, \qquad \hat{K} = K\,; \\ \text{SchemeIII}: \quad & \ln \frac{H^2}{\Lambda^2} = \frac{1}{4} + \ln \alpha\,, \quad \hat{K} = K\,. \end{aligned} \tag{6.6}$$

In the limit $\frac{H}{\Lambda} \to 0$ we recover the inverse Kretschmann scalar of the extremal KS solution (E.5), represented by a horizontal red dashed line. As H approached $H^B_{\rm max}$, represented by vertical dashed black line, the Kretschmann scalar at the AH of the holographic dual to TypeB de Sitter vacua of the cascading gauge theory appears to grow faster than any polynomial of $\Lambda/(H^B_{\rm max} - H)$ — we take $H^B_{\rm max}$ in (6.5) as the limiting value for the existence of TypeB vacua. In the right panel of figure 26 we associate the growth of the Kretschmann scalar in the limit $H \to H^B_{\rm max}$ with the collapse of the 3-cycle (the S^3 supporting the RR 3-form flux (2.6)) at the horizon, see (B.37),

$$R^2_{S^3} = \frac{f^h_{a,0}(h^h_0)^{1/2}}{3} = P g_s^{1/2}\, \frac{\hat{f}^h_{a,0}(\hat{h}^h_0)^{1/2}}{3}\,, \tag{6.7}$$

where in the second equality we used (C.5).

7 Conclusion

In this paper we presented a comprehensive analysis of the vacua structure of the cascading gauge theory in de Sitter. The cascading gauge theory in Minkowski space-time is characterized by a single modulus g_s and the strong coupling scale Λ; it confines with the spontaneous breaking of the chiral symmetry. de Sitter space-time presents a new mass scale — the Hubble constant H. There are three distinct types of de Sitter vacua

JHEP05(2020)035

of the theory — TypeA_s (resembling the thermal deconfined states of KS theory with the unbroken chiral symmetry), TypeA_b (resembling the thermal deconfined states of KS theory with the spontaneously broken chiral symmetry) and TypeB (resembling the thermal confined states of KS theory with the spontaneously broken chiral symmetry) — with the different (Euclidean) topology, and the global symmetry. All three types play a role of being an attractor of the late-time de Sitter dynamics, depending on the interplay of the strong coupling scale Λ and the Hubble constant H. We discover an intriguing pattern of the chiral symmetry breaking in the theory depending on the ratio $\frac{H}{\Lambda}$. While it is natural to expect that the chiral symmetry is spontaneously broken for sufficiently small $\frac{H}{\Lambda}$ (in fact, the extremal KS solution is a limiting case $\frac{H}{\Lambda} \to 0$), we find that the chiral symmetry is spontaneously broken as well when $H \in [H^b_{\rm min}, H_{\rm max}]$, with $\{H^b_{\rm min}, H_{\rm max}\} \sim \Lambda$. In the former case, TypeB de Sitter vacua, the vacuum entanglement entropy density vanishes[25] much like for the confining thermal states, while in the latter, TypeA$_b$ de Sitter vacua, the vacuum entanglement entropy is finite, much like for the thermal deconfined states. Since $H^s_{\rm min} < H^b_{\rm min}$, the chiral symmetry breaking and the confinement/deconfinement are two separate transitions in the cascading gauge theory in de Sitter. This is in contrast to thermal transitions in the cascading gauge theory in Minkowski space-time, where the chiral symmetry breaking is always accompanied by the confinement [13, 14].

There is a number of open questions and future directions:

- We argued that vacua TypeA$_s$ do not exist for sufficiently small $\frac{H}{\Lambda}$. It is important to rigorously establish this fact. Indeed, TypeA$_s$ vacua, unlike TypeB vacua, are characterized by the nonzero entanglement entropy density, and thus, when exist, will always dominate over TypeB vacua as the late-time dynamical attractors.

- We mentioned that TypeA$_b$ vacua resemble the thermal states of the deconfined cascading gauge theory with $\mathbb{Z}_2$ chiral symmetry. The holographic dual of these states is a Klebanov-Strassler black hole [14], which is unstable to local energy density perturbations — the sound waves in the cascading gauge theory plasma. It would be interesting to study the fate of spatial inhomogeneities in TypeA$_b$ de Sitter vacua.

- Ideally, we would like to develop numerical simulations of the cascading gauge theory in de Sitter, akin to the model studied in [24]. As a first step, it would be interesting to compute the spectrum (the quasinormal modes) of the chiral symmetry breaking fluctuations about TypeA$_s$ vacua for $H \in [H^b_{\rm min}, H_{\rm max}]$.

- It is important to explore the spontaneous symmetry breaking and the role played by the de Sitter vacuum entanglement entropy in other top-down examples of massive holography.

- In this paper we studied confinement/deconfinement and chiral symmetry breaking of strongly coupled gauge theories in de Sitter. It would be extremely interesting to pursue these questions in other curved background space-times, and specifically in anti-de Sitter.

[25] More precisely it is order $\mathcal{O}(N^0)$.

JHEP05(2020)035

There is an ample literature on the subject,[26] mostly from the field theory perspective. A natural starting point would be to understand the dynamics of $\mathcal{N}=2^*$ gauge theory in AdS_4, expanding on [35].

Acknowledgments

Research at Perimeter Institute is supported by the Government of Canada through Industry Canada and by the Province of Ontario through the Ministry of Research & Innovation. This work was further supported by NSERC through the Discovery Grants program.

A EF frame equations of motion

Within Eddington-Finkelstein metric ansatz (with spatially homogeneous and isotropic background metric of the cascading gauge theory — $d\boldsymbol{x}^2$)

$$ds_{10}^2 = 2dt\ (dr - A\ dt) + \Sigma^2\ d\boldsymbol{x}^2 + \Omega_1^2\ g_5^2 + \Omega_2^2\ (g_3^2+g_4^2) + \Omega_3^2\ (g_1^2+g_2^2)\,, \tag{A.1}$$

with

$$A = A(t,r)\,,\ \Sigma = \Sigma(t,r)\,,\ \Omega_i = \Omega_i(t,r)\,,\ K_i = K_i(t,r)\,,\ \Phi = \ln g(t,r)\,, \tag{A.2}$$

we find from (2.1) the following evolution ($' \equiv \partial_r$ and $d_+ \equiv \partial_t + A\partial_r$):

$$\begin{aligned}
0 =\ & (d_+\Sigma)' + \left(\frac{d_+\Omega_2}{\Omega_2} + \frac{d_+\Omega_3}{\Omega_3} + \frac{d_+\Omega_1}{2\Omega_1}\right)\Sigma' + \left(\frac{\Omega_2'}{\Omega_2} + \frac{\Omega_3'}{\Omega_3} + 2\frac{\Sigma'}{\Sigma} + \frac{\Omega_1'}{2\Omega_1}\right) d_+\Sigma \\
& - \frac{P^2 g\Sigma K_2'}{1296\Omega_2^2\Omega_3^2}\ d_+K_2 - \frac{\Sigma K_1'}{1152\Omega_3^4P^2g}\ d_+K_1 - \frac{\Sigma K_3'}{1152\Omega_2^4P^2g}\ d_+K_3 - \frac{\Sigma(K_1-K_3)^2}{4608\Omega_3^2\Omega_2^2\Omega_1^2P^2g} \\
& - \frac{P^2gK_2^2\Sigma(\Omega_2^4+\Omega_3^4)}{5184\Omega_2^4\Omega_1^2\Omega_3^4} + \frac{P^2gK_2\Sigma}{1296\Omega_2^4\Omega_1^2} - \frac{P^2g\Sigma}{1296\Omega_2^4\Omega_1^2} - \frac{\Sigma(K_1K_2-K_3K_2-2K_1)^2}{373248\Omega_1^2\Omega_2^4\Omega_3^4}\,,
\end{aligned} \tag{A.3}$$

$$\begin{aligned}
0 =\ & (d_+\Omega_1)' + \left(\frac{3\Sigma'}{2\Sigma} + \frac{\Omega_2'}{\Omega_2} + \frac{\Omega_3}{\Omega_3}\right) d_+\Omega_1 + \left(\frac{d_+\Omega_2}{\Omega_2} + \frac{d_+\Omega_3}{\Omega_3} + \frac{3d_+\Sigma}{2\Sigma}\right)\Omega_1' \\
& - \frac{K_1'\Omega_1}{1152P^2g\Omega_3^4}\ d_+K_1 - \frac{\Omega_1P^2gK_2'}{1296\Omega_3^2\Omega_2^2}\ d_+K_2 - \frac{\Omega_1K_3'}{1152\Omega_2^4P^2g}\ d_+K_3 + \frac{(K_3-K_1)^2}{1536\Omega_3^2\Omega_2^2\Omega_1P^2g} \\
& + \frac{(K_3K_2-K_1K_2+2K_1)^2}{373248\Omega_3^4\Omega_1\Omega_2^4} - \frac{(2\Omega_1^2+\Omega_2^2-\Omega_3^2)(2\Omega_1^2-\Omega_2^2+\Omega_3^2)}{8\Omega_3^2\Omega_2^2\Omega_1} + \frac{P^2gK_2^2(\Omega_2^4+\Omega_3^4)}{1728\Omega_3^4\Omega_1\Omega_2^4} \\
& - \frac{P^2gK_2}{432\Omega_1\Omega_2^4} + \frac{P^2g}{432\Omega_1\Omega_2^4}\,,
\end{aligned} \tag{A.4}$$

$$\begin{aligned}
0 =\ & (d_+\Omega_2)' + \left(\frac{\Omega_2'}{\Omega_2} + \frac{\Omega_3'}{\Omega_3} + \frac{3\Sigma'}{2\Sigma} + \frac{\Omega_1'}{2\Omega_1}\right) d_+\Omega_2 + \left(\frac{d_+\Omega_3}{\Omega_3} + \frac{d_+\Omega_1}{2\Omega_1} + \frac{3d_+\Sigma}{2\Sigma}\right)\Omega_2' \\
& + \frac{P^2gK_2'}{1296\Omega_2\Omega_3^2}\ d_+K_2 - \frac{\Omega_2K_1'}{1152\Omega_3^4P^2g}\ d_+K_1 + \frac{K_3'}{384\Omega_2^3P^2g}\ d_+K_3 + \frac{(K_1-K_3)^2}{4608\Omega_3^2\Omega_2\Omega_1^2P^2g}
\end{aligned} \tag{A.5}$$

[26] See e.g., [34] and references/citations there.

$$
\begin{aligned}
&- \frac{K_2^2 P^2 g(\Omega_2^4 - 3\Omega_3^4)}{5184\Omega_2^3\Omega_1^2\Omega_3^4} - \frac{K_2 P^2 g}{432\Omega_2^3\Omega_1^2} + \frac{P^2 g}{432\Omega_2^3\Omega_1^2} + \frac{(K_1K_2 - K_3K_2 - 2K_1)^2}{373248\Omega_2^3\Omega_1^2\Omega_3^4} \\
&+ \frac{4\Omega_1^4 - 8\Omega_1^2\Omega_3^2 - \Omega_2^4 + \Omega_3^4}{16\Omega_3^2\Omega_2\Omega_1^2}\,,
\end{aligned}
$$

$$
\begin{aligned}
0 = {} & (d_+\Omega_3)' + \left(\frac{\Omega_2'}{\Omega_2} + \frac{\Omega_3'}{\Omega_3} + \frac{3\Sigma'}{2\Sigma} + \frac{\Omega_1'}{2\Omega_1}\right) d_+\Omega_3 + \left(\frac{d_+\Omega_2}{\Omega_2} + \frac{d_+\Omega_1}{2\Omega_1} + \frac{3d_+\Sigma}{2\Sigma}\right) \Omega_3' \\
&+ \frac{P^2 g K_2'}{1296\Omega_2^2\Omega_3}\, d_+K_2 + \frac{K_1'}{384\Omega_3^3 P^2 g}\, d_+K_1 - \frac{\Omega_3 K_3'}{1152\Omega_2^4 P^2 g}\, d_+K_3 + \frac{(K_1 - K_3)^2}{4608\Omega_3\Omega_2^2\Omega_1^2 P^2 g} \\
&+ \frac{P^2 g K_2^2(3\Omega_2^4 - \Omega_3^4)}{5184\Omega_2^4\Omega_1^2\Omega_3^3} + \frac{P^2 g K_2\Omega_3}{1296\Omega_2^4\Omega_1^2} - \frac{P^2 g\Omega_3}{1296\Omega_2^4\Omega_1^2} + \frac{(K_1K_2 - K_3K_2 - 2K_1)^2}{373248\Omega_2^4\Omega_1^2\Omega_3^3} \\
&+ \frac{4\Omega_1^4 - 8\Omega_1^2\Omega_2^2 + \Omega_2^4 - \Omega_3^4}{16\Omega_3\Omega_2^2\Omega_1^2}\,,
\end{aligned} \tag{A.6}
$$

$$
\begin{aligned}
0 = {} & (d_+K_1)' + \left(\frac{d_+\Omega_2}{\Omega_2} - \frac{d_+\Omega_3}{\Omega_3} + \frac{d_+\Omega_1}{2\Omega_1} + \frac{3d_+\Sigma}{2\Sigma} - \frac{d_+g}{2g}\right) K_1' + \left(\frac{\Omega_2'}{\Omega_2} - \frac{\Omega_3'}{\Omega_3} + \frac{3\Sigma'}{2\Sigma}\right. \\
&\left. + \frac{\Omega_1'}{2\Omega_1} - \frac{g'}{2g}\right) d_+K_1 - \frac{\Omega_3^2(K_1 - K_3)}{4\Omega_2^2\Omega_1^2} - \frac{P^2 g(K_2 - 2)(K_1K_2 - K_3K_2 - 2K_1)}{648\Omega_2^4\Omega_1^2}\,,
\end{aligned} \tag{A.7}
$$

$$
\begin{aligned}
0 = {} & (d_+K_2)' + \left(\frac{d_+\Omega_1}{2\Omega_1} + \frac{3d_+\Sigma}{2\Sigma} + \frac{d_+g}{2g}\right) K_2' + \left(\frac{\Omega_1'}{2\Omega_1} + \frac{g'}{2g} + \frac{3\Sigma'}{2\Sigma}\right) d_+K_2 \\
&- \frac{(K_3 - K_1)(K_3K_2 - K_1K_2 + 2K_1)}{576\Omega_1^2\Omega_2^2\Omega_3^2 P^2 g} - \frac{K_2(\Omega_2^4 + \Omega_3^4)}{4\Omega_1^2\Omega_2^2\Omega_3^2} + \frac{\Omega_3^2}{2\Omega_1^2\Omega_2^2}\,,
\end{aligned} \tag{A.8}
$$

$$
\begin{aligned}
0 = {} & (d_+K_3)' + \left(\frac{3d_+\Sigma}{2\Sigma} - \frac{d_+g}{2g} - \frac{d_+\Omega_2}{\Omega_2} + \frac{d_+\Omega_3}{\Omega_3} + \frac{d_+\Omega_1}{2\Omega_1}\right) K_3' + \left(\frac{\Omega_3'}{\Omega_3} - \frac{\Omega_2'}{\Omega_2} + \frac{\Omega_1'}{2\Omega_1}\right. \\
&\left. - \frac{g'}{2g} + \frac{3\Sigma'}{2\Sigma}\right) d_+K_3 - \frac{\Omega_2^2(K_3 - K_1)}{4\Omega_3^2\Omega_1^2} - \frac{P^2 g K_2(K_3K_2 - K_1K_2 + 2K_1)}{648\Omega_1^2\Omega_3^4}\,,
\end{aligned} \tag{A.9}
$$

$$
\begin{aligned}
0 = {} & (d_+g)' + \left(\frac{d_+\Omega_2}{\Omega_2} + \frac{d_+\Omega_3}{\Omega_3} + \frac{d_+\Omega_1}{2\Omega_1} + \frac{3d_+\Sigma}{2\Sigma}\right) g' - \frac{P^2 g^2 K_2'}{324\Omega_2^2\Omega_3^2}\, d_+K_2 \\
&+ \frac{K_3'}{288\Omega_2^4 P^2}\, d_+K_3 + \frac{K_1'}{288\Omega_3^4 P^2}\, d_+K_1 + \left(\frac{\Omega_2'}{\Omega_2} + \frac{\Omega_3'}{\Omega_3} + \frac{\Omega_1'}{2\Omega_1} - \frac{g'}{g} + \frac{3\Sigma'}{2\Sigma}\right) d_+g \\
&+ \frac{(K_3 - K_1)^2}{1152\Omega_3^2\Omega_2^2\Omega_1^2 P^2} - \frac{P^2 g^2 K_2^2(\Omega_2^4 + \Omega_3^4)}{1296\Omega_1^2\Omega_2^4\Omega_3^4} + \frac{P^2 g^2 K_2}{324\Omega_1^2\Omega_2^4} - \frac{P^2 g^2}{324\Omega_1^2\Omega_2^4}\,,
\end{aligned} \tag{A.10}
$$

$$
\begin{aligned}
0 = {} & A'' - \left(\frac{2\Omega_2'}{\Omega_1\Omega_2} + \frac{2\Omega_3'}{\Omega_1\Omega_3} + \frac{3\Sigma'}{\Sigma\Omega_1}\right) d_+\Omega_1 - \left(\frac{2\Omega_2'}{\Omega_2^2} + \frac{4\Omega_3'}{\Omega_2\Omega_3} + \frac{6\Sigma'}{\Sigma\Omega_2} + \frac{2\Omega_1'}{\Omega_1\Omega_2}\right) d_+\Omega_2 \\
&- \left(\frac{4\Omega_2'}{\Omega_2\Omega_3} + \frac{2\Omega_3'}{\Omega_3^2} + \frac{6\Sigma'}{\Sigma\Omega_3} + \frac{2\Omega_1'}{\Omega_1\Omega_3}\right) d_+\Omega_3 - \left(\frac{6\Omega_2'}{\Omega_2\Sigma} + \frac{6\Omega_3'}{\Omega_3\Sigma} + \frac{6\Sigma'}{\Sigma^2} + \frac{3\Omega_1'}{\Omega_1\Sigma}\right) d_+\Sigma \\
&+ \frac{g'}{2g^2}\, d_+g + \frac{P^2 g K_2'}{648\Omega_2^2\Omega_3^2}\, d_+K_2 + \frac{K_1'}{576\Omega_3^4 P^2 g}\, d_+K_1 + \frac{K_3'}{576\Omega_2^4 P^2 g}\, d_+K_3 \\
&- \frac{(K_1 - K_3)^2}{768\Omega_3^2\Omega_2^2\Omega_1^2 P^2 g} - \frac{P^2 g K_2^2(\Omega_2^4 + \Omega_3^4)}{864\Omega_2^4\Omega_1^2\Omega_3^4} + \frac{P^2 g K_2}{216\Omega_2^4\Omega_1^2} - \frac{P^2 g}{216\Omega_2^4\Omega_1^2} \\
&- \frac{(K_1K_2 - K_3K_2 - 2K_1)^2}{93312\Omega_1^2\Omega_2^4\Omega_3^4} - \frac{4\Omega_1^4 - 8\Omega_1^2\Omega_2^2 - 8\Omega_1^2\Omega_3^2 + \Omega_2^4 - 2\Omega_2^2\Omega_3^2 + \Omega_3^4}{8\Omega_2^2\Omega_3^2\Omega_1^2}\,;
\end{aligned} \tag{A.11}
$$

JHEP05(2020)035

and the constraint equations

$$0=\Sigma''+\frac{\Sigma}{6}\left(\frac{(g')^2}{g^2}+\frac{4\Omega_3''}{\Omega_3}+\frac{4\Omega_2''}{\Omega_2}+\frac{2\Omega_1''}{\Omega_1}+\frac{P^2g(K_2')^2}{162\Omega_3^2\Omega_2^2}+\frac{(K_3')^2}{144P^2g\Omega_2^4}+\frac{(K_1')^2}{144P^2g\Omega_3^4}\right), \tag{A.12}$$

$$\begin{aligned}0=&d_+^2\Sigma+\frac{\Sigma}{3\Omega_1}\,d_+^2\Omega_1+\frac{2\Sigma}{3\Omega_2}\,d_+^2\Omega_2+\frac{2\Sigma}{3\Omega_3}\,d_+^2\Omega_3-\left(\frac{\Sigma}{3\Omega_1}\,d_+\Omega_1+\frac{2\Sigma}{3\Omega_2}\,d_+\Omega_2\right.\\&\left.+\frac{2\Sigma}{3\Omega_3}\,d_+\Omega_3+d_+\Sigma\right)A'+\frac{\Sigma P^2g}{972\Omega_2^2\Omega_3^2}\,(d_+K_2)^2+\frac{\Sigma}{864\Omega_2^4P^2g}\,(d_+K_3)^2\\&+\frac{\Sigma}{864\Omega_3^4P^2g}\,(d_+K_1)^2+\frac{\Sigma}{6g^2}\,(d_+g)^2.\end{aligned} \tag{A.13}$$

To derive the late-time geometry dual to the cascading gauge theory vacuum in de Sitter, we introduce following [19]

$$\lim_{t\to\infty}\left\{A(t,r)\,,\,\frac{\Sigma(t,r)}{e^{Ht}}\,,\,K_i(t,r)\,,\,g(t,r)\right\}=\{a(r)\,,\,\sigma(r)\,,\,K_i(r)\,,\,g(r)\}\;; \tag{A.14}$$

furthermore,

$$\lim_{t\to\infty}\left\{\Omega_1^2(t,r)\,,\,\Omega_2^2(t,r)\,,\,\Omega_3^2(t,r)\right\}=\left\{\frac{1}{9}w_{c2}(r)\,,\,\frac{1}{6}w_{a2}(r)\,,\,\frac{1}{6}w_{b2}(r)\right\}. \tag{A.15}$$

We find from (A.3)–(A.13) in the $t\to\infty$ limit 9 second order ODEs:

$$\begin{aligned}0=&\sigma''+\frac{5(\sigma')^2}{4\sigma}+\frac{5a'\sigma'}{8a}+\frac{\sigma}{16}\left(\frac{2\sigma'}{\sigma}-\frac{a'}{a}\right)\left(\frac{w_{c2}'}{w_{c2}}+\frac{2w_{a2}'}{w_{a2}}+\frac{2w_{b2}'}{w_{b2}}\right)+\frac{H\sigma}{16a}\left(\frac{30\sigma'}{\sigma}+\frac{w_{c2}'}{w_{c2}}\right.\\&\left.+\frac{2w_{a2}'}{w_{a2}}+\frac{2w_{b2}'}{w_{b2}}\right)-\frac{\sigma}{8}\left(\frac{1}{2}\left(\frac{w_{a2}'}{w_{a2}}+\frac{w_{b2}'}{w_{b2}}\right)^2+\frac{w_{a2}'w_{b2}'}{w_{a2}w_{b2}}+\frac{w_{a2}'w_{c2}'}{w_{a2}w_{c2}}+\frac{w_{c2}'w_{b2}'}{w_{c2}w_{b2}}\right)+\frac{\sigma(g')^2}{16g^2}\\&-\frac{2gP^2(K_2')^2}{9w_{b2}w_{a2}}-\frac{(K_3')^2}{4gP^2w_{a2}^2}-\frac{(K_1')^2}{4gP^2w_{b2}^2}-\frac{27\sigma(K_3-K_1)^2}{256w_{b2}w_{a2}aw_{c2}gP^2}-\frac{\sigma}{128aw_{b2}^2w_{a2}^2w_{c2}}\\&\times\left(5K_2^2(K_3-K_1)^2+2w_{b2}w_{a2}(9w_{b2}^2-18w_{b2}w_{a2}-48w_{b2}w_{c2}+9w_{a2}^2-48w_{a2}w_{c2}+16w_{c2}^2)\right.\\&\left.+20K_1(K_3K_2-K_1K_2+K_1)\right)-\frac{3\sigma gP^2(K_2(w_{b2}^2K_2+w_{a2}^2K_2-4w_{b2}^2)+4w_{b2}^2)}{32aw_{b2}^2w_{a2}^2w_{c2}};\end{aligned} \tag{A.16}$$

$$\begin{aligned}0=&a''+\frac{21a'\sigma'}{4\sigma}+\frac{a}{8}\left(\frac{18\sigma'}{\sigma}+\frac{7a'}{a}\right)\left(\frac{w_{c2}'}{w_{c2}}+\frac{2w_{a2}'}{w_{a2}}+\frac{2w_{b2}'}{w_{b2}}\right)+\frac{3H}{8}\left(\frac{26\sigma'}{\sigma}+\frac{3w_{c2}'}{w_{c2}}\right.\\&\left.+\frac{6w_{a2}'}{w_{a2}}+\frac{6w_{b2}'}{w_{b2}}\right)+\frac{3a}{8}\left(\frac{12(\sigma')^2}{\sigma^2}+\frac{2w_{a2}'w_{c2}'}{w_{a2}w_{c2}}+\frac{2w_{c2}'w_{b2}'}{w_{c2}w_{b2}}+\frac{2w_{a2}'w_{b2}'}{w_{a2}w_{b2}}+\left(\frac{w_{a2}}{w_{a2}}+\frac{w_{b2}'}{w_{b2}}\right)^2\right)\\&-\frac{3(g')^2a}{8g^2}-\frac{5a}{32}\left(\frac{8gP^2(K_2')^2}{9w_{b2}w_{a2}}+\frac{(K_3')^2}{gP^2w_{a2}^2}+\frac{(K_1')^2}{gP^2w_{b2}^2}\right)+\frac{9(K_3-K_1)^2}{128w_{b2}w_{a2}w_{c2}gP^2}\\&-\frac{1}{64w_{c2}w_{a2}^2w_{b2}^2}\left(K_2^2(K_3-K_1)^2-6w_{b2}w_{a2}(9w_{b2}^2-18w_{b2}w_{a2}-48w_{b2}w_{c2}+9w_{a2}^2\right.\\&\left.-48w_{a2}w_{c2}+16w_{c2}^2)+4K_1((K_3-K_1)K_2+K_1)\right)+\frac{gP^2}{16w_{c2}w_{b2}^2w_{a2}^2}\left((w_{a2}^2+w_{b2}^2)K_2^2\right.\\&\left.+4(1-K_2)w_{b2}^2\right);\end{aligned} \tag{A.17}$$

JHEP05(2020)035

$$0 = w_{a2}'' + \frac{w_{a2}a'}{8a}\left(\frac{6w_{a2}'}{w_{a2}} - \frac{6\sigma'}{\sigma} - \frac{2w_{b2}'}{w_{b2}} - \frac{w_{c2}'}{w_{c2}}\right) - \frac{w_{a2}}{8}\left(\frac{(w_{a2}')^2}{w_{a2}^2} - \frac{4w_{a2}'w_{b2}'}{w_{a2}w_{b2}} + \frac{(w_{b2}')^2}{w_{b2}^2}\right. \tag{A.18}$$
$$\left. - \frac{12w_{a2}'\sigma'}{w_{a2}\sigma} + \frac{12w_{b2}'\sigma'}{\sigma w_{b2}} + \frac{12(\sigma')^2}{\sigma^2} - \frac{2w_{a2}'w_{c2}'}{w_{a2}w_{c2}}) + \frac{2w_{c2}'w_{b2}'}{w_{c2}w_{b2}} + \frac{6w_{c2}'\sigma'}{\sigma w_{c2}}\right) + \frac{(g')^2 w_{a2}}{8g^2}$$
$$+ \frac{gP^2(K_2')^2}{12w_{b2}} - \frac{w_{a2}(K_1')^2}{32w_{b2}^2 gP^2} + \frac{7(K_3')^2}{32w_{a2}gP^2} + \frac{3Hw_{a2}}{8a}\left(\frac{2w_{a2}'}{w_{a2}} - \frac{2w_{b2}'}{w_{b2}} - \frac{6\sigma'}{\sigma} - \frac{w_{c2}'}{w_{c2}}\right)$$
$$+ \frac{9(K_3-K_1)^2}{128w_{b2}w_{c2}agP^2} + \frac{3}{64w_{b2}^2 w_{c2}w_{a2}a}\left(K_2^2(K_3-K_1)^2 + 2w_{b2}w_{a2}(16w_{c2}^2 - 48w_{c2}w_{b2}\right.$$
$$\left. + 16w_{a2}w_{c2} + 9w_{b2}^2 + 6w_{a2}w_{b2} - 15w_{a2}^2) + 4K_1(K_3K_2 - K_1K_2 + K_1)\right)$$
$$+ \frac{gP^2}{16w_{b2}^2 w_{c2}w_{a2}a}\left(K_2^2(5w_{b2}^2 - 3w_{a2}^2) + 20(1-K_2)w_{b2}^2\right);$$

$$0 = w_{b2}'' + \frac{a'w_{b2}}{8a}\left(\frac{6w_{b2}'}{w_{b2}} - \frac{6\sigma'}{\sigma} - \frac{2w_{a2}'}{w_{a2}} - \frac{w_{c2}'}{w_{c2}}\right) - \frac{w_{b2}}{8}\left(\frac{(w_{a2}')^2}{w_{a2}^2} - \frac{4w_{a2}'w_{b2}'}{w_{a2}w_{b2}} + \frac{(w_{b2}')^2}{w_{b2}^2}\right. \tag{A.19}$$
$$\left. + \frac{12w_{a2}'\sigma'}{w_{a2}\sigma} - \frac{12w_{b2}'\sigma'}{\sigma w_{b2}} + \frac{12(\sigma')^2}{\sigma^2} + \frac{2w_{a2}'w_{c2}'}{w_{a2}w_{c2}} - \frac{2w_{c2}'w_{b2}'}{w_{c2}w_{b2}} + \frac{6w_{c2}'\sigma'}{\sigma w_{c2}}\right) + \frac{(g')^2 w_{b2}}{8g^2}$$
$$+ \frac{gP^2(K_2')^2}{12w_{a2}} + \frac{7(K_1')^2}{32w_{b2}gP^2} - \frac{w_{b2}(K_3')^2}{32w_{a2}^2 gP^2} - \frac{3Hw_{b2}}{8a}\left(\frac{2w_{a2}'}{w_{a2}} - \frac{2w_{b2}'}{w_{b2}} + \frac{6\sigma'}{\sigma} + \frac{w_{c2}'}{w_{c2}}\right)$$
$$+ \frac{9(K_3-K_1)^2}{128w_{a2}gP^2 w_{c2}a} + \frac{3}{64w_{b2}w_{a2}^2 w_{c2}a}\left(K_2^2(K_3-K_1)^2 + 2w_{a2}w_{b2}(16w_{c2}^2 + 16w_{c2}w_{b2}\right.$$
$$\left. - 48w_{a2}w_{c2} - 15w_{b2}^2 + 6w_{a2}w_{b2} + 9w_{a2}^2) + 4K_1(K_3K_2 - K_1K_2 + K_1)\right)$$
$$- \frac{gP^2}{16w_{b2}w_{a2}^2 w_{c2}a}\left(K_2^2(3w_{b2}^2 - 5w_{a2}^2) + 12(1-K_2)w_{b2}^2\right);$$

$$0 = w_{c2}'' - \frac{w_{c2}a'}{8a}\left(\frac{2w_{b2}'}{w_{b2}} + \frac{6\sigma'}{\sigma} - \frac{7w_{c2}'}{w_{c2}} + \frac{2w_{a2}'}{w_{a2}}\right) - \frac{w_{c2}}{8}\left(\frac{(w_{a2}')^2}{w_{a2}^2} + \frac{4w_{a2}'w_{b2}'}{w_{a2}w_{b2}} + \frac{(w_{b2}')^2}{w_{b2}^2}\right. \tag{A.20}$$
$$\left. + \frac{12w_{a2}'\sigma'}{w_{a2}\sigma} + \frac{12w_{b2}'\sigma'}{\sigma w_{b2}} + \frac{12(\sigma')^2}{\sigma^2} - \frac{6w_{a2}'w_{c2}'}{w_{a2}w_{c2}} - \frac{6w_{c2}'w_{b2}'}{w_{c2}w_{b2}} - \frac{18w_{c2}'\sigma'}{\sigma w_{c2}} + \frac{4(w_{c2}')^2}{w_{c2}^2}\right)$$
$$+ \frac{(g')^2 w_{c2}}{8g^2} - \frac{w_{c2}gP^2(K_2')^2}{36w_{b2}w_{a2}} - \frac{w_{c2}(K_1')^2}{32w_{b2}^2 gP^2} - \frac{w_{c2}(K_3')^2}{32w_{a2}^2 gP^2} - \frac{3Hw_{c2}}{8a}\left(\frac{2w_{a2}'}{w_{a2}} + \frac{2w_{b2}'}{w_{b2}} + \frac{6\sigma'}{\sigma}\right.$$
$$\left. - \frac{3w_{c2}'}{w_{c2}}\right) + \frac{45(K_3-K_1)^2}{128w_{a2}w_{b2}gP^2 a} + \frac{3}{64w_{b2}^2 w_{a2}^2 a}\left(K_2^2(K_3-K_1)^2 - 2w_{a2}w_{b2}(48w_{c2}^2\right.$$
$$\left. - 16w_{c2}w_{b2} - 16w_{a2}w_{c2} - 21w_{b2}^2 + 42w_{a2}w_{b2} - 21w_{a2}^2) + 4K_1(K_3K_2 - K_1K_2 + K_1)\right)$$
$$+ \frac{5gP^2}{16w_{b2}^2 w_{a2}^2 a}\left(K_2^2(w_{b2}^2 + w_{a2}^2) + 4(1-K_2)w_{b2}^2\right);$$

$$0 = K_1'' + \left(\frac{3H}{2a} + \frac{w_{a2}'}{w_{a2}} + \frac{w_{c2}'}{2w_{c2}} - \frac{w_{b2}'}{w_{b2}} + \frac{3\sigma'}{\sigma} + \frac{a'}{a} - \frac{g'}{g}\right)K_1' - \frac{9w_{b2}(K_1-K_3)}{4w_{a2}aw_{c2}} \tag{A.21}$$
$$- \frac{(K_2-2)(K_2K_1 - K_2K_3 - 2K_1)gP^2}{2aw_{c2}w_{a2}^2};$$

JHEP05(2020)035

$$0 = K_2'' + \left(\frac{a'}{a} + \frac{3H}{2a} + \frac{w_{c2}'}{2w_{c2}} + \frac{g'}{g} + \frac{3\sigma'}{\sigma}\right)K_2' - \frac{9(K_1-K_3)(K_2(K_1-K_3)-2K_1)}{16w_{a2}w_{b2}gP^2w_{c2}a} \tag{A.22}$$
$$- \frac{9((w_{a2}^2+w_{b2}^2)K_2-2w_{b2}^2)}{4w_{a2}w_{b2}w_{c2}a};$$
$$0 = K_3'' + \left(\frac{3H}{2a} - \frac{w_{a2}'}{w_{a2}} + \frac{3\sigma'}{\sigma} + \frac{w_{c2}'}{2w_{c2}} + \frac{w_{b2}'}{w_{b2}} + \frac{a'}{a} - \frac{g'}{g}\right)K_3' + \frac{9w_{a2}(K_1-K_3)}{4w_{b2}aw_{c2}} \tag{A.23}$$
$$+ \frac{K_2(K_2(K_1-K_3)-2K_1)gP^2}{2aw_{b2}^2w_{c2}};$$
$$0 = g'' + \left(\frac{3H}{2a} + \frac{a'}{a} + \frac{w_{c2}'}{2w_{c2}} - \frac{g'}{g} + \frac{w_{b2}'}{w_{b2}} + \frac{w_{a2}'}{w_{a2}} + \frac{3\sigma'}{\sigma}\right)g' - \frac{g^2P^2(K_2')^2}{9w_{b2}w_{a2}} + \frac{(K_1')^2}{8P^2w_{b2}^2} \tag{A.24}$$
$$+ \frac{(K_3')^2}{8P^2w_{a2}^2} + \frac{9(K_1-K_3)^2}{32aw_{b2}w_{c2}w_{a2}P^2} - \frac{g^2P^2(K_2^2(w_{a2}^2+w_{b2}^2)+4(1-K_2)w_{b2}^2)}{4w_{b2}^2aw_{c2}w_{a2}^2},$$

and 2 first order ODEs:

$$0 = \sigma' + \frac{\sigma}{2a}\left(H - a'\right); \tag{A.25}$$
$$0 = \frac{(g')^2}{g^2} - \frac{3H}{a}\left(\frac{2w_{b2}'}{w_{b2}} + \frac{4\sigma'}{\sigma} + \frac{2w_{a2}'}{w_{a2}} + \frac{w_{c2}'}{w_{c2}} + \frac{a'}{a} - \frac{H}{a}\right) - \frac{2w_{a2}'a'}{aw_{a2}} - \frac{6\sigma'a'}{\sigma a} - \frac{4w_{b2}'w_{a2}'}{w_{b2}w_{a2}} \tag{A.26}$$
$$- \frac{12w_{b2}'\sigma'}{\sigma w_{b2}} - \frac{12w_{a2}'\sigma'}{\sigma w_{a2}} - \frac{2w_{b2}'a'}{aw_{b2}} - \frac{6w_{c2}'\sigma'}{\sigma w_{c2}} - \frac{w_{c2}'a'}{aw_{c2}} - \frac{2w_{b2}'w_{c2}'}{w_{b2}w_{c2}} - \frac{2w_{c2}'w_{a2}'}{w_{c2}w_{a2}} - \frac{(w_{b2}')^2}{w_{b2}^2}$$
$$- \frac{12(\sigma')^2}{\sigma^2} - \frac{(w_{a2}')^2}{w_{a2}^2} + \frac{2P^2g(K_2')^2}{9w_{b2}w_{a2}} + \frac{(K_1')^2}{4w_{b2}^2P^2g} + \frac{(K_3')^2}{4w_{a2}^2P^2g} - \frac{9(K_1-K_3)^2}{16aw_{c2}gP^2w_{b2}w_{a2}}$$
$$- \frac{1}{8aw_{b2}^2w_{c2}w_{a2}^2}\Big(K_2^2(K_1-K_3)^2 + 2w_{a2}w_{b2}(9w_{a2}^2 - 18w_{b2}w_{a2} - 48w_{c2}w_{a2} + 9w_{b2}^2$$
$$- 48w_{b2}w_{c2} + 16w_{c2}^2) - 4K_1((K_1-K_3)K_2 - K_1)\Big) - \frac{P^2g}{2w_{b2}^2aw_{c2}w_{a2}^2}\Big(K_2^2(w_{a2}^2+w_{b2}^2)$$
$$+ 4(1-K_2)w_{b2}^2\Big).$$

It is straightforward to verify the (A.16)–(A.24) are consistent with (A.25)–(A.26); thus the latter ODEs can be used for drop (A.16) and (A.20) and eliminate σ' and w_{c2}' in the remaining second order ODEs.

The cascading gauge theory de Sitter vacuum equations of motion (A.16)–(A.26) are invariant under the following symmetries ($\lambda \equiv$ const),

- symmetry SEF1:

$$r \to r+\lambda, \qquad \{H, P, a, \sigma, w_{a2,b2,c2}, K_{1,2,3}, g\} \to \{H, P, a, \sigma, w_{a2,b2,c2}, K_{1,2,3}, g\}\ ; \tag{A.27}$$

- symmetry SEF2:

$$P \to \lambda P, \qquad g \to \frac{g}{\lambda}, \quad \{r, H, a, \sigma, w_{a2,b2,c2}, K_{1,2,3}\} \to \{r, H, a, \sigma, w_{a2,b2,c2}, K_{1,2,3}\}\ ; \tag{A.28}$$

JHEP05(2020)035

- symmetry SEF3:

$$\begin{aligned}\{P,r,a,w_{a2,b2,c2}\} &\to \lambda\{P,r,a,w_{a2,b2,c2}\}\,, \qquad \sigma \to \lambda^{1/2}\sigma\,, \qquad \{K_{1,3}\} \to \lambda^2\{K_{1,3}\}\,,\\ \{H,K_2,g\} &\to \{H,K_2,g\}\,;\end{aligned} \tag{A.29}$$

- symmetry SEF4:

$$\begin{aligned}\{r,H\} &\to \lambda\{r,H\}\,, \qquad \{P,\sigma,w_{a2,b2,c2},K_{1,2,3},g\} \to \{P,\sigma,w_{a2,b2,c2},K_{1,2,3},g\}\\ a &\to \lambda^2 a\,.\end{aligned} \tag{A.30}$$

B FG frame equations of motion, asymptotics, relation to EF frame and extremal Klebanov-Strassler solution

Fefferman-Graham frame can be used to describe only (the patch of) the gravitational dual to the cascading gauge theory de Sitter vacua. It is useful to setup the asymptotic boundary conditions, analytical continuation to Euclidean (Bunch-Davies) vacua, and study the $H \to 0$ limit in which one recovers the KS solution [2].

Within the metric ansatz

$$\begin{aligned}ds_{10}^2 &= \frac{1}{h^{1/2}\rho^2}\left(d\mathcal{M}_4^{f,c}\right)^2 + \frac{h^{1/2}}{\rho^2}(d\rho)^2 + \frac{f_c h^{1/2}}{9}g_5^2 + \frac{f_a h^{1/2}}{6}(g_3^2+g_4^2) + \frac{f_b h^{1/2}}{6}(g_1^2+g_2^2)\\ \left(d\mathcal{M}_4^f\right)^2 &= -d\tau^2 + e^{2H\tau}d\boldsymbol{x}^2\,, \qquad (d\mathcal{M}_4^c)^2 = -d\tau^2 + \frac{1}{H^2}\cosh^2(H\tau)\left(dS^3\right)^2\,,\end{aligned} \tag{B.1}$$

where we used the FG frame time τ and the radial coordinate ρ to distinguish them from the EF frame time t and the radial coordinate r in (A.1),

$$f_{a,b,c} = f_{a,b,c}(\rho)\,, \qquad h = h(\rho)\,, \qquad K_{1,2,3} = K_{1,2,3}(\rho)\,, \qquad g = g(\rho)\,, \tag{B.2}$$

we find the following equations of motion (independent of whether we use the flat boundary spatial slicing $\left(d\mathcal{M}_4^f\right)^2$ or the closed boundary spatial slicing $(d\mathcal{M}_4^c)^2$) describing de Sitter vacuum of the cascading gauge theory [31]:

$$\begin{aligned}0 = {} & f_c'' - \frac{3f_c'}{\rho} - 3hf_cH^2 - \frac{(f_c')^2}{2f_c} + \frac{5f_c}{\rho^2} + \frac{f_c(g')^2}{8g^2} + \frac{3f_b'f_c'}{4f_b} + \frac{63f_a}{16f_b\rho^2} + \frac{63f_b}{16f_a\rho^2} + \frac{3f_c}{f_a\rho^2}\\ & - \frac{f_c(f_a')^2}{8f_a^2} + \frac{3f_a'f_c'}{4f_a} + \frac{f_c(h')^2}{8h^2} - \frac{f_c(f_b')^2}{8f_b^2} + \frac{3f_c}{f_b\rho^2} - \frac{63}{8\rho^2} - \frac{K_1^2}{8f_a^2h^2f_b^2\rho^2} + \frac{3gP^2}{2f_a^2h\rho^2}\\ & - \frac{f_cf_a'f_b'}{2f_af_b} - \frac{27K_1K_3}{32f_ahf_bgP^2\rho^2} - \frac{K_2^2K_1^2}{32f_a^2h^2f_b^2\rho^2} + \frac{K_2K_1^2}{8f_a^2h^2f_b^2\rho^2} - \frac{K_2^2K_3^2}{32f_a^2h^2f_b^2\rho^2} - \frac{3f_c(K_1')^2}{32hf_b^2gP^2}\\ & - \frac{3f_c(K_3')^2}{32f_a^2hgP^2} + \frac{3gP^2K_2^2}{8hf_b^2\rho^2} + \frac{3gP^2K_2^2}{8f_a^2h\rho^2} - \frac{3gP^2K_2}{2f_a^2h\rho^2} - \frac{9f_c^2}{f_af_b\rho^2} + \frac{f_ch'}{h\rho} + \frac{K_2^2K_1K_3}{16f_a^2h^2f_b^2\rho^2}\\ & - \frac{K_2K_1K_3}{8f_a^2h^2f_b^2\rho^2} - \frac{gP^2f_c(K_2')^2}{12f_ahf_b} + \frac{27K_1^2}{64f_ahf_bgP^2\rho^2} + \frac{27K_3^2}{64f_ahf_bgP^2\rho^2}\,,\\ 0 = {} & f_a'' - \frac{45f_a^2}{16f_cf_b\rho^2} + \frac{f_ah'}{h\rho} + \frac{gP^2(K_2')^2}{36hf_b} + \frac{5(K_3')^2}{32f_ahgP^2} - \frac{f_af_b'f_c'}{4f_cf_b} - \frac{(f_a')^2}{8f_a} + \frac{5f_a}{\rho^2} - \frac{3f_a'}{\rho}\\ & - \frac{K_2^2K_1^2}{32f_cf_ah^2f_b^2\rho^2} + \frac{K_2K_1^2}{8f_cf_ah^2f_b^2\rho^2} - \frac{K_2^2K_3^2}{32f_cf_ah^2f_b^2\rho^2} - \frac{3gP^2K_2}{2f_cf_ah\rho^2} + \frac{3gP^2K_2^2}{8f_cf_ah\rho^2}\end{aligned} \tag{B.3}$$

JHEP05(2020)035

$$
\begin{aligned}
&- \frac{9K_3^2}{64f_c h f_b g P^2 \rho^2} - \frac{9K_1^2}{64f_c h f_b g P^2 \rho^2} + \frac{3f_a}{f_b \rho^2} + \frac{3f_c}{f_b \rho^2} + \frac{9K_1 K_3}{32 f_c h f_b g P^2 \rho^2} + \frac{K_2^2 K_1 K_3}{16 f_c f_a h^2 f_b^2 \rho^2} \\
&- \frac{K_2 K_1 K_3}{8 f_c f_a h^2 f_b^2 \rho^2} - \frac{5 f_a g P^2 K_2^2}{8 f_c h f_b^2 \rho^2} - \frac{K_1^2}{8 f_c f_a h^2 f_b^2 \rho^2} + \frac{3gP^2}{2 f_c f_a h \rho^2} - \frac{3 f_a (K_1')^2}{32 h f_b^2 g P^2} - \frac{9}{\rho^2} + \frac{f_a (g')^2}{8g^2} \\
&- 3 f_a h H^2 + \frac{f_a' f_b'}{2 f_b} + \frac{f_c' f_a'}{4 f_c} - \frac{f_a (f_b')^2}{8 f_b^2} + \frac{9 f_a}{8 f_c \rho^2} + \frac{f_a (h')^2}{8h^2} + \frac{27 f_b}{16 f_c \rho^2}\,, \qquad \text{(B.4)}
\end{aligned}
$$

$$
\begin{aligned}
0 = {} & f_b'' - \frac{3f_b'}{\rho} - \frac{(f_b')^2}{8f_b} + \frac{5f_b}{\rho^2} - \frac{45 f_b^2}{16 f_c f_a \rho^2} + \frac{f_b h'}{h\rho} - \frac{K_1^2}{8 f_c h^2 f_a^2 f_b \rho^2} - \frac{3 f_b (K_3')^2}{32 h g f_a^2 P^2} \\
&- \frac{K_2^2 K_1^2}{32 f_c h^2 f_a^2 f_b \rho^2} + \frac{K_2 K_1^2}{8 f_c h^2 f_a^2 f_b \rho^2} - \frac{K_2^2 K_3^2}{32 f_c h^2 f_a^2 f_b \rho^2} - \frac{9K_1^2}{64 f_c h g f_a P^2 \rho^2} + \frac{3gP^2 K_2^2}{f_c h f_b \rho^2} \\
&- \frac{9K_3^2}{64 f_c h g f_a P^2 \rho^2} - \frac{5 g f_b P^2}{2 f_c h f_a^2 \rho^2} + \frac{3 f_b}{f_a \rho^2} + \frac{3 f_c}{f_a \rho^2} - \frac{f_b f_c' f_a'}{4 f_c f_a} + \frac{5 (K_1')^2}{32 h g f_b P^2} + \frac{g P^2 (K_2')^2}{36 h f_a} \\
&- \frac{9}{\rho^2} + \frac{27 f_a}{16 f_c \rho^2} + \frac{9 f_b}{8 f_c \rho^2} + \frac{K_2^2 K_1 K_3}{16 f_c h^2 f_a^2 f_b \rho^2} - \frac{K_2 K_1 K_3}{8 f_c h^2 f_a^2 f_b \rho^2} + \frac{5 g f_b P^2 K_2}{2 f_c h f_a^2 \rho^2} - \frac{5 g f_b P^2 K_2^2}{8 f_c h f_a^2 \rho^2} \\
&+ \frac{9 K_1 K_3}{32 f_c h g f_a P^2 \rho^2} + \frac{f_b (g')^2}{8g^2} - 3 h f_b H^2 + \frac{f_a' f_b'}{2 f_a} - \frac{f_b (f_a')^2}{8 f_a^2} + \frac{f_b' f_c'}{4 f_c} + \frac{f_b (h')^2}{8h^2}\,, \qquad \text{(B.5)}
\end{aligned}
$$

$$
\begin{aligned}
0 = {} & h'' + \frac{K_2^2 K_1^2}{4 f_c f_a^2 f_b^2 h \rho^2} - \frac{K_2 K_1^2}{f_c f_a^2 f_b^2 h \rho^2} + \frac{K_2^2 K_3^2}{4 f_c f_a^2 f_b^2 h \rho^2} + \frac{9 K_1^2}{16 f_c f_a f_b \rho^2 g P^2} + \frac{9 K_3^2}{16 f_c f_a f_b \rho^2 g P^2} \\
&+ \frac{2h f_c'}{f_c \rho} + \frac{4h f_b'}{f_b \rho} + \frac{4h f_a'}{f_a \rho} + \frac{(K_1')^2}{8 f_b^2 g P^2} + \frac{(K_3')^2}{8 f_a^2 g P^2} + \frac{g P^2 K_2^2}{2 f_c f_b^2 \rho^2} + \frac{g P^2 K_2^2}{2 f_c f_a^2 \rho^2} - \frac{2 g P^2 K_2}{f_c f_a^2 \rho^2} + \frac{f_c' h'}{2 f_c} \\
&+ \frac{h' f_b'}{f_b} + \frac{h' f_a'}{f_a} - \frac{16h}{\rho^2} - \frac{(h')^2}{h} + 12 h^2 H^2 - \frac{K_2^2 K_1 K_3}{2 f_c f_a^2 f_b^2 h \rho^2} + \frac{K_2 K_1 K_3}{f_c f_a^2 f_b^2 h \rho^2} + \frac{K_1^2}{f_c f_a^2 f_b^2 h \rho^2} \\
&+ \frac{2 g P^2}{f_c f_a^2 \rho^2} + \frac{g P^2 (K_2')^2}{9 f_a f_b)} - \frac{9 K_1 K_3}{8 f_c f_a f_b \rho^2 g P^2} - \frac{3h'}{\rho}\,, \qquad \text{(B.6)}
\end{aligned}
$$

$$
\begin{aligned}
0 = {} & K_1'' - \frac{g K_2^2 K_1 P^2}{f_c f_a^2 h \rho^2} + \frac{g K_2^2 K_3 P^2}{f_c f_a^2 h \rho^2} + \frac{4 g K_2 K_1 P^2}{f_c f_a^2 h \rho^2} - \frac{2 g K_2 K_3 P^2}{f_c f_a^2 h \rho^2} - \frac{9 f_b K_1}{2 f_c f_a \rho^2} + \frac{9 f_b K_3}{2 f_c f_a \rho^2} \\
&- \frac{4 g K_1 P^2}{f_c f_a^2 h \rho^2} + \frac{K_1' f_c'}{2 f_c} - \frac{K_1' g'}{g} - \frac{K_1' h'}{h} + \frac{f_a' K_1'}{f_a} - \frac{3 K_1'}{\rho} - \frac{K_1' f_b'}{f_b}\,, \qquad \text{(B.7)}
\end{aligned}
$$

$$
\begin{aligned}
0 = {} & K_3'' + \frac{g K_2^2 K_1 P^2}{f_c f_b^2 h \rho^2} - \frac{g K_2^2 K_3 P^2}{f_c f_b^2 h \rho^2} - \frac{2 g K_2 K_1 P^2}{f_c f_b^2 h \rho^2} + \frac{9 f_a K_1}{2 f_c f_b \rho^2} - \frac{9 f_a K_3}{2 f_c f_b \rho^2} + \frac{K_3' f_c'}{2 f_c} \\
&- \frac{K_3' g'}{g} + \frac{f_b' K_3'}{f_b} - \frac{K_3' h'}{h} - \frac{3 K_3'}{\rho} - \frac{K_3' f_a'}{f_a}\,, \qquad \text{(B.8)}
\end{aligned}
$$

$$
\begin{aligned}
0 = {} & K_2'' - \frac{9 f_b K_2}{2 f_c f_a \rho^2} - \frac{9 f_a K_2}{2 f_c f_b \rho^2)} + \frac{9 f_b}{f_c f_a \rho^2} - \frac{9 K_2 K_1^2}{8 f_c g P^2 h f_b f_a \rho^2} + \frac{9 K_2 K_1 K_3}{4 f_c g P^2 h f_b f_a \rho^2} \\
&- \frac{9 K_2 K_3^2}{8 f_c g P^2 h f_b f_a \rho^2} + \frac{9 K_1^2}{4 f_c g P^2 h f_b f_a \rho^2} - \frac{9 K_1 K_3}{4 f_c g P^2 h f_b f_a \rho^2} + \frac{K_2' f_c'}{2 f_c} + \frac{K_2' g'}{g} - \frac{K_2' h'}{h} \\
&- \frac{3 K_2'}{\rho}\,, \qquad \text{(B.9)}
\end{aligned}
$$

JHEP05(2020)035

$$
\begin{aligned}
0 = {} & g'' - \frac{g^2P^2K_2^2}{2f_cf_a^2h\rho^2} - \frac{g^2P^2K_2^2}{2f_cf_b^2h\rho^2} + \frac{2g^2P^2K_2}{f_cf_a^2h\rho^2} + \frac{9K_1^2}{16f_cf_af_bh\rho^2P^2} + \frac{9K_3^2}{16f_cf_af_bh\rho^2P^2} \\
& - \frac{(g')^2}{g} - \frac{9K_1K_3}{8f_cf_af_bh\rho^2P^2} + \frac{(K_3')^2}{8f_a^2hP^2} + \frac{(K_1')^2}{8f_b^2hP^2} - \frac{2g^2P^2}{f_cf_a^2h\rho^2} - \frac{g^2P^2(K_2')^2}{9f_af_bh} + \frac{g'f_c'}{2f_c} \\
& + \frac{g'f_a'}{f_a} + \frac{g'f_b'}{f_b} - \frac{3g'}{\rho}\,.
\end{aligned}
\tag{B.10}
$$

Additionally, we have the first order constraint

$$
\begin{aligned}
0 = {} & \frac{8}{9}g^2(K_2')^2f_bf_aP^4 + (K_3')^2f_b^2 + (K_1')^2f_a^2 - \frac{4g^2K_2^2f_a^2P^4}{f_c\rho^2} + \frac{4gf_a^2f_b^2P^2(h')^2}{h} \\
& + \frac{4h(g')^2f_a^2f_b^2P^2}{g} + \frac{96hgf_a^2f_bP^2}{\rho^2} + \frac{96hgf_af_b^2P^2}{\rho^2} - \frac{96hgf_a^2f_b^2P^2}{\rho^2} - \frac{4gK_1^2P^2}{f_ch\rho^2} \\
& + 96h^2gf_a^2f_b^2P^2H^2 + \frac{9K_1K_3f_bf_a}{f_c\rho^2} + \frac{32gf_a^2f_b^2P^2h'}{\rho} + \frac{16g^2K_2f_b^2P^4}{f_c\rho^2} - \frac{4g^2K_2^2f_b^2P^4}{f_c\rho^2} \\
& - \frac{gK_2^2K_1^2P^2}{f_ch\rho^2} + \frac{4gK_2K_1^2P^2}{f_ch\rho^2} - \frac{gK_2^2K_3^2P^2}{f_ch\rho^2} + \frac{64hgf_a^2f_bP^2f_b'}{\rho} + \frac{64hgf_af_b^2P^2f_a'}{\rho} \\
& - 16hgf_af_bP^2f_a'f_b' - \frac{32f_chgf_af_bP^2}{\rho^2} - \frac{18hgf_af_b^3P^2}{f_c\rho^2} - \frac{18hgf_a^3f_bP^2}{f_c\rho^2} + \frac{36hgf_a^2f_b^2P^2}{f_c\rho^2} \\
& - \frac{9K_3^2f_bf_a}{f_c\rho^2} - 4hgf_b^2P^2(f_a')^2 - 4hgf_a^2P^2(f_b')^2 - \frac{16g^2f_b^2P^4}{f_c\rho^2} + \frac{2gK_2^2K_1K_3P^2}{f_ch\rho^2} \\
& - \frac{4gK_2K_1K_3P^2}{f_ch\rho^2} - \frac{8hgf_b^2f_aP^2f_c'f_a'}{f_c} + \frac{32hgf_a^2f_b^2P^2f_c'}{f_c\rho} - \frac{8hgf_a^2f_bP^2f_b'f_c'}{f_c} - \frac{9K_1^2f_bf_a}{2f_c\rho^2}\,.
\end{aligned}
\tag{B.11}
$$

The cascading gauge theory de Sitter vacuum equations of motion (B.3)–(B.11) are invariant under the following symmetries ($\lambda \equiv$ const) (compare with (A.27)–(A.30)):

- symmetry SFG1:

$$
\begin{pmatrix} \rho \\ H \\ P \\ h \\ f_{a,b,c} \\ K_{1,2,3} \\ g \end{pmatrix} \longrightarrow \begin{pmatrix} \rho/(1+\lambda\,\rho) \\ H \\ P \\ (1+\lambda\,\rho)^4\;h \\ (1+\lambda\,\rho)^{-2}\;f_{a,b,c} \\ K_{1,2,3} \\ g \end{pmatrix}; \tag{B.12}
$$

- symmetry SFG2:

$$
P \to \lambda P\,,\;\; g \to \frac{g}{\lambda}\,,\;\; \{\rho, H, f_{a,b,c}, h, K_{1,2,3}\} \to \{\rho, H, f_{a,b,c}, h, K_{1,2,3}\}\,; \tag{B.13}
$$

- symmetry SFG3:

$$
P \to \lambda P\,,\;\; \rho \to \frac{\rho}{\lambda}\,,\;\; \{h, K_{1,3}\} \to \lambda^2\{h, K_{1,3}\}\,,\;\; \{H, f_{a,b,c}, K_2, g\} \to \{H, f_{a,b,c}, K_2, g\}\,; \tag{B.14}
$$

JHEP05(2020)035

- symmetry SFG4:

$$\rho \to \lambda\rho\,,\ H \to \frac{H}{\lambda}\,,\ \{P, f_{a,b,c}, h, K_{1,2,3}, g\} \to \{P, f_{a,b,c}, h, K_{1,2,3}, g\}\,. \tag{B.15}$$

FG frame makes analytical continuation to Euclidean Bunch-Davies vacuum obvious:

$$(d\mathcal{M}_4^c)^2 \underbrace{\longrightarrow}_{\tau\to i\frac{\theta+\pi/2}{H}} \frac{1}{H^2}\left((d\theta)^2+\sin^2(\theta)\ \left(dS^3\right)^2\right) = \frac{1}{H^2}\ \left(dS^4\right)^2\,. \tag{B.16}$$

B.1 Asymptotics

The general UV (as $\rho \to 0$) asymptotic solution of (B.3)–(B.11) describing the phase of the cascading gauge theory with spontaneously broken chiral symmetry takes the form

$$\begin{aligned}
f_c =& 1+f_{a,1,0}\rho+\left(-\frac{3}{8}P^2g_sH^2-\frac{1}{4}K_0H^2+\frac{1}{4}f_{a,1,0}^2+\frac{1}{2}P^2g_sH^2\ln\rho\right)\rho^2\\
&-\frac{1}{4}P^2g_sH^2f_{a,1,0}\rho^3+\sum_{n=4}^{\infty}\sum_k f_{c,n,k}\ \rho^n\ln^k\rho\,,
\end{aligned} \tag{B.17}$$

$$\begin{aligned}
f_a =& 1+f_{a,1,0}\rho+\left(-\frac{1}{2}P^2g_sH^2-\frac{1}{4}K_0H^2+\frac{1}{4}f_{a,1,0}^2+\frac{1}{2}P^2g_sH^2\ln\rho\right)\rho^2+f_{a,3,0}\rho^3\\
&+\sum_{n=4}^{\infty}\sum_k f_{a,n,k}\ \rho^n\ln^k\rho\,,
\end{aligned} \tag{B.18}$$

$$\begin{aligned}
f_b =& 1+f_{a,1,0}\rho+\left(-\frac{1}{2}P^2g_sH^2-\frac{1}{4}K_0H^2+\frac{1}{4}f_{a,1,0}^2+\frac{1}{2}P^2g_sH^2\ln\rho\right)\rho^2\\
&-\left(\frac{1}{2}P^2g_sH^2f_{a,1,0}+f_{a,3,0}\right)\rho^3+\sum_{n=4}^{\infty}\sum_k f_{b,n,k}\ \rho^n\ln^k\rho\,,
\end{aligned} \tag{B.19}$$

$$\begin{aligned}
h =& \frac{1}{8}P^2g_s+\frac{1}{4}K_0-\frac{1}{2}P^2g_s\ln\rho+\left(P^2g_s\ln\rho-\frac{1}{2}K_0\right)f_{a,1,0}\rho+\left(\left(-\frac{1}{4}P^2g_s\right.\right.\\
&\left.-\frac{5}{4}P^2g_s\ln\rho+\frac{5}{8}K_0\right)f_{a,1,0}^2+\frac{119}{576}P^4g_s^2H^2+\frac{31}{96}P^2g_sH^2K_0+\frac{1}{8}H^2K_0^2+\frac{1}{2}P^4g_s^2H^2\ln\rho^2\\
&-\frac{31}{48}P^4g_s^2H^2\ln\rho-\frac{1}{2}P^2g_sH^2K_0\ln\rho\Big)\rho^2+\left(\left(\frac{5}{4}P^2g_s\ln\rho+\frac{11}{24}P^2g_s-\frac{5}{8}K_0\right)f_{a,1,0}^3\right.\\
&+\left(-\frac{3}{2}P^4g_s^2\ln\rho^2+\frac{23}{16}P^4g_s^2\ln\rho-\frac{19}{64}P^4g_s^2+\frac{3}{2}P^2g_sK_0\ln\rho-\frac{23}{32}P^2g_sK_0\right.\\
&\left.\left.-\frac{3}{8}K_0^2\right)H^2f_{a,1,0}\right)\rho^3+\sum_{n=4}^{\infty}\sum_k h_{n,k}\ \rho^n\ln^k\rho\,,
\end{aligned} \tag{B.20}$$

$$\begin{aligned}
K_1 =& K_0-2P^2g_s\ln\rho+P^2g_sf_{a,1,0}\rho+\left(-\frac{1}{4}P^2f_{a,1,0}^2g_s-\frac{1}{4}P^4g_s^2H^2\ln\rho+\frac{9}{16}P^4g_s^2H^2\right.\\
&\left.+\frac{1}{8}P^2g_sH^2K_0\right)\rho^2+\left(\frac{1}{12}f_{a,1,0}^3P^2g_s+\frac{1}{48}P^2g_s\Big(36P^2g_s\ln\rho-13P^2g_s\right.\\
&\left.-6K_0\Big)H^2f_{a,1,0}+\frac{2}{3}P^2g_s\Big(3f_{a,3,0}\ln\rho+f_{a,3,0}+k_{2,3,0}\Big)\right)\rho^3\\
&+\sum_{n=4}^{\infty}\sum_k k_{1,n,k}\ \rho^n\ln^k\rho\,,
\end{aligned} \tag{B.21}$$

JHEP05(2020)035

$$K_2 = 1 + \left(k_{2,3,0} + \frac{3}{4} H^2 f_{a,1,0} P^2 g_s \ln\rho + 3 f_{a,3,0} \ln\rho \right) \rho^3 + \sum_{n=4}^{\infty} \sum_k k_{2,n,k}\ \rho^n \ln^k \rho\,, \tag{B.22}$$

$$\begin{aligned} K_3 = {} & K_0 - 2P^2 g_s \ln\rho + P^2 g_s f_{a,1,0} \rho + \left(-\frac{1}{4} P^2 g_s f_{a,1,0}^2 - \frac{1}{4} P^4 g_s^2 H^2 \ln\rho + \frac{9}{16} P^4 g_s^2 H^2 \right. \\ & \left. + \frac{1}{8} P^2 g_s H^2 K_0 \right) \rho^2 + \left(\frac{1}{12} f_{a,1,0}^3 P^2 g_s - \frac{1}{48} P^2 g_s \left(12 P^2 g_s \ln\rho + 29 P^2 g_s \right. \right. \\ & \left. \left. + 6 K_0 \right) H^2 f_{a,1,0} - \frac{2}{3} P^2 g_s \left(3 f_{a,3,0} \ln\rho + f_{a,3,0} + k_{2,3,0} \right) \right) \rho^3 \\ & + \sum_{n=4}^{\infty} \sum_k k_{3,n,k}\ \rho^n \ln^k \rho\,, \end{aligned} \tag{B.23}$$

$$g = g_s \left(1 - \frac{1}{2} P^2 g_s H^2 \rho^2 + \frac{1}{2} f_{a,1,0} P^2 g_s H^2 \rho^3 + \sum_{n=4}^{\infty} \sum_k g_{n,k}\ \rho^n \ln^k \rho \right). \tag{B.24}$$

It is characterized by 11 parameters:

$$\{ K_0\,,\ H\,,\ g_s\,,\ f_{a,1,0}\,,\ \underbrace{f_{a,3,0}\,,\ k_{2,3,0}}_{\mathcal{O}_3^\alpha}\,,\ \underbrace{g_{4,0}\,,\ f_{c,4,0}}_{\mathcal{O}_4^\beta}\,,\ \underbrace{f_{a,6,0}}_{\mathcal{O}_6}\,,\ \underbrace{f_{a,7,0}}_{\mathcal{O}_7}\,,\ \underbrace{f_{a,8,0}}_{\mathcal{O}_8} \}\,, \tag{B.25}$$

where we indicated the dual cascading gauge theory operators which expectation values these parameters characterize. g_s is the asymptotic string coupling, and K_0 is related to strong coupling scale Λ of the cascading gauge theory (see appendix B.3) as [31]

$$\Lambda^2 = \frac{1}{P^2 g_s}\ e^{-\frac{K_0}{P^2 g_s}}\,. \tag{B.26}$$

Finally, $f_{a,1,0}$ corresponds to a diffeomorphism parameter (-2λ) in symmetry transformation SFG1, see (B.12).

To understand IR asymptotics of the FG frame solutions it is convenient to consider Euclidean continuation of the background geometry (B.1). For a fixed radial coordinate ρ the resulting Euclidean space is topologically $S^4 \times S^2 \times S^3$, where S^4 is an analytical continuation of $\mathcal{M}^c$ (B.16), and $S^2 \times S^3$ is a compact part of the warped deformed conifold.[27] Without loss of generality we assume that the radial coordinate

$$\rho\ \in\ [0, +\infty)\,, \tag{B.27}$$

so that $y \equiv \frac{1}{\rho}$ corresponds to the IR asymptotic. The range (B.27) can always be enforced with an appropriate symmetry transformation SFG1 (B.12). Ten dimensional Euclidean manifold is geodesically complete if one of the compact factors S^4 or S^2 smoothly shrinks to zero size as $y \to 0$. Note that S^3 can not shrink to zero size without causing a naked singularity since it supports nonzero (when $P \neq 0$) RR 3-form flux (2.5). Thus, from purely topological considerations we expect several inequivalent de Sitter vacua of the cascading gauge theory: TypeA (shrinking S^4) and TypeB (shrinking S^2).

[27] See [4] for a nice review.

JHEP05(2020)035

- TypeA de Sitter vacua of the cascading gauge theory. To identify smooth Euclidean FG frame geometries with vanishing S^4 as $y \to 0$ we introduce[28]

$$h^h \equiv y^{-2}\, h\,, \qquad f^h_{a,b,c} \equiv y\, f_{a,b,c}\,. \tag{B.28}$$

The IR asymptotic expansion

$$\begin{aligned} f^h_{a,b,c} &= \sum_{n=0} f^h_{a,b,c,n} y^n\,, & h^h &= \frac{1}{4H^2} + \sum_{n=1} h^h_n y^n\,, \\ K_{1,2,3} &= \sum_{n=0} K^h_{1,2,3,n} y^n\,, & g &= \sum_{n=0} g^h_n y^n\,, \end{aligned} \tag{B.29}$$

is characterized by 7 parameters:

$$\{f^h_{a,0}\,,\ f^h_{b,0}\,,\ f^h_{c,0}\,,\ K^h_{1,0}\,,\ K^h_{2,0}\,,\ K^h_{3,0}\,,\ g^h_0\}\,. \tag{B.30}$$

Note that given (B.29),

$$\begin{aligned} &\frac{1}{h^{1/2}\rho^2}\,(d\mathcal{M}^c_4)^2 + \frac{h^{1/2}}{\rho^2}\,(d\rho)^2 \quad \underbrace{\longrightarrow}_{\tau\to i\frac{\theta+\pi/2}{H}} \quad \frac{1}{h^{1/2}\rho^2}\,\frac{1}{H^2}(dS^4)^2 + \frac{h^{1/2}}{\rho^2}\,(d\rho)^2 \\ &= \frac{y}{(h^h)^{1/2}}\,\frac{1}{H^2}(dS^4)^2 + \frac{(h^h)^{1/2}}{y}\,(dy)^2 \quad \underbrace{\longrightarrow}_{y\equiv z^2\to 0} \quad \frac{2}{H}\left(z^2(dS^4)^2 + (dz)^2\right), \end{aligned} \tag{B.31}$$

i.e., S^4 indeed smoothly shrinks to zero size as $y \to 0$. It is important to emphasize that TypeA vacua defined by (B.29) have either U(1) or $\mathbb{Z}_2$ chiral symmetry — chiral symmetry is unbroken in the former (TypeA$_s$), and spontaneously broken in the latter (TypeA$_b$).

- TypeB de Sitter vacua of the cascading gauge theory. To identify smooth Euclidean FG frame geometries with vanishing S^2 as $y \to 0$ we introduce [31]

$$h^h \equiv y^{-4}\, h\,, \qquad f^h_{a,b,c} \equiv y^2\, f_{a,b,c}\,. \tag{B.32}$$

The IR asymptotic expansion

$$\begin{aligned} &f^h_a = f^h_{a,0} + \sum_{n=1} f^h_{a,n} y^{2n}\,, \quad f^h_b = 3y^2 + \sum_{n=2} f^h_{b,n} y^{2n}\,, \quad f^h_c = \frac{3}{4} f^h_{a,0} + \sum_{n=1} f^h_{c,n} y^{2n}\,, \\ &K_1 = k^h_{1,3} y^3 + \sum_{n=2} k^h_{1,n} y^{2n+1}\,, \qquad K_2 = k^h_{2,2} y^2 + k^h_{2,4} y^4 + \sum_{n=3} k^h_{2,n} y^{2n}\,, \\ &K_3 = k^h_{3,1} y + \sum_{n=1} k^h_{3,n} y^{2n+1}\,, \qquad h^h = h^h_0 + \sum_{n=1} h^h_n y^{2n}\,, \qquad g = g^h_0 + \sum_{n=1} g^h_n y^{2n}\,, \end{aligned} \tag{B.33}$$

is characterized by 7 parameters:

$$\{f^h_{a,0}\,,\ h^h_0\,,\ k^h_{1,3}\,,\ k^h_{2,2}\,,\ k^h_{2,4}\,,\ k^h_{3,1}\,,\ g^h_0\}\,. \tag{B.34}$$

[28] Other holographic models in this class were discussed earlier in [29, 30, 36–38].

JHEP05(2020)035

Note that given (B.33),

$$\frac{h^{1/2}}{\rho^2}\,(d\rho)^2+\frac{f_b h^{1/2}}{6}(g_1^2+g_2^2)=(h^h)^{1/2}\,(dy)^2+(h^h)^{1/2}y^2\;\frac{1}{2}(g_1^2+g_2^2)\Big|_{2-\text{cycle}}$$
$$\underbrace{\longrightarrow}_{y\to 0}\qquad \left(h_0^h\right)^{1/2}\;\left(y^2(dS^2)^2+(dy)^2\right), \tag{B.35}$$

where $\Big|_{S^2}$ means restriction to a 2-cycle. Following [4], this means setting $\psi=0$, $\phi_2=-\phi_1$, $\theta_2=-\theta_1$ in one-forms $\{g_i\}$ on $T^{1,1}$:

$$\left(g_1^2+g_2^2\right)\Big|_{2-\text{cycle}}=2\left((d\theta_1)^2+\sin^2\theta_1\,(d\phi_1)^2\right)=2\left(dS^2\right)^2\,. \tag{B.36}$$

On the other hand, the 3-cycle supporting RR flux remains finite, provided $f^h_{a,0}h^h_0\neq 0$:

$$\frac{f_c h^{1/2}}{9}g_5^2+\frac{f_a h^{1/2}}{6}(g_3^2+g_4^2)=\frac{f_c^h(h^h)^{1/2}}{9}g_5^2+\frac{f_a^h(h^h)^{1/2}}{6}(g_3^2+g_4^2) \tag{B.37}$$
$$\underbrace{\longrightarrow}_{y\to 0}\qquad \frac{f^h_{a,0}(h^h_0)^{1/2}}{6}\;\left(\frac{1}{2}g_5^2+g_3^2+g_4^2\right)\Big|_{3-\text{cycle: }\theta_2=\phi_2=0,\theta_1=2\eta,\psi=\xi_1+\xi_2,\phi_1=\xi_1-\xi_2}$$
$$=\frac{f^h_{a,0}(h^h_0)^{1/2}}{6}\;2\left((d\eta)^2+\cos^2\eta(d\xi_1)^2+\sin^2\eta(d\xi_2)^2\right)=\frac{f^h_{a,0}(h^h_0)^{1/2}}{3}\;\left(dS^3\right)^2\,.$$

From (B.35), S^2 indeed smoothly shrinks to zero size as $y\to 0$. Because $f_a\neq f_b$ as $y\to 0$, TypeB vacua defined by (B.33) have $\mathbb{Z}_2$ chiral symmetry — chiral symmetry is spontaneously broken.

B.1.1 TypeA$_s$ vacua asymptotics

We provide here connection with the extensive earlier studies of TypeA$_s$ vacua in [31].

Chirally symmetric de Sitter vacua of the cascading gauge theory (TypeA$_s$) correspond to a consistent truncation

$$f_c\equiv f_2\,,\qquad f_a=f_b\equiv f_3\,,\qquad K_1=K_3\equiv K\,,\qquad K_2=1\,. \tag{B.38}$$

We find:

- in the UV, i.e., as $\rho\to 0$,

$$f_2=1+f_{2,1,0}\;\rho+\left(-\frac{3}{8}H^2P^2g_s-\frac{1}{4}H^2K_0+\frac{1}{4}f^2_{2,1,0}+\frac{1}{2}H^2P^2g_s\ln\rho\right)\rho^2$$
$$-\frac{1}{4}H^2P^2g_sf_{2,1,0}\;\rho^3+\sum_{n=4}^{\infty}\sum_k f_{2,n,k}\;\rho^n\ln^k\rho\,, \tag{B.39}$$
$$f_3=1+f_{2,1,0}\;\rho+\left(-\frac{1}{2}H^2P^2g_s-\frac{1}{4}H^2K_0+\frac{1}{4}f^2_{2,1,0}+\frac{1}{2}H^2P^2g_s\ln\rho\right)\rho^2$$
$$-\frac{1}{4}H^2P^2g_sf_{2,1,0}\;\rho^3+\sum_{n=4}^{\infty}\sum_k f_{3,n,k}\;\rho^n\ln^k\rho\,, \tag{B.40}$$

JHEP05(2020)035

$$
\begin{aligned}
h = {} & \frac{1}{8}P^2 g_s + \frac{1}{4}K_0 - \frac{1}{2}P^2 g_s \ln\rho - \frac{1}{2}f_{2,1,0}(-2P^2 g_s \ln\rho + K_0)\ \rho + \bigg(\frac{119}{576}H^2P^4 g_s^2 \\
& + \frac{31}{96}H^2 K_0 P^2 g_s - \frac{1}{4}P^2 g_s f_{2,1,0}^2 + \frac{1}{8}H^2 K_0^2 + \frac{5}{8}f_{2,1,0}^2 K_0 - \frac{1}{96}P^2 g_s(62H^2P^2 g_s \\
& + 48H^2 K_0 + 120 f_{2,1,0}^2)\ln\rho + \frac{1}{2}H^2P^4 g_s^2 \ln^2\rho\bigg)\ \rho^2 - \frac{1}{192}f_{2,1,0}\bigg(288H^2P^4 g_s^2 \ln^2\rho \\
& + \bigg(-276H^2P^4 g_s^2 - 288H^2 K_0 P^2 g_s - 240P^2 g_s f_{2,1,0}^2\bigg)\ln\rho + 57H^2P^4 g_s^2 \\
& + 138H^2 K_0 P^2 g_s - 88P^2 f_{2,1,0}^2 g_s + 72H^2 K_0^2 + 120 f_{2,1,0}^2 K_0\bigg)\ \rho^3 \\
& + \sum_{n=4}^{\infty}\sum_k h_{n,k}\ \rho^n \ln^k\rho\,, \qquad \text{(B.41)}
\end{aligned}
$$

$$
\begin{aligned}
K = {} & K_0 - 2P^2 g_s \ln\rho + P^2 g_s f_{2,1,0}\ \rho + \frac{1}{16}P^2 g_s(-4H^2P^2 g_s \ln\rho + 9H^2P^2 g_s + 2H^2 K_0 \\
& - 4f_{2,1,0}^2)\ \rho^2 - \frac{1}{48}P^2 g_s f_{2,1,0}(-12H^2P^2 g_s \ln\rho + 21H^2P^2 g_s + 6H^2 K_0 - 4f_{2,1,0}^2)\ \rho^3 \\
& + \sum_{n=4}^{\infty}\sum_k k_{n,k}\ \rho^n \ln^k\rho\,, \qquad \text{(B.42)}
\end{aligned}
$$

$$
g = g_s\bigg(1 - \frac{1}{2}H^2P^2 g_s\ \rho^2 + \frac{1}{2}H^2P^2 g_s f_{2,1,0}\ \rho^3 + \sum_{n=4}^{\infty}\sum_k g_{n,k}\rho^n \ln^k\rho\bigg)\,, \qquad \text{(B.43)}
$$

characterized by 8 parameters:

$$
\{K_0\,,\ H\,,\ g_s\,,\ f_{2,1,0}\,,\ g_{4,0}\,,\ f_{2,4,0}\,,\ f_{2,6,0}f_{2,8,0}\}\,; \qquad \text{(B.44)}
$$

- in the IR, i.e., as $y \equiv \frac{1}{\rho} \to 0$,

$$
\begin{aligned}
f_{2,3}^h &= \sum_{n=0} f_{2,3,n}^h y^n\,, & h^h &= \frac{1}{4H^2} + \sum_{n=1} h_n^h y^n\,, \\
K &= \sum_{n=0} K_n^h y^n\,, & g &= \sum_{n=0} g_n^h y^n\,,
\end{aligned} \qquad \text{(B.45)}
$$

characterized by 4 parameters:

$$
\{f_{2,0}^h\,,\ f_{3,0}^h\,,\ K_0^h\,,\ g_0^h\}\,. \qquad \text{(B.46)}
$$

JHEP05(2020)035

Comparing (B.17)–(B.24) with (B.39)–(B.43) to $\mathcal{O}(\rho^8)$ we identify

$$f_{a,1,0}=f_{2,1,0}\,,\qquad f_{a,3,0}=-\frac{1}{4}H^2P^2g_sf_{2,1,0}\,,\qquad k_{2,3,0}=0\,,\qquad f_{c,4,0}=f_{2,4,0}\,, \tag{B.47}$$

$$\begin{aligned}f_{a,6,0}=&\left(-\frac{96087}{4096000}K_0P^4g_s^2-\frac{3409}{409600}K_0^2P^2g_s-\frac{11056513}{245760000}P^6g_s^3\right)H^6\\&+\left(\frac{1171}{20480}P^4g_s^2f_{2,1,0}^2-\frac{13}{10240}K_0P^2g_sf_{2,1,0}^2\right)H^4+\left(-\frac{1}{512}P^2g_sf_{2,1,0}^4-\frac{307}{1280}P^2g_sf_{2,4,0}\right.\\&\left.+\frac{31}{320}P^2g_sg_{4,0}-\frac{87}{640}K_0f_{2,4,0}\right)H^2-\frac{1}{4}f_{2,6,0}+\frac{3}{16}f_{2,1,0}^2f_{2,4,0}\,,\end{aligned} \tag{B.48}$$

$$\begin{aligned}f_{a,7,0}=&\left(\frac{13331}{196608}P^6g_s^3f_{2,1,0}+\frac{753}{16384}P^4g_s^2f_{2,1,0}K_0+\frac{547}{24576}K_0^2f_{2,1,0}P^2g_s\right)H^6\\&+\left(-\frac{2077}{18432}P^4g_s^2f_{2,1,0}^3-\frac{77}{3072}K_0P^2g_sf_{2,1,0}^3\right)H^4+\left(\frac{21}{1280}P^2g_sf_{2,1,0}^5+\frac{19}{64}K_0f_{2,1,0}f_{2,4,0}\right.\\&\left.+\frac{61}{128}f_{2,1,0}P^2g_sf_{2,4,0}-\frac{7}{32}f_{2,1,0}P^2g_sg_{4,0}\right)H^2-\frac{3}{8}f_{2,1,0}^3f_{2,4,0}+\frac{1}{2}f_{2,1,0}f_{2,6,0}\,,\end{aligned} \tag{B.49}$$

$$\begin{aligned}f_{a,8,0}=&\frac{1}{70K_0-141P^2g_s}\left[\left(-\frac{40244584228943}{5689958400000}K_0P^8g_s^4-\frac{12213914790101}{3034644480000}K_0^2P^6g_s^3\right.\right.\\&\left.-\frac{931679}{4915200}K_0^4P^2g_s-\frac{9161577517}{7225344000}K_0^3P^4g_s^2+\frac{25292565670124671}{19118260224000000}P^{10}g_s^5\right)H^8\\&+\left(-\frac{173957}{81920}P^2g_sK_0^3f_{2,1,0}^2-\frac{5131309293043}{303464448000}P^8g_s^4f_{2,1,0}^2-\frac{12991428547}{1032192000}K_0P^6g_s^3f_{2,1,0}^2\right.\\&\left.+\frac{504197}{1433600}P^4g_s^2f_{2,1,0}^2K_0^2\right)H^6+\left(\frac{1892623}{92160}P^4g_s^2K_0f_{2,1,0}^4+\frac{63}{8}P^2g_sK_0^2f_{2,1,0}^4\right.\\&+\frac{2093}{768}P^2g_sK_0^2g_{4,0}-\frac{11179}{2560}K_0^3f_{2,4,0}+\frac{176710639657}{4741632000}P^6g_s^3f_{2,4,0}-\frac{2470057}{1290240}P^6g_s^3f_{2,1,0}^4\\&-\frac{259362731}{33868800}P^6g_s^3g_{4,0}-\frac{132413627}{16128000}K_0P^4g_s^2f_{2,4,0}-\frac{6266917}{537600}K_0^2P^2g_sf_{2,4,0}\\&\left.+\frac{698651}{80640}P^4g_s^2K_0g_{4,0}\right)H^4+\left(-\frac{15365}{3072}P^4g_s^2f_{2,1,0}^6-\frac{69139}{960}P^4g_s^2f_{2,6,0}\right.\\&-\frac{2751}{128}K_0^2f_{2,1,0}^2f_{2,4,0}-\frac{3675}{512}P^2g_sK_0f_{2,1,0}^6-\frac{1215}{128}P^4g_s^2f_{2,1,0}^2g_{4,0}-\frac{1699}{16}P^2g_sK_0f_{2,6,0}\\&-\frac{14827}{320}P^2g_sK_0f_{2,1,0}^2f_{2,4,0}+\frac{2177}{64}P^2g_sK_0f_{2,1,0}^2g_{4,0}-\frac{385}{16}K_0^2f_{2,6,0}\\&\left.-\frac{1540367}{17920}P^4g_s^2f_{2,1,0}^2f_{2,4,0}\right)H^2+\frac{3085}{32}P^2g_sf_{2,1,0}^4f_{2,4,0}-\frac{1375}{8}P^2g_sf_{2,1,0}^2f_{2,6,0}\\&+21P^2g_sf_{2,4,0}g_{4,0}-\frac{2527}{10}K_0f_{2,4,0}^2+70K_0f_{2,8,0}-\frac{63}{2P^2g_s}K_0^2f_{2,4,0}^2+\frac{2275}{16}K_0f_{2,1,0}^4f_{2,4,0}\\&\left.-\frac{875}{4}K_0f_{2,1,0}^2f_{2,6,0}+42K_0f_{2,4,0}g_{4,0}+14P^2g_sg_{4,0}^2+104P^2g_sf_{2,8,0}-\frac{45539}{280}P^2g_sf_{2,4,0}^2\right].\end{aligned} \tag{B.50}$$

Comparing (B.29) with (B.45) we identify

$$f_{c,0}^h=f_{2,0}^h\,,\qquad f_{a,0}^h=f_{b,0}^h=f_{3,0}^h\,,\qquad K_{1,0}^h=K_{3,0}^h=K_0^h\,,\qquad K_{2,0}^h=1\,. \tag{B.51}$$

JHEP05(2020)035

B.2 From FG to EF frame

A general map between the FG and EF frame de Sitter vacua of the holographic duals was worked out in [19]. Specifically, given

$$\begin{aligned} ds^2\Big|_{EF} &= 2dt\ \ (dr - a(r)\ dt) + \sigma(r)^2 e^{2Ht}\ d\boldsymbol{x}^2 + \cdots\,, \\ ds^2\Big|_{FG} &= c_1(\rho)^2\ \ \left(-d\tau^2 + e^{2H\tau}\ d\boldsymbol{x}^2\right) + c_2(\rho)^2\ (d\rho)^2 + \cdots\,, \end{aligned} \tag{B.52}$$

where $\cdots$ are metric components along the compact directions,

$$\begin{aligned} r &= -\int^{\rho} ds\ c_1(s)c_2(s) + \text{const}\,, & t &= \tau - H\int_0^{\rho} ds\ \frac{c_2(s)}{c_1(s)}\,, \\ a(r) &= \frac{1}{2}c_1(\rho)^2\,, & \sigma(r) &= c_1(\rho)\ \exp\left[H\int_0^{\rho} ds\ \frac{c_2(s)}{c_1(s)}\right]. \end{aligned} \tag{B.53}$$

Using (B.1), we find from (B.53):

$$r = \frac{1}{\rho} + \text{const} = y + \text{const}\,, \qquad a = \frac{1}{2h^{1/2}\rho^2}\,, \qquad t = \tau - H\int_0^{\rho} ds\ h(s)^{1/2}\,. \tag{B.54}$$

Note that asymptotically in UV, i.e., as $\rho \to 0$, the EF and the FG times coincide:

$$t - \tau \qquad \sim \qquad -H\int_0^{\rho} ds\ \left(-\frac{1}{2}P^2 g_s \ln s\right)^{1/2} \qquad \longrightarrow \qquad 0\,. \tag{B.55}$$

Without loss of generality we fix const in (B.54) so that $r = 0 \iff \frac{1}{\rho} \equiv y = 0$. Introducing

$$z \equiv -r\,, \tag{B.56}$$

we find from (B.28)–(B.29), (B.32)–(B.33), and (B.33) the following asymptotic expansions for the EF frame vacua:

- TypeA$_s$ vacua:

$$\begin{aligned} a &= -Hz + \frac{H((f^h_{2,0})^2(f^h_{3,0})^2 - 6f^h_{2,0}(f^h_{3,0})^3 + 3H^2P^2(f^h_{3,0})^2 g^h_0 + 10H^4(K^h_0)^2)}{5(f^h_{3,0})^4 f^h_{2,0}} z^2 + \mathcal{O}(z^3)\,, \\ \sigma &= s^h_0\left(1 - \frac{(f^h_{2,0})^2(f^h_{3,0})^2 - 6f^h_{2,0}(f^h_{3,0})^3 + 3H^2P^2(f^h_{3,0})^2 g^h_0 + 10H^4(K^h_0)^2}{5(f^h_{3,0})^4 f^h_{2,0}} z + \mathcal{O}(z^2)\right), \\ w_{c2} &\equiv f^h_2\left(h^h\right)^{1/2} = \frac{f^h_{2,0}}{2H} - \frac{2}{5H}\frac{4(f^h_{2,0})^2(f^h_{3,0})^2 - 3H^2P^2(f^h_{3,0})^2 g^h_0 - 4H^4(K^h_0)^2}{(f^h_{3,0})^4} z + \mathcal{O}(z^2)\,, \\ w_{a2} = w_{b2} &\equiv f^h_3\left(h^h\right)^{1/2} = \frac{f^h_{3,0}}{2H} \\ &\quad + \frac{2}{5H}\frac{2(f^h_{2,0})^2(f^h_{3,0})^2 - 6f^h_{2,0}(f^h_{3,0})^3 + H^2P^2(f^h_{3,0})^2 g^h_0 + 4H^4(K^h_0)^2}{(f^h_{3,0})^3 f^h_{2,0}} z + \mathcal{O}(z^2)\,, \\ K_1 = K_3 &\equiv K = K^h_0 - \frac{16}{5}\frac{H^2P^2K^h_0 g^h_0}{(f^h_{3,0})^2 f^h_{2,0}} z + \mathcal{O}(z^2)\,, \qquad K_2 = 1\,, \\ g &= g^h_0 - \frac{8}{5}\frac{H^2P^2(g^h_0)^2}{(f^h_{3,0})^2 f^h_{2,0}} z + \mathcal{O}(z^2)\,; \end{aligned} \tag{B.57}$$

JHEP05(2020)035

- TypeA$_b$ vacua:

$$
\begin{aligned}
a =& -Hz + \frac{H}{80(f^h_{a,0})^2(f^h_{b,0})^2 g^h_0 f^h_{c,0} P^2}\Big(24H^2(g^h_0)^2((K^h_{2,0})^2(f^h_{a,0})^2+(K^h_{2,0})^2(f^h_{b,0})^2\\
&-4K^h_{2,0}(f^h_{b,0})^2+4(f^h_{b,0})^2)P^4+g^h_0(40H^4(K^h_{1,0})^2(K^h_{2,0})^2-80H^4K^h_{1,0}(K^h_{2,0})^2K^h_{3,0}\\
&+40H^4(K^h_{2,0})^2(K^h_{3,0})^2-160H^4(K^h_{1,0})^2K^h_{2,0}+160H^4K^h_{1,0}K^h_{2,0}K^h_{3,0}\\
&+160H^4(K^h_{1,0})^2+9(f^h_{a,0})^3f^h_{b,0}-18(f^h_{a,0})^2(f^h_{b,0})^2-48(f^h_{a,0})^2f^h_{b,0}f^h_{c,0}+9f^h_{a,0}(f^h_{b,0})^3\\
&-48f^h_{a,0}(f^h_{b,0})^2f^h_{c,0}+16f^h_{a,0}f^h_{b,0}(f^h_{c,0})^2)P^2+27H^2f^h_{a,0}f^h_{b,0}(K^h_{1,0}-K^h_{3,0})^2\Big)z^2\\
&+\mathcal{O}(z^3)\,, \qquad \text{(B.58)}\\
\sigma =& s^h_0\Bigg(1-\frac{1}{80(f^h_{a,0})^2(f^h_{b,0})^2 g^h_0 f^h_{c,0} P^2)}\Big(24H^2(g^h_0)^2((K^h_{2,0})^2(f^h_{a,0})^2+(K^h_{2,0})^2(f^h_{b,0})^2\\
&-4K^h_{2,0}(f^h_{b,0})^2+4(f^h_{b,0})^2)P^4+g^h_0(40H^4(K^h_{1,0})^2(K^h_{2,0})^2-80H^4K^h_{1,0}(K^h_{2,0})^2K^h_{3,0}\\
&+40H^4(K^h_{2,0})^2(K^h_{3,0})^2-160H^4(K^h_{1,0})^2K^h_{2,0}+160H^4K^h_{1,0}K^h_{2,0}K^h_{3,0}\\
&+160H^4(K^h_{1,0})^2+9(f^h_{a,0})^3f^h_{b,0}-18(f^h_{a,0})^2(f^h_{b,0})^2-48(f^h_{a,0})^2f^h_{b,0}f^h_{c,0}+9f^h_{a,0}(f^h_{b,0})^3\\
&-48f^h_{a,0}(f^h_{b,0})^2f^h_{c,0}+16f^h_{a,0}f^h_{b,0}(f^h_{c,0})^2)P^2+27H^2f^h_{a,0}f^h_{b,0}(K^h_{1,0}-K^h_{3,0})^2\Big)z\\
&+\mathcal{O}(z^2)\Bigg)\,, \qquad \text{(B.59)}\\
w_{c2} \equiv f^h_c(h^h)^{1/2} =& \frac{f^h_{c,0}}{2H}+\frac{1}{H(f^h_{a,0})^2(f^h_{b,0})^2 g^h_0 P^2}\Big(\frac{3}{5}H^2(g^h_0)^2((K^h_{2,0})^2(f^h_{a,0})^2\\
&+(K^h_{2,0})^2(f^h_{b,0})^2-4K^h_{2,0}(f^h_{b,0})^2+4(f^h_{b,0})^2)P^4+\frac{1}{10}g^h_0(4H^4(K^h_{1,0})^2(K^h_{2,0})^2\\
&-8H^4K^h_{1,0}(K^h_{2,0})^2K^h_{3,0}+4H^4(K^h_{2,0})^2(K^h_{3,0})^2-16H^4(K^h_{1,0})^2K^h_{2,0}\\
&+16H^4K^h_{1,0}K^h_{2,0}K^h_{3,0}+16H^4(K^h_{1,0})^2+9(f^h_{a,0})^3f^h_{b,0}-18(f^h_{a,0})^2(f^h_{b,0})^2\\
&+9f^h_{a,0}(f^h_{b,0})^3-16f^h_{a,0}f^h_{b,0}(f^h_{c,0})^2)P^2+\frac{27}{40}H^2f^h_{a,0}f^h_{b,0}(K^h_{1,0}-K^h_{3,0})^2\Big)z+\mathcal{O}(z^2)\,, \qquad \text{(B.60)}\\
w_{a2} \equiv f^h_a(h^h)^{1/2} =& \frac{f^h_{a,0}}{2H}+\frac{1}{f^h_{a,0}H(f^h_{b,0})^2 g^h_0 f^h_{c,0} P^2}\Big(-\frac{1}{5}H^2(g^h_0)^2((K^h_{2,0})^2(f^h_{a,0})^2\\
&-3(K^h_{2,0})^2(f^h_{b,0})^2+12K^h_{2,0}(f^h_{b,0})^2-12(f^h_{b,0})^2)P^4+\frac{1}{20}g^h_0(8H^4(K^h_{1,0})^2(K^h_{2,0})^2\\
&-16H^4K^h_{1,0}(K^h_{2,0})^2K^h_{3,0}+8H^4(K^h_{2,0})^2(K^h_{3,0})^2-32H^4(K^h_{1,0})^2K^h_{2,0}+32H^4K^h_{1,0}K^h_{2,0}K^h_{3,0}\\
&+32H^4(K^h_{1,0})^2-9(f^h_{a,0})^3f^h_{b,0}+9f^h_{a,0}(f^h_{b,0})^3-48f^h_{a,0}(f^h_{b,0})^2f^h_{c,0}+16f^h_{a,0}f^h_{b,0}(f^h_{c,0})^2)P^2\\
&+\frac{9}{40}H^2f^h_{a,0}f^h_{b,0}(K^h_{1,0}-K^h_{3,0})^2\Big)z+\mathcal{O}(z^2)\,, \qquad \text{(B.61)}\\
w_{b2} \equiv f^h_b(h^h)^{1/2} =& \frac{f^h_{b,0}}{2H}+\frac{1}{f^h_{b,0}H(f^h_{a,0})^2 g^h_0 f^h_{c,0} P^2}\Big(\frac{1}{5}H^2(g^h_0)^2(3(K^h_{2,0})^2(f^h_{a,0})^2\\
&-(K^h_{2,0})^2(f^h_{b,0})^2+4K^h_{2,0}(f^h_{b,0})^2-4(f^h_{b,0})^2)P^4+\frac{1}{20}g^h_0(8H^4(K^h_{1,0})^2(K^h_{2,0})^2\\
&-16H^4K^h_{1,0}(K^h_{2,0})^2K^h_{3,0}+8H^4(K^h_{2,0})^2(K^h_{3,0})^2-32H^4(K^h_{1,0})^2K^h_{2,0}+32H^4K^h_{1,0}K^h_{2,0}K^h_{3,0}
\end{aligned}
$$

JHEP05(2020)035

$$+32H^4(K^h_{1,0})^2+9(f^h_{a,0})^3f^h_{b,0}-48(f^h_{a,0})^2f^h_{b,0}f^h_{c,0}-9f^h_{a,0}(f^h_{b,0})^3+16f^h_{a,0}f^h_{b,0}(f^h_{c,0})^2)P^2$$
$$+\frac{9}{40}H^2f^h_{a,0}f^h_{b,0}(K^h_{1,0}-K^h_{3,0})^2\Big)z+\mathcal{O}(z^2)\,, \tag{B.62}$$

$$K_1=K^h_{1,0}-\frac{1}{5(f^h_{a,0})^2f^h_{c,0}}\Big(8H^2g^h_0(K^h_{2,0}-2)(K^h_{1,0}K^h_{2,0}-K^h_{2,0}K^h_{3,0}-2K^h_{1,0})P^2$$
$$+9f^h_{a,0}f^h_{b,0}(K^h_{1,0}-K^h_{3,0})\Big)z+\mathcal{O}(z^2)\,, \tag{B.63}$$

$$K_2=K^h_{2,0}-\frac{9}{5f^h_{a,0}f^h_{b,0}g^h_0f^h_{c,0}P^2}\Big(g^h_0(K^h_{2,0}(f^h_{a,0})^2+K^h_{2,0}(f^h_{b,0})^2-2(f^h_{b,0})^2)P^2$$
$$+H^2(K^h_{1,0}-K^h_{3,0})(K^h_{1,0}K^h_{2,0}-K^h_{2,0}K^h_{3,0}-2K^h_{1,0})\Big)z+\mathcal{O}(z^2)\,, \tag{B.64}$$

$$K_3=K^h_{3,0}+\frac{1}{5(f^h_{b,0})^2f^h_{c,0}}\Big(8H^2K^h_{2,0}g^h_0(K^h_{1,0}K^h_{2,0}-K^h_{2,0}K^h_{3,0}-2K^h_{1,0})P^2$$
$$+9f^h_{a,0}f^h_{b,0}(K^h_{1,0}-K^h_{3,0})\Big)z+\mathcal{O}(z^2)\,, \tag{B.65}$$

$$g=g^h_0-\frac{H^2}{10(f^h_{a,0})^2(f^h_{b,0})^2f^h_{c,0}P^2}\Big(8(g^h_0)^2((K^h_{2,0})^2(f^h_{a,0})^2+(K^h_{2,0})^2(f^h_{b,0})^2-4K^h_{2,0}(f^h_{b,0})^2$$
$$+4(f^h_{b,0})^2)P^4-9f^h_{a,0}(K^h_{1,0}-K^h_{3,0})^2f^h_{b,0})z+\mathcal{O}(z^2)\,; \tag{B.66}$$

- TypeB vacua:

$$a=\frac{1}{2(h^h_0)^{1/2}}+\mathcal{O}(z^2)\,,\qquad \sigma=s^h_0\Big(1+(h^h_0)^{1/2}Hz+\mathcal{O}(z^2)\Big)\,,$$
$$w_{c2}\equiv f^h_c(h^h)^{1/2}=\frac{3}{4}f^h_{a,0}(h^h_0)^{1/2}+\mathcal{O}(z^2)\,,\qquad w_{a2}\equiv f^h_a(h^h)^{1/2}=f^h_{a,0}(h^h_0)^{1/2}+\mathcal{O}(z^2)\,,$$
$$w_{b2}\equiv f^h_b(h^h)^{1/2}=3(h^h_0)^{1/2}z^2+\mathcal{O}(z^4)\,,\qquad K_1=-k^h_{1,3}z^3+\mathcal{O}(z^5)\,, \tag{B.67}$$
$$K_2=k^h_{2,2}z^2+\mathcal{O}(z^4)\,,\qquad K_3=-k^h_{3,1}z+\mathcal{O}(z^3)\,,\qquad g=g^h_0+\mathcal{O}(z^2)\,,$$

where

$$s^h_0=\sigma\Big|^{\text{FG frame}}_{y=0}\,. \tag{B.68}$$

B.3 Extremal KS solution limit $H\to 0$

We review here extremal KS solution [2] following [31] and identify the relation of the strong coupling scale Λ (B.26) to the conifold deformation parameter ϵ (B.70).

JHEP05(2020)035

We use the radial coordinate $\hat{r} \in [0, \infty)$ to describe KS solution:

$$
\begin{aligned}
ds_5^2 &= H_{KS}^{-1/2}\ \left(-dt^2 + d\boldsymbol{x}^2\right) + H_{KS}^{1/2}\ \omega_{1,KS}^2\ d\hat{r}^2\,, \\
\Omega_i &= \omega_{i,KS}\ H_{KS}^{1/4}\,, \qquad\qquad K_i = K_{i,KS}\,, \qquad\qquad \text{(B.69)} \\
K_{1,KS} &= \frac{2}{3}P^2 g_s\ \frac{\cosh\hat{r}-1}{\sinh\hat{r}}\left(\frac{\hat{r}\cosh\hat{r}}{\sinh\hat{r}}-1\right), \qquad K_{2,KS} = 1 - \frac{\hat{r}}{\sinh\hat{r}}\,, \\
K_{3,KS} &= \frac{2}{3}P^2 g_s\ \frac{\cosh\hat{r}+1}{\sinh\hat{r}}\left(\frac{\hat{r}\cosh\hat{r}}{\sinh\hat{r}}-1\right), \qquad g = g_s\,, \qquad\qquad \text{(B.70)} \\
\omega_{1,KS} &= \frac{\epsilon^{2/3}}{\sqrt{6}\hat{K}_{KS}}\,, \qquad \omega_{2,KS} = \frac{\epsilon^{2/3}\hat{K}_{KS}^{1/2}}{\sqrt{2}}\cosh\frac{\hat{r}}{2}\,, \qquad \omega_{3,KS} = \frac{\epsilon^{2/3}\hat{K}_{KS}^{1/2}}{\sqrt{2}}\sinh\frac{\hat{r}}{2}\,,
\end{aligned}
$$

with

$$
\hat{K}_{KS} = \frac{(\sinh(2\hat{r})-2\hat{r})^{1/3}}{2^{1/3}\sinh\hat{r}}\,,\ H'_{KS} = \frac{2}{27}\ \frac{(K_{1,KS}-K_{3,KS})K_{2,KS}-2K_{1,KS}}{\epsilon^{8/3}\hat{K}_{KS}^2\sinh^2\hat{r}}\,, \qquad \text{(B.71)}
$$

where now $\hat{r}\to\infty$ is the boundary and $\hat{r}\to 0$ is the IR.

Comparing the metric ansatz in (B.69) and (B.1) we identify

$$
\frac{(d\rho)^2}{\rho^4} = (w_{1,KS}(\hat{r}))^2(d\hat{r})^2\,. \qquad \text{(B.72)}
$$

Introducing

$$
z \equiv e^{-\hat{r}/3}\,, \qquad \text{(B.73)}
$$

we find from (B.72)

$$
\frac{1}{\rho} = \frac{\sqrt{6}\ (2\epsilon)^{2/3}}{4}\ \int_1^z du\ \frac{u^6-1}{u^2(1-u^{12}+12u^6\ln u)^{1/3}}\,. \qquad \text{(B.74)}
$$

In the UV, $\hat{r}\to\infty$, $z\to 0$ and $\rho\to 0$ we have

$$
\begin{aligned}
e^{-\hat{r}/3} \equiv z = \frac{\sqrt{6}\ (2\epsilon)^{2/3}}{4}\rho\Bigg(1 &+ \mathcal{Q}\rho + \mathcal{Q}^2\rho^2 + \mathcal{Q}^3\rho^3 + \mathcal{Q}^4\rho^4 + \mathcal{Q}^5\rho^5 + \Bigg(\frac{27}{80}\epsilon^4\ln 3 + \mathcal{Q}^6 \\
&+ \frac{27}{800}\epsilon^4 - \frac{9}{16}\epsilon^4\ln 2 + \frac{9}{20}\epsilon^4\ln\epsilon + \frac{27}{40}\epsilon^4\ln\rho\Bigg)\rho^6 + \Bigg(-\frac{63}{16}\epsilon^4\mathcal{Q}\ln 2 + \frac{189}{80}\epsilon^4\mathcal{Q}\ln 3 + \mathcal{Q}^7 \\
&+ \frac{729}{800}\mathcal{Q}\epsilon^4 + \frac{63}{20}\epsilon^4\mathcal{Q}\ln\epsilon + \frac{189}{40}\mathcal{Q}\epsilon^4\ln\rho\Bigg)\rho^7 + \Bigg(\frac{2403}{400}\epsilon^4\mathcal{Q}^2 - \frac{63}{4}\epsilon^4\mathcal{Q}^2\ln 2 + \frac{189}{20}\epsilon^4\mathcal{Q}^2\ln 3 \\
&+ \frac{63}{5}\epsilon^4\mathcal{Q}^2\ln\epsilon + \mathcal{Q}^8 + \frac{189}{10}\epsilon^4\mathcal{Q}^2\ln\rho\Bigg)\rho^8 + \Bigg(\frac{189}{5}\epsilon^4\mathcal{Q}^3\ln\epsilon + \frac{9729}{400}\epsilon^4\mathcal{Q}^3 - \frac{189}{4}\epsilon^4\mathcal{Q}^3\ln 2 \\
&+ \frac{567}{20}\epsilon^4\mathcal{Q}^3\ln 3 + \mathcal{Q}^9 + \frac{567}{10}\epsilon^4\mathcal{Q}^3\ln\rho\Bigg)\rho^9 + \mathcal{O}(\rho^{10}\ln\rho)\Bigg)\,, \qquad \text{(B.75)}
\end{aligned}
$$

where

$$
\begin{aligned}
\mathcal{Q} &= \frac{\sqrt{6}\ (2\epsilon)^{2/3}}{4}\left\{\int_0^1 du\left(\frac{1-u^6}{u^2(1-u^{12}+12u^6\ln u)^{1/3}} - \frac{1}{u^2}\right) - 1\right\} \\
&= -\frac{\sqrt{6}\ (2\epsilon)^{2/3}}{4}\ \times\ 0.839917(9)\,.
\end{aligned} \qquad \text{(B.76)}
$$

JHEP05(2020)035

In the IR, $\hat{r}\to 0$, $z\to 1_-$ and $\frac{1}{\rho}\to 0$ we have

$$\hat{r}=\frac{\sqrt{6}\ 2^{1/3}}{3^{1/3}\ \epsilon^{2/3}}\ y\left(1-\frac{2^{2/3}\ 3^{1/3}}{15\ \epsilon^{4/3}}\ y^2+\frac{71\ 3^{2/3}\ 2^{1/3}}{2625\ \epsilon^{8/3}}\ y^4+\mathcal{O}(y^6)\right). \tag{B.77}$$

Using (B.75) and (B.77), and the exact analytic solution describing the Klebanov-Strassler Minkowski vacuum of the cascading gauge theory (B.70), (B.71) we can identify parameters (B.25):

$$\begin{aligned}
&K_0=P^2g_s\left(-\ln 3+\frac{5}{3}\ \ln 2-\frac{4}{3}\ \ln\epsilon-\frac{2}{3}\right), && f_{a,1,0}=-2\mathcal{Q},\\
&k_{2,3,0}=\frac{3\sqrt{6}}{8}\epsilon^2(3\ln 3-5\ln 2+4\ln\epsilon), \qquad f_{c,4,0}=0, && f_{a,3,0}=\frac{3\sqrt{6}}{4}\ \epsilon^2,\\
&f_{a,6,0}=\left(-\frac{27}{16}\ln 2+\frac{81}{50}+\frac{81}{80}\ln 3+\frac{27}{20}\ln\epsilon\right)\epsilon^4+\frac{3\sqrt{6}}{4}\mathcal{Q}^3\epsilon^2,\\
&f_{a,7,0}=\left(\frac{27}{5}\ln\epsilon-\frac{27}{4}\ln 2+\frac{81}{20}\ln 3+\frac{1701}{200}\right)\epsilon^4\mathcal{Q}+\frac{3\sqrt{6}}{4}\epsilon^2\mathcal{Q}^4,\\
&f_{a,8,0}=\left(\frac{27}{2}\ln\epsilon-\frac{135}{8}\ln 2+\frac{81}{8}\ln 3+\frac{405}{16}\right)\mathcal{Q}^2\epsilon^4+\frac{3\sqrt{6}}{4}\mathcal{Q}^5\epsilon^2, \qquad g_{4,0}=0,
\end{aligned} \tag{B.78}$$

in the UV, and parameters (B.34):

$$\begin{aligned}
&f^h_{a,0}=2^{1/3}\ 3^{2/3}\ \epsilon^{4/3}, && h^h_0=P^2g_s\ \epsilon^{-8/3}\ \times\ 0.056288(0),\\
&k^h_{1,3}=\frac{4\sqrt{6}}{9\ \epsilon^2}\ P^2g_s, && k^h_{2,2}=\frac{2^{2/3}}{3^{2/3}\ \epsilon^{4/3}}, \qquad k^h_{2,4}=-\frac{11\ 2^{1/3}\ 3^{2/3}}{45\ \epsilon^{8/3}},\\
&k^h_{3,1}=\frac{4\sqrt{6}\ 2^{1/3}\ 3^{2/3}}{27\epsilon^{2/3}}\ P^2g_s, \qquad g^h_0=g_s,
\end{aligned} \tag{B.79}$$

in the IR.

Given (B.26), we identify from (B.78)

$$\Lambda=\frac{3^{1/2}e^{1/3}\epsilon^{2/3}}{2^{5/6}(P^2g_s)^{1/2}}=\frac{2^{1/6}e^{1/3}\epsilon^{2/3}}{3^{3/2}M\alpha' g_s^{1/2}}=\frac{2^{1/6}e^{1/3}g_s^{1/2}}{3^{3/2}}\ m_{\text{glueball}}\ \approx\ 0.3g_s^{1/2}m_{\text{glueball}}, \tag{B.80}$$

where in the second equality we used (2.7); the glueball mass scale is defined as in (1.10).

C Numerical procedure

C.1 FG frame de Sitter vacua

Equations of motion for the FG frame de Sitter vacua of the cascading gauge theory, along with the asymptotics and the symmetries of the dual holographic formulation, are presented in appendix B. Generically, we have eight functions of the radial coordinate ρ, see (B.2). When the chiral symmetry is unbroken, there are only five functions, see (B.38). The solution to the equations of motion is unique[29] once we fix the Hubble constant H, the

[29] Apart from the discrete choices associated with the IR boundary conditions leading to classification of topologically distinct holographic vacua: TypeA$_{s,b}$ or TypeB, see appendix B.1.

JHEP05(2020)035

asymptotic string coupling g_s, the 3-form flux P (alternatively the rank difference of gauge group factors M in the cascading theory), see (2.6) and (2.7), and the strong coupling scale Λ of the cascading gauge theory (alternatively K_0, see (B.26), or the conifold deformation parameter ϵ, see (B.80)). Of these, parameters H, Λ, P are dimensionful. The radial coordinate ρ is dimensionful as well, albeit in units of 'mass'. As a result, UV/IR parameters of the solutions, see (B.25), (B.30) and (B.34), have complicated dimensional dependence. It is possible to completely eliminate the dimensional dependence (and the g_s dependence) from all the equations of motion and the asymptotic expansions with appropriate rescaling:

$$\begin{aligned} &\{\rho\,,\ f_{a,b,c}\,,\ h\,,\ K_{1,2,3}\,,\ g\} \qquad \Longrightarrow \qquad \{\hat{\rho}\,,\ \hat{f}_{a,b,c}\,,\ \hat{h}\,,\ \hat{K}_{1,2,3}\,,\ \hat{g}\}\,; \\ &\rho = \frac{1}{HPg_s^{1/2}}\,\hat{\rho}\,, \qquad f_{a,b,c} = \hat{f}_{a,b,c}\,, \qquad h = P^2 g_s\,\hat{h}\,, \\ &K_{1,3} = P^2 g_s\,\hat{K}_{1,3}\,, \qquad K_2 = \hat{K}_2\,, \qquad g = g_s\,\hat{g}\,. \end{aligned} \tag{C.1}$$

Additionally we introduce a dimensionless parameter k_s as

$$k_s \equiv \frac{K_0}{P^2 g_s} + \ln\left(H^2 P^2 g_s\right)\,, \tag{C.2}$$

leading from (B.26) to the identification

$$k_s = \ln\frac{H^2}{\Lambda^2}\,. \tag{C.3}$$

Notice that the conformal limit in the cascading gauge theory, i.e., $H \gg \Lambda$, corresponds to $k_s \to \infty$.

We do not present the relations between all the UV/IR parameters stemming from (C.1) and (C.2) — they are straightforward to work out, but too long to be illuminating — and instead focus on the few ones for which we are reporting the numerical results:

- TypeA$_{s,b}$ vacua,

$$f^h_{a,b,c,0} = HPg_s^{1/2}\,\hat{f}^h_{a,b,c,0}\,, \quad K^h_{1,3,0} = P^2 g_s\,\hat{K}^h_{1,3,0}\,, \quad K^h_{2,0} = \hat{K}^h_{2,0}\,, \quad g^h_0 = g_s\,\hat{g}^h_0\,; \tag{C.4}$$

- TypeB vacua,

$$\begin{aligned} &f^h_{a,0} = H^2P^2 g_s\,\hat{f}^h_{a,0}\,, \quad h^h_0 = \frac{\hat{h}^h_0}{H^4P^2 g_s}\,, \quad k^h_{1,3} = \frac{\hat{k}^h_{1,3}}{H^3 P g_s^{1/2}}\,, \quad k^h_{2,2} = \frac{\hat{k}^h_{2,2}}{H^2P^2 g_s} \\ &k^h_{2,4} = \frac{\hat{k}^h_{2,4}}{H^4P^4 g_s^2}\,, \qquad k^h_{3,1} = \frac{Pg_s^{1/2}}{H}\,\hat{k}^h_{3,1}\,, \quad g^h_0 = g_s\,\hat{g}^h_0\,. \end{aligned} \tag{C.5}$$

Numerical analysis of the bulk differential equations describing de Sitter vacua are rather involved. To trust them, we would like to have various consistency checks. Here, the symmetry transformations SFG2-SFG4 (B.13)–(B.15) are very useful: we can produce different data sets fixing three of the four parameters $\{H, P, g_s, K_0\}$. As we demonstrate,

JHEP05(2020)035

with appropriate rescaling, the distinct data sets must collapse. We find it useful to implement three different computational schemes:

$$\begin{aligned}
&\text{SchemeI}: && H=P=g_s=1\,, && k_s && \text{is varied}\,;\\
&\text{SchemeII}: && H=g_s=K_0=1\,, && b\equiv P^2 && \text{is varied}\,;\\
&\text{SchemeIII}: && P=g_s=1\,,\ K_0=\frac{1}{4}\,, && \alpha\equiv H^2 && \text{is varied}\,.
\end{aligned} \tag{C.6}$$

Note that:

- SchemeI is equivalent to performing computations in the hatted variables in (C.1), with (C.2);
- SchemeII is convenient to take a conformal limit to Klebanov-Witten solution [3] in TypeA$_s$ vacua: $b\to 0$;
- SchemeIII is convenient to study the extremal KS [2] limit in TypeB vacua: $\alpha\to 0$.

Numerical computations are done adopting the algorithms developed in [12]. Altogether, there are 8 second order differential equations (B.3)–(B.10) and a single first order constraint (B.11) for 8 functions $\{f_a, f_b, f_c, h, K_1, K_2, K_2, g\}$. Notice that the constraint (B.11) involves f_c' linearly. Thus, we can use the latter equation and eliminate the redundant equation (B.3). The final set of ODEs — 7 second order equations and 1 first order equation — necessitates $15=2\times 7+1$ parameters.

- TypeA$_{s,b}$ vacua: the result of the numerical computations are the data files with entries for the 8 UV parameters $\{f_{a,1,0}, f_{a,3,0}, k_{2,3,0}, g_{4,0}, f_{c,4,0}, f_{a,6,0}, f_{a,7,0}, f_{a,8,0}\}$ and the 7 IR parameters $\{f^h_{a,0}, f^h_{b,0}, f^h_{c,0}, K^h_{1,0}, K^h_{2,0}, K^h_{3,0}, g^h_0\}$ (see appendix B.1) labeled by k_s (for the computational scheme SchemeI), b (for the computational scheme SchemeII) or α (for the computational scheme SchemeIII). The number of parameters are reduced to 5 (in the UV) and 4 (in the IR) when chiral symmetry is unbroken (see appendix B.1.1).

- TypeB vacua: the result of the numerical computations are the data files with entries for the 8 UV parameters $\{f_{a,1,0}, f_{a,3,0}, k_{2,3,0}, g_{4,0}, f_{c,4,0}, f_{a,6,0}, f_{a,7,0}, f_{a,8,0}\}$ and the 7 IR parameters $\{f^h_{a,0}, h^h_0, k^h_{1,3}, k^h_{2,2}, k^h_{2,4}, k^h_{3,1}, g^h_0\}$ (see appendix B.1) labeled[30] by k_s (for the computational scheme SchemeI), or α (for the computational scheme SchemeIII).

C.2 EF frame de Sitter vacua

In total, there are 11 (8 with unbroken chiral symmetry) coupled ODEs (A.16)–(A.26) describing EF frame de Sitter vacua involving 5 metric warp factors $\{a, \sigma, w_{a2}, w_{b2}, w_{c2}\}$ (see (2.13)), 3 flux functions $\{K_1, K_2, K_3\}$ (see (2.11)) and the string coupling g as a function of a radial coordinate $z\equiv -r$, see (B.56). The full set of ODEs is redundant, and in practice we use 9 equations (A.17)–(A.25): we drop (A.16) in favor of (A.25), and we use (A.20) (it involves w_{c2}'' linearly) instead of (A.26) (though it involves w_{c2}' linearly). The reason for this is to reduce the complexity of the system of ODEs — unlike construction

[30] We will not use the computation scheme SchemeII here.

JHEP05(2020)035

of de Sitter vacua in FG frame which is a boundary value problem, representation of de Sitter vacua in EF frame is an initial value problem, and thus we can get away with using a higher order system of ODEs.

The initial conditions for these equations are set at $z \to 0_+$ with asymptotic expansions (B.57) for TypeA$_s$ de Sitter vacua, and with asymptotic expansions (B.58)–(B.66) for TypeA_b de Sitter vacua. The EF frame equations of motion are integrated on the interval

$$z \in [0, z_{AH}]\,, \tag{C.7}$$

where z_{AH} is the first zero of the AH location function $\mathcal{L}_{AH}$ (see (3.32)):

$$\mathcal{L}_{AH}(z) \equiv 3H\ \sigma^3 \omega_{c2}^{1/2} \omega_{a2} \omega_{b2} - a \frac{d}{dz}\left\{\sigma^3 \omega_{c2}^{1/2} \omega_{a2} \omega_{b2}\right\}. \tag{C.8}$$

Using (B.57)–(B.66),

$$\begin{aligned} \text{TypeA}_s: &\qquad \mathcal{L}_{AH} = \frac{3\sqrt{2}}{8H^{3/2}} (s_0^h)^3 (f_{2,0}^h)^{1/2} (f_{3,0}^h)^2 + \mathcal{O}(z)\,; \\ \text{TypeA}_b: &\qquad \mathcal{L}_{AH} = \frac{3\sqrt{2}}{8H^{3/2}} (s_0^h)^3 (f_{c,0}^h)^{1/2} f_{a,0}^h f_{b,0}^h + \mathcal{O}(z)\,, \end{aligned} \tag{C.9}$$

i.e., both for TypeA$_s$ and TypeA$_b$ vacua

$$\mathcal{L}_{AH}(z=0) > 0\,, \qquad \frac{d}{dz}\mathcal{L}_{AH}(z=0)\ <\ 0\,, \tag{C.10}$$

where the second inequality is a numerical observation. Notice that to set-up the initial conditions for (A.17)–(A.25), besides the FG frame IR data (B.30) (or (B.46) when the chiral symmetry is unbroken), one needs parameter s_0^h, see (B.68),

$$\begin{aligned} s_0^h = \lim_{z\to 0_+} \sigma(z) &= \lim_{\rho\to+\infty} \left\{ c_1(\rho)\ \exp\left[H \int_0^\rho ds\ \frac{c_2(s)}{c_1(s)} \right] \right\} \\ &= \lim_{\rho\to+\infty} \left\{ \frac{1}{(h(\rho))^{1/4}\rho}\ \exp\left[H \int_0^\rho ds\ (h(s))^{1/2} \right] \right\}, \end{aligned} \tag{C.11}$$

where we used (B.53) and explicit expressions

$$c_1 = \frac{1}{h^{1/4}\rho}\,, \qquad c_2 = \frac{h^{1/4}}{\rho} \tag{C.12}$$

from comparing (B.52) and (2.12). The limit in (C.11) must be taken carefully, as the integral is divergent at the upper limit of integration: using the asymptotic expression for h as $y \equiv \frac{1}{\rho} \to 0$ (B.28) and (B.29) we can regulate it as follows,

$$\int_0^\rho ds\ (h(s))^{1/2} = \int_0^\rho ds \left((h(s))^{1/2} - \frac{P g_s^{1/2}}{2(HP g_s^{1/2} s + 1)} \right) + \frac{1}{2H}\ \ln\left(1 + HP g_s^{1/2} \rho\right)\,, \tag{C.13}$$

or in dimensionless/rescaled quantities (C.1)

$$\frac{1}{H}\int_0^{\hat\rho} d\hat s\ (\hat h(\hat s))^{1/2} = \frac{1}{H}\int_0^{\hat\rho} d\hat s \left((\hat h(\hat s))^{1/2} - \frac{1}{2(\hat s + 1)} \right) + \frac{1}{2H}\ \ln(1+\hat\rho)\,, \tag{C.14}$$

JHEP05(2020)035

leading to

$$s_0^h = 2^{1/2}\ HP^{1/2} g_s^{1/4}\ \exp\left[\int_0^{\hat{\rho}} d\hat{s}\ \left((\hat{h}(\hat{s}))^{1/2} - \frac{1}{2(\hat{s}+1)}\right)\right] \equiv HP^{1/2} g_s^{1/4}\ \hat{s}_0^h\,, \tag{C.15}$$

where the last equality defines dimensionless/rescaled $\hat{s}_0^h$.

D $b \to 0$ of TypeA$_s$ vacua

D.1 FG frame

The conformal, i.e., $H \gg \Lambda$, limit of TypeA$_s$ vacua is best described in computational SchemeII (C.6). Using perturbative expansions (4.11) we find ($' = \frac{d}{d\rho}$),

- for $n = 1$:

$$0 = k_1'' - \frac{\rho+6}{2\rho(1+\rho)} k_1' - \frac{8}{(1+\rho)\rho^2}\,, \tag{D.1}$$

$$0 = g_1'' - \frac{\rho+6}{2\rho(1+\rho)} g_1' + (k_1')^2 - \frac{4}{(1+\rho)\rho^2}\,, \tag{D.2}$$

$$\begin{aligned} 0 = {} & f_{21}' + h_1' + 4f_{31}' + \frac{(1+\rho)\rho}{2(\rho+2)}(k_1')^2 + \frac{2}{\rho(\rho+2)}\left(f_{21} + 4f_{31} - 4k_1 - 1\right) \\ & + \frac{(\rho+4)(3\rho+4)}{2(\rho+2)(1+\rho)\rho} h_1\,, \end{aligned} \tag{D.3}$$

$$\begin{aligned} 0 = {} & f_{31}'' + \frac{1}{4}(k_1')^2 + \frac{(\rho+2)}{2\rho(1+\rho)} h_1' - \frac{(\rho+6)}{2\rho(1+\rho)} f_{31}' + \frac{1}{(1+\rho)\rho^2}\left(5f_{21} + 8f_{31} - 4k_1 - 1\right) \\ & - \frac{3\rho^2 - 16\rho - 16}{4(1+\rho)^2\rho^2} h_1\,, \end{aligned} \tag{D.4}$$

$$\begin{aligned} 0 = {} & h_1'' + \frac{1}{2}(k_1')^2 - \frac{(3\rho+10)}{2\rho(1+\rho)} h_1 + \frac{2}{(1+\rho)\rho^2}\left(3 + 20k_1 - 9f_{21} - 36f_{31}\right) \\ & + \frac{(3\rho^2 - 80\rho - 80}{2(1+\rho)^2\rho^2} h_1\,; \end{aligned} \tag{D.5}$$

- for $n = 2$:

$$\begin{aligned} 0 = {} & k_2'' - \frac{\rho+6}{2\rho(1+\rho)} k_2' - \frac{1}{4\rho(1+\rho)(\rho+2)}\Big((4g_1' + 6h_1' + 8f_{31}')\rho^3 + (12g_1' + 18h_1' + 3h_1 \\ & + 24f_{31}')\rho^2 + (8g_1' + 12h_1' - 16k_1 + 4f_{21} + 16h_1 + 16f_{31}' + 16f_{31})\rho - 16k_1 + 4f_{21} \\ & + 16h_1 + 16f_{31} - 4\rho - 4\Big) k_1' - \frac{(1+\rho)\rho}{4(\rho+2)}(k_1')^3 - \frac{8(k_1 + g_1 - f_{21} - h_1 - 2f_{31})}{(1+\rho)\rho^2}\,, \end{aligned} \tag{D.6}$$

$$\begin{aligned} 0 = {} & g_2'' - \frac{\rho+6}{2\rho(1+\rho)} g_2' - (g_1')^2 + 2k_1' k_2' - \frac{1}{4\rho(\rho+2)(1+\rho)}\Big((k_1')^2\rho^4 + (2(k_1')^2\rho^3 \\ & + 2h_1')\rho^3 + ((k_1')^2 + 3h_1 + 6h_1')\rho^2 + (16f_{31} + 4f_{21} + 16h_1 + 4h_1' - 16k_1)\rho + 16f_{31} \\ & + 4f_{21} + 16h_1 - 16k_1 - 4\rho - 4\Big) g_1' - (2f_{31} + h_1)(k_1')^2 + \frac{4(2f_{31} - 2g_1 + f_{21} + h_1)}{(1+\rho)\rho^2}\,, \end{aligned} \tag{D.7}$$

$$0 = f_{22}' + 4f_{32}' + h_2' + \frac{1}{\rho+2}\Big(f_{31}'\rho^2 + (f_{21} - h_1 + f_{31}')\rho + 2f_{21} - 2h_1\Big) h_1'$$

$$+\frac{5\rho(1+\rho)}{2(\rho+2)}(f_{31}')^2+\frac{\rho(1+\rho)}{4(\rho+2)}(g_1')^2+\frac{\rho(1+\rho)}{4(\rho+2)}(h_1')^2+\frac{(1+\rho)\rho}{2(\rho+2)^2}\Big(f_{31}'\rho^2+(f_{21}-g_1$$
$$-h_1-2f_{31}+f_{31}')\rho+2f_{21}-2g_1-2h_1-4f_{31}\Big)(k_1')^2+\frac{\rho(1+\rho)}{\rho+2}k_1'k_2'$$
$$+\frac{1}{2(\rho+2)^2}\Big((8f_{21}+3h_1-8f_{31})\rho^2+(36f_{21}-16k_1+16h_1-16f_{31})\rho+36f_{21}-16k_1$$
$$+16h_1-16f_{31}-4\rho-4\Big)f_{31}'+\frac{1}{2(\rho+2)\rho(1+\rho)}\Big(3f_{21}h_1\rho^2+(-8f_{21}f_{31}+32k_1h_1$$
$$+64k_1f_{31}+4f_{22}-16k_2)\rho-8f_{21}f_{31}+32k_1h_1+64k_1f_{31}-8k_1^2-4f_{21}^2+(16f_{32}-4f_{21}^2$$
$$-8k_1^2-64h_1f_{31}-4g_1+4h_1-24h_1^2+16h_2+8f_{31}-68f_{31}^2)\rho-64h_1f_{31}+-4g_1-16k_2$$
$$+4f_{22}+8f_{31}+16f_{32}+4h_1+16h_2-24h_1^2-68f_{31}^2+3h_2\rho^2\Big), \tag{D.8}$$

$$0=f_{32}''-\frac{\rho+6}{2\rho(1+\rho)}f_{32}'+\frac{\rho+2}{2\rho(1+\rho)}h_2'+\frac{1}{2}k_1'k_2'+\frac{1}{8}(g_1')^2+\frac{1}{8}(h_1')^2+\frac{1}{4}(f_{31}')^2-\frac{1}{4}(g_1$$
$$+h_1+f_{31})(k_1')^2-\frac{\rho+2}{2\rho(1+\rho)}(h_1-f_{31})h_1'+\frac{1}{4(1+\rho)^2\rho^2}\Big((4f_{21}+16f_{21}k_1-16f_{21}h_1$$
$$-36f_{21}f_{31}+32k_1h_1+48k_1f_{31}+20f_{22}-16k_2-8f_{21}^2-8k_1^2-48h_1f_{31}-4g_1+4h_1$$
$$-24h_1^2+16h_2+4f_{31}-36f_{31}^2+32f_{32})\rho+16f_{21}k_1-36f_{21}f_{31}+32k_1h_1+48k_1f_{31}$$
$$-8f_{21}^2-8k_1^2-3h_1f_{31}\rho^2-48h_1f_{31}-4g_1-16k_2+4f_{21}+20f_{22}+4f_{31}+32f_{32}+4h_1$$
$$+16h_2-24h_1^2-36f_{31}^2-16f_{21}h_1-3h_2\rho^2\Big), \tag{D.9}$$

$$0=h_2''-\frac{3\rho+10}{2\rho(1+\rho)}h_2'-\frac{7}{4}(h_1')^2-\frac{5}{2}(f_{31}')^2-\frac{1}{4(\rho+2)}\Big((h_1'+2f_{31}')\rho^2+(h_1'+2g_1$$
$$+4f_{31}+2f_{31}')\rho+4g_1+8f_{31}\Big)(k_1')^2-\frac{1}{4}(g_1')^2+k_1'k_2'-\frac{1}{4\rho(1+\rho)(\rho+2)}\Big(4f_{31}'\rho^3+(3h_1$$
$$+12f_{31}')\rho^2+(4f_{21}-16k_1+16h_1+16f_{31}+8f_{31}')\rho+4f_{21}-16k_1+16h_1+16f_{31}-4\rho$$
$$-4\Big)h_1'-\frac{1}{2\rho(1+\rho)(\rho+2)}\Big(3h_1\rho^2+(4f_{21}-16k_1+16h_1+16f_{31})\rho+4f_{21}-16k_1$$
$$+16h_1+16f_{31}-4\rho-4\Big)f_{31}'-\frac{1}{2(1+\rho)^2\rho^2}\Big((80f_{21}k_1-44f_{21}h_1-152f_{21}f_{31}+80k_1h_1$$
$$+320k_1f_{31}+36f_{22}-80k_2-40f_{21}^2-40k_1^2-176h_1f_{31}-12g_1-40h_1^2+80h_2+24f_{31}$$
$$-388f_{31}^2+144f_{32}+12f_{21})\rho+80f_{21}k_1-152f_{21}f_{31}+80k_1h_1+320k_1f_{31}-40f_{21}^2$$
$$-40k_1^2-176h_1f_{31}-44f_{21}h_1-12g_1-80k_2+12f_{21}+36f_{22}+24f_{31}+144f_{32}+80h_2$$
$$-40h_1^2-388f_{31}^2-3(h_1^2+h_2)\rho^2\Big). \tag{D.10}$$

The UV ($\rho\to 0$) and the IR ($y\equiv\frac{1}{\rho}\to 0$) asymptotic expansions can be obtained from (B.39)–(B.43) and (B.45) correspondingly, using the SchemeII parameters (C.6),

JHEP05(2020)035

where

$$
\begin{aligned}
&f_{2,1,0} = 1 + f_{2,1,0;1}\, b + f_{2,1,0;2}\, b^2 + \mathcal{O}(b^3)\,, \qquad g_{4,0} = g_{4,0;1}\, b + g_{4,0;2}\, b^2 + \mathcal{O}(b^3)\,,\\
&f_{2,4,0} = \left(-\frac{1}{12} + \frac{4}{3}\, k_{4,0;1}\right) b + \left(-\frac{139}{1152} + \frac{1}{24}\, f_{2,1,0;1} - \frac{22}{9} k_{4,0;1} + \frac{2}{3} g_{4,0;1}\right.\\
&\qquad\qquad \left. + \frac{4}{3} k_{4,0;2}\right) b^2 + \mathcal{O}(b^3)\,,\\
&f_{2,6,0} = f_{2,6,0;1}\, b + f_{2,6,0;2}\, b^2 + \mathcal{O}(b^3)\,, \qquad f_{2,8,0} = f_{2,8,0;1}\, b + f_{2,8,0;2}\, b^2 + \mathcal{O}(b^3)\,,\\
&f^h_{2,0} = 1 + f^h_{2,0;1}\, b + f^h_{2,0;2}\, b^2 + \mathcal{O}(b^3)\,, \qquad f^h_{3,0} = 1 + f^h_{3,0;1}\, b + f^h_{3,0;2}\, b^2 + \mathcal{O}(b^3)\,,\\
&K^h_0 = 1 + K^h_{0;1}\, b + K^h_{0;2}\, b^2 + \mathcal{O}(b^3)\,, \qquad g^h_0 = 1 + g^h_{0;1}\, b + g^h_{0;2}\, b^2 + \mathcal{O}(b^3)\,.
\end{aligned}
\tag{D.11}
$$

Note that in lieu of $f_{2,4,0;1}$ and $f_{2,4,0;2}$ in (D.11) we used $k_{4,0;1}$ and $k_{4,0;2}$:

$$
\begin{aligned}
k_1 &= -2\ln\rho + \rho - \frac{1}{8}\rho^2 - \frac{1}{24}\rho^3 + \left(\frac{3}{64}\ln\rho + k_{4,0;1}\right)\rho^4 + \mathcal{O}(\rho^5)\,,\\
k_2 &= f_{2,1,0;1}\,\rho + \left(-\frac{1}{4}\ln\rho + \frac{9}{16} - \frac{1}{2} f_{2,1,0;1}\right)\rho^2 + \left(\frac{1}{4}\ln\rho - \frac{7}{16} + \frac{1}{8} f_{2,1,0;1}\right)\rho^3\\
&\quad + \left(-\frac{3}{16}\ln^2\rho + \left(\frac{11}{64} - 4k_{4,0;1}\right)\ln\rho + k_{4,0;1}\right)\rho^4 + \mathcal{O}(\rho^5)\,.
\end{aligned}
\tag{D.12}
$$

This is done for computational convenience — the equations for k_1 (see (D.1)) and k_2 (see (D.6)) decouple from all the other equations at the corresponding order.

We are able to solve analytically only the equation for k_1 (D.1),

$$
k_1 = \frac{\rho}{4} + \frac{1}{4+4\rho} - \frac{1}{4} - 4\ln 2 + \frac{\rho^3 - 6\rho^2 - 24\rho - 16}{8(1+\rho)^{3/2}}\,\ln\frac{\sqrt{1+\rho}-1}{\sqrt{1+\rho}+1}\,,
\tag{D.13}
$$

resulting in

$$
k_{4,0;1} = \frac{29}{259} - \frac{3}{32}\ln 2\,, \qquad K^h_{0;1} = \frac{5}{3} - 4\ln 2\,,
\tag{D.14}
$$

and the equation for g_1 (D.2),

$$
\begin{aligned}
g_1 &= -\frac{\rho^2}{32} - \frac{7\rho}{16} - \frac{1}{32(1+\rho)^2} - \frac{3}{8+8\rho} + \frac{13}{32} - \frac{\rho^4(\rho+2)}{32(1+\rho)^{5/2}}\,\ln\frac{\sqrt{1+\rho}-1}{\sqrt{1+\rho}+1}\\
&\quad + \left(\frac{23}{64} - \frac{\rho^3}{128} + \frac{15\rho^2}{128} - \frac{15\rho}{64} + \frac{9}{64(1+\rho)^2} - \frac{63}{128+128\rho} - \frac{1}{128(1+\rho)^3}\right)\\
&\quad \times \ln^2\frac{\sqrt{1+\rho}-1}{\sqrt{1+\rho}+1}\,;
\end{aligned}
\tag{D.15}
$$

$$
g_{4,0;1} = -\frac{17}{32} + \frac{3}{8}\,\ln^2 2 + \frac{1}{8}\,\ln 2\,, \qquad g^h_{0;1} = -\frac{13}{18}\,.
\tag{D.16}
$$

All the remaining equations are solved numerically, using the shooting algorithm developed

JHEP05(2020)035

in [12]. We find:

$$\begin{aligned}
f_{2,1,0;1} &= 0.434278\,, & f_{2,1,0;2} &= 0.357298\,,\\
g_{4,0;1} &= -0.264437\,, & g_{4,0;2} &= -0.64466\,,\\
k_{4,0;1} &= 0.0482987\,, & k_{4,0;2} &= 0.184174\,,\\
f_{2,6,0;1} &= -0.407036\,, & f_{2,6,0;2} &= -0.489017\,,\\
f_{2,8,0;1} &= -0.427022\,, & f_{2,8,0;2} &= -0.609369\,,\\
f^h_{2,0;1} &= -0.156614\,, & f^h_{2,0;2} &= 0.54009\,,\\
f^h_{3,0;1} &= -0.378836\,, & f^h_{3,0;2} &= 0.638051\,,\\
K^h_{0;1} &= -1.10592\,, & K^h_{0;2} &= 1.65245\,,\\
g^h_{0;1} &= -0.722222\,, & g^h_{0;2} &= 0.311658\,,
\end{aligned} \tag{D.17}$$

where we used the same numerical methods to solve (D.1) and (D.2). Comparing the numerical results for $\{k_{4,0;1},\ g_{4,0;1},\ K^h_{0;1},\ g^h_{0;1}\}$ from (D.17) with the analytic predictions (D.14) and (D.16) we find agreement at the fractional level of $\sim 10^{-10}$ or better.

D.2 EF frame

Using perturbative expansions (4.14) and $w_{c2n} \equiv v_n - w_{a2n}$, we find from (A.17)–(A.25) ($' = \frac{d}{dz}$),

- for $n = 1$:

$$0 = k_1'' + \frac{5(2z-1)}{2(z-1)z}\, k_1' - \frac{8}{(z-1)z}\,, \tag{D.18}$$

$$0 = v_1'' - \frac{27}{(z-1)z}\, v_1 - \frac{15(2z-1)}{2(z-1)z}\, a_1' + \frac{11}{4}\,(k_1')^2 + \frac{60}{(z-1)z}\, k_1 - \frac{15(2z^2-2z+1)}{2z^2(z-1)^2}\, a_1 + \frac{9}{(z-1)z}\,, \tag{D.19}$$

$$0 = a_1'' + \frac{7(2z-1)}{2(z-1)z}\, a_1' + \frac{10z^2-10z+3}{2z^2(z-1)^2}\, a_1 - \frac{1}{4}(k_1')^2 + \frac{9}{(z-1)z}\, v_1 - \frac{20}{(z-1)z}\, k_1 - \frac{3}{(z-1)z}\,, \tag{D.20}$$

$$0 = w_{a21}'' + \frac{5(2z-1)}{2(z-1)z}\, w_{a21}' - \frac{12}{(z-1)z}\, w_{a21} - \frac{(2z-1)}{2(z-1)z}\, v_1' - \frac{3(2z-1)}{2(z-1)z}\, a_1' + \frac{3}{4}\,(k_1')^2 - \frac{3}{(z-1)z}\, v_1 - \frac{3(2z^2-2z+1)}{2z^2(z-1)^2}\, a_1 + \frac{12}{(z-1)z}\, k_1 + \frac{1}{(z-1)z}\,, \tag{D.21}$$

$$0 = s_1' - \frac{1}{2}a_1' + \frac{1}{2(z-1)z}\, a_1\,, \tag{D.22}$$

$$0 = g_1'' + \frac{5(1-2z)}{2z(1-z)}\, g_1' + (k_1')^2 + \frac{4}{z(1-z)}\,; \tag{D.23}$$

- for $n = 2$:

$$0 = k_2'' + \frac{5(2z-1)}{2(z-1)z}\, k_2' + \left(\frac{1}{2}v_1' + \frac{5}{2}a_1' - 2w_{a21}' - g_1'\right) k_1' - \frac{8(k_1 - a_1 - v_1 + g_1 + 2w_{a21})}{(z-1)z}\,, \tag{D.24}$$

JHEP05(2020)035

$$
\begin{aligned}
0 = {} & v_2'' - \frac{27}{(z-1)z}\, v_2 - \frac{15(2z-1)}{2(z-1)z}\, a_2' + \frac{11}{2}\, k_1' k_2' + \frac{60}{(z-1)z}\, k_2 - \frac{15(2z^2-2z+1)}{2z^2(z-1)^2}\, a_2 \\
& - \frac{1}{2}(v_1')^2 + \left(\frac{11}{2} w_{a21}' - \frac{10(2z-1)}{(z-1)z}\, w_{a21} + \frac{2(2z-1)}{(z-1)z}\, v_1 \right) v_1' + \frac{3(2z-1)(5a_1-v_1)}{2(z-1)z}\, a_1' \\
& - \frac{15}{4}(a_1')^2 - \left(\frac{11}{4} g_1 + \frac{1}{4} v_1 + \frac{3}{2} w_{a21} \right) (k_1')^2 - \frac{55}{4}(w_{a21}')^2 - \frac{10(2z-1)(v_1-5w_{a21})}{(z-1)z}\, w_{a21}' \\
& + \frac{5}{8}(g_1')^2 + \frac{15v_1^2}{(z-1)z} + \frac{30k_1^2}{(z-1)z} + \frac{75w_{a21}^2}{(z-1)z} + \frac{15(4z^2-4z+3)a_1^2}{4z^2(z-1)^2} - \frac{12(5a_1+4v_1)k_1}{(z-1)z} \\
& + \left(\frac{3(16z^2-16z-1)v_1}{2z^2(z-1)^2} - \frac{9}{(z-1)z} \right) a_1 - \frac{2(15v_1-1)w_{a21}}{(z-1)z} + \frac{9g_1-4v_1}{(z-1)z}\,, \qquad \text{(D.25)} \\
0 = {} & a_2'' + \frac{7(2z-1)}{2(z-1)z}\, a_2' + \frac{10z^2-10z+3}{2z^2(z-1)^2}\, a_2 + \frac{9}{(z-1)z}\, v_2 - \frac{1}{2} k_1' k_2' - \frac{20}{(z-1)z}\, k_2 \\
& + \left(-\frac{1}{4} a_1 + \frac{1}{4} g_1 + \frac{1}{2} w_{a21} \right) (k_1')^2 + \frac{1}{8}(g_1')^2 + \frac{5}{4}(w_{a21}')^2 + \frac{3}{4}(a_1')^2 - \frac{1}{2} w_{a21}' v_1' - \frac{10k_1^2}{(z-1)z} \\
& - \frac{105w_{a21}^2}{(z-1)z} + \frac{20v_1k_1}{(z-1)z} - \frac{10v_1^2}{(z-1)z} - \frac{3a_1^2}{4z^2(z-1)^2} + \frac{6(7v_1-1)w_{a21}}{(z-1)z} + \frac{3(v_1-g_1)}{(z-1)z}\,, \qquad \text{(D.26)} \\
0 = {} & w_{a22}'' + \frac{5(2z-1)}{2z(z-1)}\, w_{a22}' - \frac{12}{(z-1)z}\, w_{a22} - \frac{3(2z-1)}{2z(z-1)}\, a_2' - \frac{2z-1}{2z(z-1)}\, v_2' \\
& - \frac{3(2z^2-2z+1)}{2z^2(z-1)^2}\, a_2 - \frac{3}{(z-1)z}\, v_2 + \frac{12}{(z-1)z}\, k_2 + \frac{3}{2} k_1' k_2' + \frac{1}{4}(w_{a21}')^2 - \frac{3}{4}(a_1')^2 \\
& - \frac{3}{4}(g_1 + w_{a21})(k_1')^2 + \frac{1}{8}(g_1')^2 + \left(\frac{5}{2} a_1' - \frac{2(2z-1)(v_1-5w_{a21})}{(z-1)z} \right) w_{a21}' \\
& + \left(\frac{(2z-1)(v_1-5w_{a21})}{2(z-1)z} - \frac{1}{2} a_1' \right) v_1' + \frac{3(2z-1)(a_1-w_{a21})}{2(z-1)z} a_1' + \frac{6v_1^2}{(z-1)z} \\
& + \frac{3(4z^2-4z+3)a_1^2}{4z^2(z-1)^2} + \frac{75w_{a21}^2}{(z-1)z} + \frac{6k_1^2}{(z-1)z} - \frac{12(v_1+a_1-w_{a21})k_1}{z(z-1)} \\
& + \frac{(3a_1-33w_{a21}-1)v_1}{z(z-1)} + \frac{g_1}{(z-1)z} + \frac{3(6z^2-6z-1)w_{a21}a_1}{2z^2(z-1)^2} - \frac{a_1-3w_{a21}}{(z-1)z}\,, \qquad \text{(D.27)} \\
0 = {} & s_2' - \frac{1}{2} a_2' + \frac{1}{2(z-1)z}\, a_2 + \frac{1}{2}(a_1-s_1) a_1' + \frac{a_1(a_1-s_1)}{2(1-z)z}\,, \qquad \text{(D.28)} \\
0 = {} & g_2' + \frac{5(2z-1)}{2(z-1)z}\, g_2' + 2k_1'k_2' - 2w_{a21}(k_1')^2 - (g_1')^2 + \left(\frac{1}{2} v_1' + 5a_1' \right) g_1' \\
& + \frac{4(v_1-2g_1+a_1-2w_{a21})}{(z-1)z}\,. \qquad \text{(D.29)}
\end{aligned}
$$

JHEP05(2020)035

Initial conditions for (D.18)–(D.29) can be deduced from (B.57) using (D.11) and (4.13):

$$
\begin{aligned}
k_1 &= K^h_{0;1} - \frac{16}{5}z + \mathcal{O}(z^2)\,,\\
v_1 &= f^h_{2,0;1} + 4f^h_{3,0;1} + \left(32K^h_{0;1} - \frac{64}{5}f^h_{2,0;1} - \frac{256}{5}f^h_{3,0;1} + \frac{28}{5}\right)z + \mathcal{O}(z^2)\,,\\
a_1 &= \left(-4K^h_{0;1} + \frac{9}{5}f^h_{2,0;1} + \frac{36}{5}f^h_{3,0;1} - \frac{3}{5}\right)z + \mathcal{O}(z^2)\,,\\
w_{a21} &= f^h_{3,0;1} + \left(\frac{32}{5}K^h_{0;1} - \frac{8}{5}f^h_{2,0;1} - \frac{56}{5}f^h_{3,0;1} + \frac{4}{5}\right)z + \mathcal{O}(z^2)\,,\\
s_1 &= s^h_{0;1} + \mathcal{O}(z)\,, \qquad g_1 = g^h_{0;1} - \frac{8}{5}z + \mathcal{O}(z^2)\,,
\end{aligned}
\tag{D.30}
$$

for $n = 1$, and

$$
\begin{aligned}
k_2 &= K^h_{0;2} + \left(\frac{32}{5}f^h_{3,0;1} - \frac{16}{5}K^h_{0;1} - \frac{16}{5}g^h_{0;1} + \frac{16}{5}f^h_{2,0;1}\right)z + \mathcal{O}(z^2)\,,\\
v_2 &= f^h_{2,0;2} + 4f^h_{3,0;2} + \left(\frac{224}{5}f^h_{2,0;1}f^h_{3,0;1} - \frac{512}{5}K^h_{0;1}f^h_{3,0;1} + 16(K^h_{0;1})^2 + 32K^h_{0;2} - \frac{64}{5}f^h_{2,0;2}\right.\\
&\quad \left. - \frac{256}{5}f^h_{3,0;2} + \frac{28}{5}g^h_{0;1} + \frac{48}{5}(f^h_{2,0;1})^2 + \frac{528}{5}(f^h_{3,0;1})^2 - 8f^h_{3,0;1} - \frac{128}{5}K^h_{0;1}f^h_{2,0;1} - \frac{16}{5}f^h_{2,0;1}\right)z\\
&\quad + \mathcal{O}(z^2)\,,\\
a_2 &= \left(-2(K^h_{0;1})^2 + 4K^h_{0;1}f^h_{2,0;1} + 16K^h_{0;1}f^h_{3,0;1} - 2(f^h_{2,0;1})^2 - \frac{38}{5}f^h_{2,0;1}f^h_{3,0;1} - \frac{97}{5}(f^h_{3,0;1})^2\right.\\
&\quad \left. - 4K^h_{0;2} + \frac{3}{5}f^h_{2,0;1} + \frac{9}{5}f^h_{2,0;2} + \frac{6}{5}f^h_{3,0;1} + \frac{36}{5}f^h_{3,0;2} - \frac{3}{5}g^h_{0;1}\right)z + \mathcal{O}(z^2)\,,\\
w_{a22} &= f^h_{3,0;2} + \left(8f^h_{2,0;1}f^h_{3,0;1} - \frac{96}{5}K^h_{0;1}f^h_{3,0;1} - \frac{32}{5}K^h_{0;1}f^h_{2,0;1} + \frac{16}{5}(K^h_{0;1})^2 + \frac{32}{5}K^h_{0;2}\right.\\
&\quad \left. - \frac{8}{5}f^h_{2,0;2} - \frac{56}{5}f^h_{3,0;2} + \frac{4}{5}g^h_{0;1} + \frac{16}{5}(f^h_{2,0;1})^2 + \frac{104}{5}(f^h_{3,0;1})^2 - \frac{4}{5}f^h_{3,0;1} - \frac{4}{5}f^h_{2,0;1}\right)z + \mathcal{O}(z^2)\,,\\
s_2 &= s^h_{0;2} + \mathcal{O}(z)\,,\\
g_2 &= g^h_{0;2} + \left(\frac{8}{5}f^h_{2,0;1} + \frac{16}{5}f^h_{3,0;1} - \frac{16}{5}g^h_{0;1}\right)z + \mathcal{O}(z^2)\,,
\end{aligned}
\tag{D.31}
$$

for $n = 2$.

E Kretschmann scalar of EF frame background geometry

We collect here the expression for the Kretschmann scalar K

$$
K \equiv \mathcal{R}_{\alpha\beta\gamma\delta}\mathcal{R}^{\alpha\beta\gamma\delta} \tag{E.1}
$$

of gravitational bulk geometries (2.13) dual to de Sitter vacua of the cascading gauge theories. Growth of K evaluated at the apparent horizon as $\frac{H^2}{\Lambda^2}$ varies signals the breakdown

JHEP05(2020)035

of the supergravity approximation. Explicitly evaluating (E.1) we find, $' = \frac{d}{dr} = -\frac{d}{dz}$,

$$
\begin{aligned}
K = {} & 4a^2\Bigg(\frac{12(\sigma'')^2}{\sigma^2}+\frac{(a'')^2}{a^2}+\frac{2(w''_{a2})^2}{w_{a2}^2}+\frac{2(w''_{b2})^2}{w_{b2}^2}+\frac{(w''_{c2})^2}{w_{c2}^2}\Bigg)+\frac{24(\sigma'')}{\sigma}\Bigg(H^2-Ha' \\
& +\frac{4Ha\sigma'}{\sigma}+\frac{2a\sigma'a'}{s}\Bigg)+\frac{4a^2w'_{c2}w''_{c2}}{w_{c2}^2}\left(\frac{a'}{a}-\frac{w'_{c2}}{w_{c2}}\right)+\frac{8a^2w'_{a2}w''_{a2}}{w_{a2}^2}\left(\frac{a'}{a}-\frac{w'_{a2}}{w_{a2}}\right)+\frac{8a^2w'_{b2}w''_{b2}}{w_{b2}^2} \\
& \times\left(\frac{a'}{a}-\frac{w'_{b2}}{w_{b2}}\right)+3H^2\left(\frac{24(\sigma')^2}{\sigma^2}+\frac{(w'_{c2})^2}{w_{c2}^2}+\frac{2(w'_{b2})^2}{w_{b2}^2}+\frac{2(w'_{a2})^2}{w_{a2}^2}\right)+2(a')^2\Bigg(\frac{12(\sigma')^2}{\sigma^2} \\
& +\frac{(w'_{c2})^2}{w_{c2}^2}+\frac{2(w'_{b2})^2}{w_{b2}^2}+\frac{2(w'_{a2})^2}{w_{a2}^2}\Bigg)+\frac{12H\sigma'a}{\sigma}\Bigg(\frac{4\sigma'a'}{a\sigma}+\frac{8(\sigma')^2}{\sigma^2}+\frac{(w'_{c2})^2}{w_{c2}^2}+\frac{2(w'_{b2})^2}{w_{b2}^2} \\
& +\frac{2(w'_{a2})^2}{w_{a2}^2}\Bigg)-2aa'\Bigg(\frac{(w'_{c2})^3}{w_{c2}^3}+\frac{2(w'_{b2})^3}{w_{b2}^3}+\frac{2(w'_{a2})^3}{w_{a2}^3}\Bigg)+\frac{12a^2(\sigma')^2}{\sigma^2}\Bigg(\frac{(w'_{c2})^2}{w_{c2}^2}+\frac{2(w'_{b2})^2}{w_{b2}^2} \\
& +\frac{2(w'_{a2})^2}{w_{a2}^2}\Bigg)+\frac{48a^2(\sigma')^4}{\sigma^4}+a^2\Bigg(\frac{2(w'_{b2})^2(w'_{c2})^2}{w_{b2}^2w_{c2}^2}+\frac{2(w'_{a2})^2(w'_{c2})^2}{w_{a2}^2w_{c2}^2}+\frac{4(w'_{a2})^2(w'_{b2})^2}{w_{a2}^2w_{b2}^2} \\
& +\frac{(w'_{c2})^4}{w_{c2}^4}+\frac{3(w'_{b2})^4}{w_{b2}^4}+\frac{3(w'_{a2})^4}{w_{a2}^4}\Bigg)+\frac{a(w'_{a2})^2}{w_{b2}w_{c2}w_{a2}^3}(27w_{a2}^2+9w_{b2}^2-36w_{b2}w_{c2}+16w_{c2}^2) \\
& +\frac{a(w'_{b2})^2}{w_{a2}w_{c2}w_{b2}^3}(9w_{a2}^2-36w_{a2}w_{c2}+27w_{b2}^2+16w_{c2}^2)+\frac{3a(w'_{c2})^2}{w_{a2}w_{b2}w_{c2}^3}(3w_{a2}^2-6w_{a2}w_{b2} \\
& +3w_{b2}^2+16w_{c2}^2)-\frac{aw'_{a2}w'_{c2}}{2w_{b2}w_{a2}^2w_{c2}^2}(63w_{a2}^2-18w_{a2}w_{b2}+24w_{a2}w_{c2}-45w_{b2}^2-24w_{b2}w_{c2} \\
& +112w_{c2}^2)+\frac{aw'_{b2}w'_{c2}}{2w_{a2}w_{c2}^2w_{b2}^2}(45w_{a2}^2+18w_{a2}w_{b2}+24w_{a2}w_{c2}-63w_{b2}^2-24w_{b2}w_{c2} \\
& -112w_{c2}^2)-\frac{aw'_{a2}w'_{b2}}{2w_{c2}w_{b2}^2w_{a2}^2}(63w_{a2}^2+18w_{a2}w_{b2}-24w_{a2}w_{c2}+63w_{b2}^2-24w_{b2}w_{c2}-80w_{c2}^2) \\
& +\frac{136w_{c2}^2}{w_{a2}^2w_{b2}^2}-\frac{144(w_{a2}+w_{b2})w_{c2}}{w_{a2}^2w_{b2}^2}+\frac{81(13w_{a2}^2+6w_{a2}w_{b2}+13w_{b2}^2)(w_{a2}-w_{b2})^2}{32w_{c2}^2w_{b2}^2w_{a2}^2} \\
& -\frac{54(w_{a2}^2-w_{b2}^2)(w_{a2}-w_{b2})}{w_{a2}^2w_{b2}^2w_{c2}}+\frac{9(9w_{a2}^2+14w_{a2}w_{b2}+9w_{b2}^2)}{w_{a2}^2w_{b2}^2}\,.
\end{aligned}
\tag{E.2}
$$

Introducing the dimensionless and rescaled functions and the radial coordinate $\hat{r} \equiv -\hat{z}$ as in (4.8),

$$
K = \frac{1}{P^2 g_s}\,\hat{K}\,. \tag{E.3}
$$

E.1 Kretschmann scalar at AH of TypeB de Sitter vacua

In section 3.4 we showed that the AH horizon of the bulk gravitational dual to TypeB de Sitter vacua of the cascading gauge theory is located at $r_{AH} = -z_{AH} = 0$, see (3.33).

JHEP05(2020)035

Using (B.67) we find from (E.2):

$$
\begin{aligned}
K_{AH}\Big|_{\text{TypeB}} &= 300h_0^h H^4 + H^2\Bigg(\frac{16P^2g_0^h(3(k_{2,2}^h)^2(f_{a,0}^h)^2+20)}{3(f_{a,0}^h)^3h_0^h} + \frac{72}{(f_{a,0}^h)^2k_{2,2}^h}\Bigg(5k_{2,4}^h(f_{a,0}^h)^2 \\
&+ 3k_{2,2}^h f_{a,0}^h + 18\Bigg) + \frac{5(k_{1,3}^h)^2k_{2,2}^h(f_{a,0}^h)^2 - 15k_{2,2}^h(k_{3,1}^h)^2 - 36k_{1,3}^hk_{3,1}^h}{k_{2,2}^hP^2(f_{a,0}^h)^2g_0^hh_0^h}\Bigg) \\
&+ \frac{1}{3840(f_{a,0}^h)^4(h_0^h)^3P^4(g_0^h)^2(k_{2,2}^h)^2}\Bigg(355(k_{1,3}^h)^4(k_{2,2}^h)^2(f_{a,0}^h)^4 - 30(k_{1,3}^h)^2(k_{2,2}^h)^2(k_{3,1}^h)^2(f_{a,0}^h)^2 \\
&+ 2283(k_{2,2}^h)^2(k_{3,1}^h)^4 + 6912k_{1,3}^hk_{2,2}^h(k_{3,1}^h)^3 + 6912(k_{1,3}^h)^2(k_{3,1}^h)^2\Bigg) \\
&+ \frac{3}{10(f_{a,0}^h)^4P^2g_0^h(h_0^h)^2(k_{2,2}^h)^2}\Bigg(25(k_{1,3}^h)^2(k_{2,2}^h)^2(f_{a,0}^h)^3 - 60k_{2,2}^hk_{2,4}^h(k_{3,1}^h)^2(f_{a,0}^h)^2 \\
&- 120k_{1,3}^hk_{2,4}^hk_{3,1}^h(f_{a,0}^h)^2 - 37(k_{2,2}^h)^2(k_{3,1}^h)^2f_{a,0}^h - 24k_{1,3}^hk_{2,2}^hk_{3,1}^hf_{a,0}^h - 216k_{2,2}^h(k_{3,1}^h)^2 \\
&- 432k_{1,3}^hk_{3,1}^h\Bigg) + \frac{1}{1080(f_{a,0}^h)^5(h_0^h)^3(k_{2,2}^h)^2}\Bigg(175(k_{1,3}^h)^2(k_{2,2}^h)^4(f_{a,0}^h)^4 \\
&+ 194400(k_{2,4}^h)^2(f_{a,0}^h)^5(h_0^h)^2 - 491(k_{2,2}^h)^4(k_{3,1}^h)^2(f_{a,0}^h)^2 + 77760k_{2,2}^hk_{2,4}^h(f_{a,0}^h)^4(h_0^h)^2 \\
&- 1152k_{1,3}^h(k_{2,2}^h)^3k_{3,1}^h(f_{a,0}^h)^2 + 746496(k_{2,2}^h)^2(f_{a,0}^h)^3(h_0^h)^2 - 2220(k_{1,3}^h)^2(k_{2,2}^h)^2(f_{a,0}^h)^2 \\
&+ 1399680k_{2,4}^h(f_{a,0}^h)^3(h_0^h)^2 + 279936k_{2,2}^h(f_{a,0}^h)^2(h_0^h)^2 - 3492(k_{2,2}^h)^2(k_{3,1}^h)^2 \\
&- 13824k_{1,3}^hk_{2,2}^hk_{3,1}^h + 2519424f_{a,0}^h(h_0^h)^2\Bigg) + \frac{8P^2g_0^h}{45k_{2,2}^h(f_{a,0}^h)^5(h_0^h)^2}\Bigg(60(k_{2,2}^h)^2k_{2,4}^h(f_{a,0}^h)^4 \\
&+ 37(k_{2,2}^h)^3(f_{a,0}^h)^3 + 216(k_{2,2}^h)^2(f_{a,0}^h)^2 + 720k_{2,4}^h(f_{a,0}^h)^2 - 756k_{2,2}^hf_{a,0}^h + 2592\Bigg) \\
&+ \frac{P^4(g_0^h)^2}{3645(h_0^h)^3(f_{a,0}^h)^6}\Bigg(881(k_{2,2}^h)^4(f_{a,0}^h)^4 + 10584(k_{2,2}^h)^2(f_{a,0}^h)^2 + 184464\Bigg)\,. \qquad \text{(E.4)}
\end{aligned}
$$

A special case of (E.4) is the Kretschmann scalar at the "AH" of the extremal KS solution, see section B.3: setting $H=0$ and using (B.79) we find

$$
\lim_{H\to 0} K_{AH}\Big|_{\text{TypeB}} = \frac{1}{P^2g_s}\,\frac{32\cdot 12^{2/3}(110\cdot 12^{1/3}+177147\delta^2)}{295245\delta^3}\,, \qquad \text{(E.5)}
$$

where we denoted, see h_0^h in (B.79),

$$
\delta \equiv 0.056288(0)\,. \qquad \text{(E.6)}
$$

JHEP05(2020)035

F Static linearized χSB fluctuations about TypeA$_s$ vacua

Static linearized χSB fluctuations about TypeA$_s$ vacua in FG frame are parameterized as in (5.1). From (B.4)–(B.5) and (B.7)–(B.9) we find, ($' = \frac{d}{d\rho}$ and $P = H = g_s = 1$):

$$
\begin{aligned}
0 = {} & \delta f'' - \frac{1}{16\rho g^2 f_2 h^2 f_3^3 (f_3'\rho - 2f_3)} \Big(-48 f_3^4 h^3 f_2 g^2 \rho^2 - 2(h')^2 g^2 f_3^4 f_2 \rho^2 - 2(g')^2 h^2 f_2 f_3^4 \rho^2 \\
& + 12 g^2 h^2 (f_3')^2 f_3^2 f_2 \rho^2 - 16 h (h') g^2 f_3^4 f_2 \rho - 16 h^2 g^2 f_3^3 (f_3') f_2 \rho - 48 f_3^4 h^2 g^2 f_2 \\
& - f_2 \rho^2 (K')^2 h f_3^2 g + 16 f_3^2 h^2 f_2^2 g^2 - 96 f_3^3 h^2 f_2 g^2 + 4 g^3 f_3^2 h + 2 g^2 K^2 \Big) \delta f' - \frac{K'}{2ghf_3} \delta k_1' \\
& - \frac{2g}{f_2 f_3 h \rho^2} \delta k_2 + \frac{1}{8 g^2 f_2 h^2 \rho^2 f_3^3 (f_3'\rho - 2f_3)} \Big(-48 g^2 f_3' f_2 h^3 f_3^3 \rho^3 + 8 g^2 (f_3')^3 f_2 h^2 f_3 \rho^3 \\
& + 48 f_3^4 h^3 f_2 g^2 \rho^2 - 2(h')^2 g^2 f_3^4 f_2 \rho^2 - 2(g')^2 h^2 f_2 f_3^4 \rho^2 - 36 g^2 h^2 (f_3')^2 f_3^2 f_2 \rho^2 \\
& - 16 h h' g^2 f_3^4 f_2 \rho + 64 h^2 g^2 f_3^3 f_3' f_2 \rho - 4 g f_3' (K')^2 f_2 h f_3 \rho^3 + 32 g^2 f_3' f_2^2 h^2 f_3 \rho - 72 g^2 f_3' h^2 f_3^3 \rho \\
& - 80 f_3^4 h^2 g^2 f_2 + 7 f_2 \rho^2 (K')^2 h f_3^2 g - 48 f_3^2 h^2 f_2^2 g^2 - 96 f_3^3 h^2 f_2 g^2 + 144 f_3^4 h^2 g^2 \\
& - 16 g^3 f_3' h f_3 \rho + 36 g^3 f_3^2 h + 2 g^2 K^2 \Big) \delta f \,, \qquad \text{(F.1)} \\
0 = {} & \delta k_1'' - \frac{1}{16\rho g^2 f_2 h^2 f_3^3 (f_3'\rho - 2f_3)} \Big(-48 f_3^4 h^3 f_2 g^2 \rho^2 - 2(h')^2 g^2 f_3^4 f_2 \rho^2 \\
& + 16 f_3^3 h f_2 g^2 \rho^2 f_3' h' - 2(g')^2 h^2 f_2 f_3^4 \rho^2 + 16 f_3^3 f_2 f_3' h^2 g g' \rho^2 + 12 g^2 h^2 (f_3')^2 f_3^2 f_2 \rho^2 \\
& - 48 h h' g^2 f_3^4 f_2 \rho - 32 f_3^4 f_2 h^2 g g' \rho - 16 h^2 g^2 f_3^3 f_3' f_2 \rho - 48 f_3^4 h^2 g^2 f_2 - f_2 \rho^2 (K')^2 h f_3^2 g \\
& + 16 f_3^2 h^2 f_2^2 g^2 - 96 f_3^3 h^2 f_2 g^2 + 4 g^3 f_3^2 h + 2 g^2 K^2 \Big) \delta k_1' + \frac{2K'}{f_3} \delta f' - \frac{9}{\rho^2 f_2} \delta k_1 \\
& + \frac{2gK}{\rho^2 f_2 h f_3^2} \delta k_2 + \frac{2(-f_3' K' f_2 h f_3 \rho^2 + 2gK)}{f_3^3 \rho^2 f_2 h} \delta f \,, \qquad \text{(F.2)} \\
0 = {} & \delta k_2'' - \frac{1}{16\rho g^2 f_2 h^2 f_3^3 (f_3'\rho - 2f_3)} \Big(-48 f_3^4 h^3 f_2 g^2 \rho^2 - 2(h')^2 g^2 f_3^4 f_2 \rho^2 \\
& + 16 f_3^3 h f_2 g^2 \rho^2 f_3' h' - 2(g')^2 h^2 f_2 f_3^4 \rho^2 - 16 f_3^3 f_2 f_3' h^2 g g' \rho^2 + 12 g^2 h^2 (f_3')^2 f_3^2 f_2 \rho^2 \\
& - 48 h h' g^2 f_3^4 f_2 \rho + 32 f_3^4 f_2 h^2 g g' \rho - 16 h^2 g^2 f_3^3 f_3' f_2 \rho - 48 f_3^4 h^2 g^2 f_2 - f_2 \rho^2 (K')^2 h f_3^2 g \\
& + 16 f_3^2 h^2 f_2^2 g^2 - 96 f_3^3 h^2 f_2 g^2 + 4 g^3 f_3^2 h + 2 g^2 K^2 \Big) \delta k_2' - \frac{9}{\rho^2 f_2} \delta k_2 + \frac{9K}{2\rho^2 f_2 f_3^2 h g} \delta k_1 \\
& - \frac{18}{f_3 \rho^2 f_2} \delta f \,. \qquad \text{(F.3)}
\end{aligned}
$$

Performing the asymptotic expansions, we determine:

- in the UV, i.e., as $\rho \to 0$, using (B.38)–(B.43),

$$
\begin{aligned}
\delta f = {} & \delta f_{1,0}\, \rho + \frac{1}{2} f_{2,1,0}\, \delta f_{1,0}\, \rho^2 + \Big(\delta f_{3,0} + \Big(\frac{1}{4} \delta f_{1,0}\, k_s - \frac{11}{8} \delta f_{1,0} \Big) \ln \rho \\
& - \frac{1}{4} \delta f_{1,0} \ln^2 \rho \Big) \rho^3 + \sum_{n=4} \sum_{k} \delta f_{n,k}\, \rho^n \ln^k \rho \,, \qquad \text{(F.4)}
\end{aligned}
$$

JHEP05(2020)035

$$\delta k_1 = -\frac{1}{2}\delta f_{1,0}\ \rho + \frac{1}{4} f_{2,1,0}\ \delta f_{1,0}\ \rho^2 + \left(\delta k_{1,3,0} + \left(-\frac{1}{24}\delta f_{1,0}\ k_s - \frac{47}{144}\delta f_{1,0} + 2\delta f_{3,0}\right)\ln\rho + \left(-\frac{4}{3}\delta f_{1,0} + \frac{1}{4}\delta f_{1,0}\ k_s\right)\ln^2\rho - \frac{1}{6}\delta f_{1,0}\ \ln^3\rho\right)\rho^3 + + \sum_{n=4}\sum_{k}\delta k_{1,n,k}\ \rho^n \ln^k\rho\,, \tag{F.5}$$

$$\delta k_2 = -\frac{9}{4}\delta f_{1,0}\ \rho + \frac{9}{8} f_{2,1,0}\ \delta f_{1,0}\ \rho^2 + \left(-\frac{13}{48}\delta f_{1,0}\ k_s - \frac{3}{8}\delta f_{1,0}\ f_{2,1,0}^2 + \frac{3}{2}\delta k_{1,3,0} - \frac{163}{144}\ \delta f_{1,0} - \delta f_{3,0} + \left(-\frac{5}{16}\ \delta f_{1,0}\ k_s + \frac{137}{96}\delta f_{1,0} + 3\delta f_{3,0}\right)\ln\rho + \left(-\frac{7}{4}\delta f_{1,0} + \frac{3}{8}\delta f_{1,0}\ k_s\right)\ln^2\rho - \frac{1}{4}\delta f_{1,0}\ \ln^3\rho\right)\rho^3 + \sum_{n=4}\sum_{k}\delta k_{2,n,k}\ \rho^n \ln^k\rho\,, \tag{F.6}$$

characterized by 4 parameters (compare with (B.25)):

$$\{\delta f_{1,0}\,,\ \underbrace{\delta f_{3,0}\,,\ \delta k_{1,3,0}}_{\mathcal{O}_3^\alpha}\,,\ \underbrace{\delta f_{7,0}}_{\mathcal{O}_7}\}\,, \tag{F.7}$$

where $\delta f_{1,0}$ is an explicit chiral symmetry breaking scale ($\propto$ the gaugino mass term), and the remaining parameters are the expectation values of the chiral symmetry breaking operators in the cascading gauge theory;

- in the IR, i.e., as $\frac{1}{\rho} = y \to 0$, using (B.45),

$$\delta f = \frac{1}{y}\sum_{n=0}\delta f_n^h\ y^n\,, \qquad \delta k_{1,2} = \sum_{n=0}\delta k_{1,2,n}^n\ y^n\,, \tag{F.8}$$

characterized by 3 parameters:

$$\{\delta f_0^h\,,\ \delta k_{1,0}^h\,,\ \delta k_{2,0}^h\}\,. \tag{F.9}$$

References

[1] I.R. Klebanov and A.A. Tseytlin, *Gravity duals of supersymmetric* SU(N) × SU($N+M$) *gauge theories*, *Nucl. Phys.* **B 578** (2000) 123 [hep-th/0002159] [INSPIRE].

[2] I.R. Klebanov and M.J. Strassler, *Supergravity and a confining gauge theory: duality cascades and χSB resolution of naked singularities*, *JHEP* **08** (2000) 052 [hep-th/0007191] [INSPIRE].

[3] I.R. Klebanov and E. Witten, *Superconformal field theory on three-branes at a Calabi-Yau singularity*, *Nucl. Phys.* **B 536** (1998) 199 [hep-th/9807080] [INSPIRE].

[4] C.P. Herzog, I.R. Klebanov and P. Ouyang, *Remarks on the warped deformed conifold*, in *Modern trends in string theory: 2nd Lisbon school on g theory superstrings*, Lisbon, Portugal, 13–17 July 2001 [hep-th/0108101] [INSPIRE].

[5] N. Seiberg, *Electric-magnetic duality in supersymmetric non-Abelian gauge theories*, *Nucl. Phys.* **B 435** (1995) 129 [hep-th/9411149] [INSPIRE].

JHEP05(2020)035

[6] A. Buchel, *Finite temperature resolution of the Klebanov-Tseytlin singularity*, *Nucl. Phys.* **B 600** (2001) 219 [hep-th/0011146] [INSPIRE].

[7] M. Krasnitz, *Correlation functions in a cascading $N = 1$ gauge theory from supergravity*, *JHEP* **12** (2002) 048 [hep-th/0209163] [INSPIRE].

[8] O. Aharony, A. Buchel and A. Yarom, *Short distance properties of cascading gauge theories*, *JHEP* **11** (2006) 069 [hep-th/0608209] [INSPIRE].

[9] A. Dymarsky, I.R. Klebanov and N. Seiberg, *On the moduli space of the cascading $\mathrm{SU}(M + p) \times \mathrm{SU}(p)$ gauge theory*, *JHEP* **01** (2006) 155 [hep-th/0511254] [INSPIRE].

[10] A. Buchel, C.P. Herzog, I.R. Klebanov, L.A. Pando Zayas and A.A. Tseytlin, *Nonextremal gravity duals for fractional D3 branes on the conifold*, *JHEP* **04** (2001) 033 [hep-th/0102105] [INSPIRE].

[11] S.S. Gubser, C.P. Herzog, I.R. Klebanov and A.A. Tseytlin, *Restoration of chiral symmetry: a supergravity perspective*, *JHEP* **05** (2001) 028 [hep-th/0102172] [INSPIRE].

[12] O. Aharony, A. Buchel and P. Kerner, *The black hole in the throat: thermodynamics of strongly coupled cascading gauge theories*, *Phys. Rev.* **D 76** (2007) 086005 [arXiv:0706.1768] [INSPIRE].

[13] A. Buchel, *Chiral symmetry breaking in cascading gauge theory plasma*, *Nucl. Phys.* **B 847** (2011) 297 [arXiv:1012.2404] [INSPIRE].

[14] A. Buchel, *Klebanov-Strassler black hole*, *JHEP* **01** (2019) 207 [arXiv:1809.08484] [INSPIRE].

[15] O. Aharony, A. Buchel and A. Yarom, *Holographic renormalization of cascading gauge theories*, *Phys. Rev.* **D 72** (2005) 066003 [hep-th/0506002] [INSPIRE].

[16] I. Bena, A. Buchel and S. Lüst, *Throat destabilization (for profit and for fun)*, arXiv:1910.08094 [INSPIRE].

[17] A. Buchel, *A holographic perspective on Gubser-Mitra conjecture*, *Nucl. Phys.* **B 731** (2005) 109 [hep-th/0507275] [INSPIRE].

[18] V. Balasubramanian, A. Buchel, S.R. Green, L. Lehner and S.L. Liebling, *Holographic thermalization, stability of anti-de Sitter space and the Fermi-Pasta-Ulam paradox*, *Phys. Rev. Lett.* **113** (2014) 071601 [arXiv:1403.6471] [INSPIRE].

[19] A. Buchel and A. Karapetyan, *De Sitter vacua of strongly interacting QFT*, *JHEP* **03** (2017) 114 [arXiv:1702.01320] [INSPIRE].

[20] A. Buchel, *Entanglement entropy of $N = 2^*$ de Sitter vacuum*, *Nucl. Phys.* **B 948** (2019) 114769 [arXiv:1904.09968] [INSPIRE].

[21] A. Buchel, *Verlinde gravity and AdS/CFT*, arXiv:1702.08590 [INSPIRE].

[22] I. Booth, *Black hole boundaries*, *Can. J. Phys.* **83** (2005) 1073 [gr-qc/0508107] [INSPIRE].

[23] P. Figueras, V.E. Hubeny, M. Rangamani and S.F. Ross, *Dynamical black holes and expanding plasmas*, *JHEP* **04** (2009) 137 [arXiv:0902.4696] [INSPIRE].

[24] A. Buchel, *Ringing in de Sitter spacetime*, *Nucl. Phys.* **B 928** (2018) 307 [arXiv:1707.01030] [INSPIRE].

[25] P.M. Chesler and L.G. Yaffe, *Numerical solution of gravitational dynamics in asymptotically anti-de Sitter spacetimes*, *JHEP* **07** (2014) 086 [arXiv:1309.1439] [INSPIRE].

JHEP05(2020)035

[26] P.M. Chesler and L.G. Yaffe, *Horizon formation and far-from-equilibrium isotropization in supersymmetric Yang-Mills plasma*, *Phys. Rev. Lett.* **102** (2009) 211601 [arXiv:0812.2053] [INSPIRE].

[27] A. Buchel, L. Lehner and R.C. Myers, *Thermal quenches in $N = 2^*$ plasmas*, *JHEP* **08** (2012) 049 [arXiv:1206.6785] [INSPIRE].

[28] A. Buchel, L. Lehner, R.C. Myers and A. van Niekerk, *Quantum quenches of holographic plasmas*, *JHEP* **05** (2013) 067 [arXiv:1302.2924] [INSPIRE].

[29] A. Buchel and A.A. Tseytlin, *Curved space resolution of singularity of fractional D3-branes on conifold*, *Phys. Rev.* **D 65** (2002) 085019 [hep-th/0111017] [INSPIRE].

[30] A. Buchel, *Gauge/gravity correspondence in accelerating universe*, *Phys. Rev.* **D 65** (2002) 125015 [hep-th/0203041] [INSPIRE].

[31] A. Buchel and D.A. Galante, *Cascading gauge theory on dS_4 and string theory landscape*, *Nucl. Phys.* **B 883** (2014) 107 [arXiv:1310.1372] [INSPIRE].

[32] A. Buchel, M.P. Heller and J. Noronha, *Entropy production, hydrodynamics and resurgence in the primordial quark-gluon plasma from holography*, *Phys. Rev.* **D 94** (2016) 106011 [arXiv:1603.05344] [INSPIRE].

[33] E. Poisson, *A relativist's toolkit*, Cambridge University Press, Cambridge, U.K. (2004).

[34] O. Aharony, M. Berkooz, D. Tong and S. Yankielowicz, *Confinement in anti-de Sitter space*, *JHEP* **02** (2013) 076 [arXiv:1210.5195] [INSPIRE].

[35] A. Buchel, *Gauge theories on hyperbolic spaces and dual wormhole instabilities*, *Phys. Rev.* **D 70** (2004) 066004 [hep-th/0402174] [INSPIRE].

[36] A. Buchel, P. Langfelder and J. Walcher, *On time dependent backgrounds in supergravity and string theory*, *Phys. Rev.* **D 67** (2003) 024011 [hep-th/0207214] [INSPIRE].

[37] A. Buchel, *Compactifications of the $N = 2^*$ flow*, *Phys. Lett.* **B 570** (2003) 89 [hep-th/0302107] [INSPIRE].

[38] A. Buchel and A. Ghodsi, *Braneworld inflation*, *Phys. Rev.* **D 70** (2004) 126008 [hep-th/0404151] [INSPIRE].

JHEP05(2020)035